Università di Pisa

Engineering PhD School “Leonardo da Vinci”

Corso di Dottorato di Ricerca in

VEICOLI TERRESTRI E SISTEMI DI TRASPORTO
SSD ING/08

Tesi di Dottorato di Ricerca

An Innovative combustion system for Diesel engines

Author

Riccardo Rossi

Tutor

Prof. Roberto Gentili

Anno 2012

SOMMARIO

La crescente attenzione alle emissioni di gas-serra e le sempre più stringenti limitazioni delle emissioni inquinanti hanno spinto la ricerca nell'ambito dei motori a combustione interna verso una combustione che consenta simultaneamente un incremento sostanziale dell'efficienza e una forte riduzione delle emissioni.
La presente attività di ricerca si è incentrata sullo studio e lo sviluppo di un nuovo concetto di combustione Diesel ad alta efficienza e basse emissioni. Il concetto consiste nel formare una carica omogenea precompressa all'esterno del cilindro combustore e nel farvela affluire gradualmente nella fase di combustione. In questo modo il controllo della combustione è affidato, anziché all'EGR, all'andamento del trasferimento della carica. Questa nuova tipologia di combustione è stata definita HCPC (Homogeneus Charge Progressive Combustion).
Per realizzare la combustione HCPC si utilizza lo "split-cycle", nel quale le fasi di aspirazione e di compressione vengono effettuate in un cilindro compressore, dal quale l'aria precompressa viene trasferita nel cilindro combustore attraverso un condotto di trasferimento. Una valvola di trasferimento è posizionata tra il cilindro compressore e il condotto di trasferimento. Durante la fase di trasferimento, nel condotto omonimo viene iniettato il combustibile, che evapora rapidamente e si miscela pressoché omogeneamente con l'aria, per poi bruciare appena giunge in camera di combustione

L'attività svolta durante il Dottorato di Ricerca ha riguardato studio del motore HCPC, sia per applicazioni leggere che pesanti, tramite tecniche di fluidodinamica computazionale (CFD). Nella prima fase dell'attività di ricerca è stata testata la validità del concetto, seguita da studi e sviluppi della geometria del motore. In seguito è stata studiata una versione per applicazioni leggere del motore, che consente di far funzionare il motore stesso con consumi specifici tipici dei motori ad accensione spontanea, a velocità di rotazione tipiche dei motori ad accensione comandata, mantenendo una combustione con basse emissioni di particolato in ogni condizione. È stata poi condotta un'attività di validazione su motori per applicazione pesante, che è consistita nel confronto dei risultati CFD con quelli sperimentali in termini di prestazioni ed emissioni inquinanti. Infine sono state studiate due versioni del motore HCPC per applicazioni pesanti, la seconda delle quali garantisce un'efficienza termica paragonabile a quella dei motori Diesel convenzionali, con bassissime emissioni inquinanti. In effetti il motore HCPC per applicazioni pesanti rispetta la normativa EURO 6 senza bisogno di complicati e costosi sistemi di post-trattamento dei gas di scarico (ad. es. SCR, LNT e/o DPF).

ABSTRACT

Due to concerns regarding the greenhouse effect and limitations on carbon dioxide emissions, the possibility of a next-generation combustion mode for internal combustion engines that can simultaneously reduce exhaust emissions and substantially improve thermal efficiency has drawn increasing attention.
The presented research activity was focused on the design and development of an innovative combustion system for Diesel engines. A new approach for a low emission – high efficiency Diesel combustion was conceived: the basic idea is to control the heat release rate by a gradual supply of an almost homogeneous charge in the combustion chamber, without relying on exhaust gas recirculation or extremely diluted mixtures to moderate the combustion reactions. This new approach was defined Homogenous Charge Progressive Combustion (HCPC).
HCPC is based on the split-cycle principle. The intake and compression phases are performed in a reciprocating external compressor, which drives the air into the combustor cylinder during the combustion process, through a transfer duct. A transfer valve is placed between the compressor cylinder and the transfer duct. The compressor piston has a fixed delay, in terms of crank-angle degrees, with respect to the combustor piston. The combustion takes place after combustor TDC, thus, during the combustion process, the combustor piston moves downwards whereas the compressor piston moves upwards. As a consequence, the air moves from the compressor cylinder to the combustor cylinder. Contemporary with the air transfer, fuel is injected into the transfer duct, evaporates and mixes with the air, bringing about the conditions needed for a nearly homogeneous combustion.

The research activity carried out during the PhD course was focused on the CFD study of the HCPC engine, both for Light-Duty and Heavy-Duty applications. Preliminary results were the concept validity was tested are presented, followed by further studies and development of the engine geometry. A light duty version of the engine is firstly presented, which can run at the even better ISFC of Diesel engines at speeds that are typical of SI engines for passenger cars, maintaining a low soot emission combustion. Next a validation activity on Heavy-Duty engines is presented, where the CFD model was tested, both for performance and emission behavior. Finally two versions of an Heavy-Duty HCPC engine are presented, the latter delivering a Diesel-like indicated thermal efficiency, with ultra-clean combustion. As a matter of fact the HCPC Heavy-Duty engine can comply with EURO 6 regulations, without needing complicated and expensive aftertreatment system (i.e. SCR, LNT and/or DPF).

ACKNOWLEDGEMENTS

I first of all would like to thanks my advisor Prof. Roberto Gentili, for giving me the chance to follow this amazing path and for his guidance during this years of staying at the University of Pisa. His deep knowledge of the subject gave me insight on the internal combustion engine universe, which I only marginally have begun to explore.
I would also like to thank my colleague Dr. Ettore Musu (Beppe), who taught me more or less everything I know about internal combustion engine numerical simulation, and especially for all the days spent together in the "Labgentili", and all the experiences we had when travelling the world to attend to symposia and conferences.
Dr. Stefano Frigo deserves a mention too, for all the fruitful conversation and the funny moments we had in these years. I will always remember all the pasta "with rinforzino" he cooked for us in the lab.
I also thank all the students I had the chance to work with as an advisor for their bachelor/master thesis work, for all the fun we had toghether.
I also want to thank all my friends in Pisa and at home, for all the fun and support they gave me throughout the years.

Being a PhD student gave me also the opportunity to live one of the most incredible experiences of my life: living and working in Madison, WI.
I had the unique chance to work with Prof. Rolf D. Reitz, who I thank for giving me the opportunity to work at the Engine Research Center, and for his guidance and all the suggestions he gave me during the research meetings.
I would like to thank also all the students, staff and faculties I had the chance to meet and work with at the ERC. A special mention goes to my friend and colleague Dr. Federico Perini (Piero), for the major help he gave me when at work, and especially for sharing with me the experience of living in Madison.

In Madison I gladly happened to be also part of another great "organization", the Madfamily. I will never forget all the family lunches and dinners we had together and I thank all the members of the family for the amazing time we spent together: Alex (Sbatta), Andres, Benè, Diogo (Cugino), Cris, Juliana, Giuseppe, Glaucio, Leandro, Leane, Luis (Palillo), Michele, Simone, Yina (Gina). Finally a special thank goes to my friend, brother, uncle Fays, for feeding me, as he would like to say, and for teaching me all those amazing recipes. I'll never forget that Saturday morning cooking together in the Med Café kitchen.

I would like to thank my parents Battista and Gabriella, who made it possible for me to reach this target, and the ones before this. Without them I won't be the person I am today.

Finally I thank Caterina, for always being at my side, even when there was an Ocean between us.

NOMENCLATURE

ATDC	=	*After Top Dead Center*
BDC	=	*Bottom Dead Center*
BMEP	=	*Break Mean Effective Pressure*
BSFC	=	*Brake Specific Fuel Consumption*
BTDC	=	*Before Top Dead Center*
CA	=	*Crank Angle*
CAD	=	*Crank Angle Degree*
CB	=	*Combustor*
CFD	=	*Computational Fluid Dynamics*
CI	=	*Compression Ignition*
CNG	=	*Compressed Natural Gas*
CO	=	*Carbon Mono-Oxide*
CP	=	*Compressor*
DDM	=	*Discrete Droplet Model*
DI	=	*Direct Injection*
DOC	=	*Diesel Oxidation Catalyst*
DPF	=	*Diesel Particulate Filter*
ECFM-3Z	=	*Extended Coherent Flamelet Model – 3 Zone*
EGR	=	*Exhaust Gas Recirculation*
EOI	=	*End Of Injection*
E-S 1, E-S 2	=	*Engine Sizing 1, Engine Sizing 2*
ETVC	=	*Effective Transfer Valve Closure*
ETVO	=	*Effective Transfer Valve Opening*
EVC	=	*Exhaust Valve Closure*
EVO	=	*Exhaust Valve Opening*
HC	=	*Unburned Hydrocarbons*
HCCI	=	*Homogeneous Charge Compression Ignition*
HCPC	=	*Homogeneous Charge Progressive Combustion*
HD	=	*Heavy Duty*
HRR	=	*Heat Release Rate*
IMEP	=	*Indicated Mean Effective Pressure*
IVC	=	*Intake Valve Closure*
IVO	=	*Intake Valve Opening*
Kgf	=	*Kilograms Of Fuel*
KH-RT	=	*Kelvin-Helmholtz Rayleigh-Taylor*
LNT	=	*Lean NOX Trap*
LPG	=	*Liquefied Petroleum Gas*
LTC	=	*Low Temperature Combustion*
NOX	=	*Oxides of Nitrogen*
OEM	=	*Original Equipment Manufacturer*

PCCI	=	*Partially Premixed Charge Compression Ignition*
PM	=	*Particulate Matter*
PPRR	=	*Peak Pressure Rise Rate*
RANS	=	*Reynolds Averaged Navier Stokes*
RCCI	=	*Reactivity Controlled Compression Ignition*
ROHR	=	*Rate Of Heat Release*
RPM	=	*Revolutions Per Minute*
SCOTE	=	*Single Cylinder Oil Test Engine*
SCR	=	*Selective Catalytic Reduction*
SI	=	*Spark Ignition*
SMD	=	*Sauter Mean Diameter*
SOI	=	*Start Of Injection*
TAB	=	*Taylor Analogy Breakup*
TDC	=	*Top Dead Center*
TSC	=	*Two-Stage Combustion*
TVC	=	*Transfer Valve Closure*
TVO	=	*Transfer Valve Opening*

TABLE OF CONTENTS

LIST OF FIGURES

LIST OF TABLES

Chapter 1

INTRODUCTION

Internal combustion engines have played a fundamental role in the power generation and transportation fields for over a century. However, due to concerns regarding the greenhouse effect and limitations on carbon dioxide emissions, as well as limited petroleum supplies, the possibility of a next-generation combustion mode for internal combustion engines that can simultaneously reduce exhaust emissions and substantially improve thermal efficiency has drawn increasing attention.

Therefore, interest in compression-ignition engines has increased both for Light-Duty and Heavy-Duty applications, being CI engines the most fuel-efficient engines developed for transportation purposes, due largely to their relatively high compression ratios and lack of throttling losses.

However, conventional Diesel engines have relatively high emissions of nitric oxides (NO_X) and soot, which represent the biggest challenge for engine design and development engineers. Although these emissions have been significantly reduced in recent years, further reductions are required to meet the increasingly stringent regulations for nowadays and beyond. EURO regulations, for instance, require a drop of 80% for NO_X emissions and 50% for soot emissions when moving from EURO 5 to EURO 6 for Heavy-Duty Diesel engines applications. Similar requirements are also determined by the United States or Japanese regulations [1]. Meeting the current emission regulations for Diesel engines has required the development of a thorough understanding of the in-cylinder processes, to try to reduce to as low as possible values in-cylinder pollutant generation. Thanks to numerous investigations, conducted mostly using advanced laser-imaging diagnostics, a greatly improved understanding of Diesel combustion was achieved, summarized by the schematic in Fig. 1.1 [2, 3]. This understanding, has been guiding engineers in substantially reducing Diesel emissions over the past fifteen years. Solutions to improve Diesel combustion were developed, like increased injection pressure, common rail systems, EGR, improved piston-bowl geometries, improved in-cylinder flows, and so on. However, Fig. 1.1 also shows the factors that limit the reduction of emissions with traditional Diesel combustion. The fuel and air first react in a fuel-rich mixture, leading to soot formation, then this rich mixture burns out in a high-temperature diffusion flame at the jet periphery, leading to NO_X formation [4]. Therefore, it appears unlikely that conventional jet-mixing controlled Diesel combustion will be able to meet

future emission requirements without complicated and expensive aftertreatment systems, like Diesel Particulate Filter (DPF) for soot emission, and Selective Catalytic Reduction (SCR) or Lean NO_X Trap (LNT) for NO_X emissions. These systems have a number of drawbacks, besides their cost. DPF and LNT work as traps, therefore they need to be periodically regenerated, by injecting additional amounts of fuel either in the cylinder during the exhaust phase or in the exhaust line, worsening fuel consumption. SCR, instead, needs to be supplied with ammonia to complete the reduction reactions needed to lower tailpipe NO_X emissions, thus requiring an additional tank for ammonia storage.

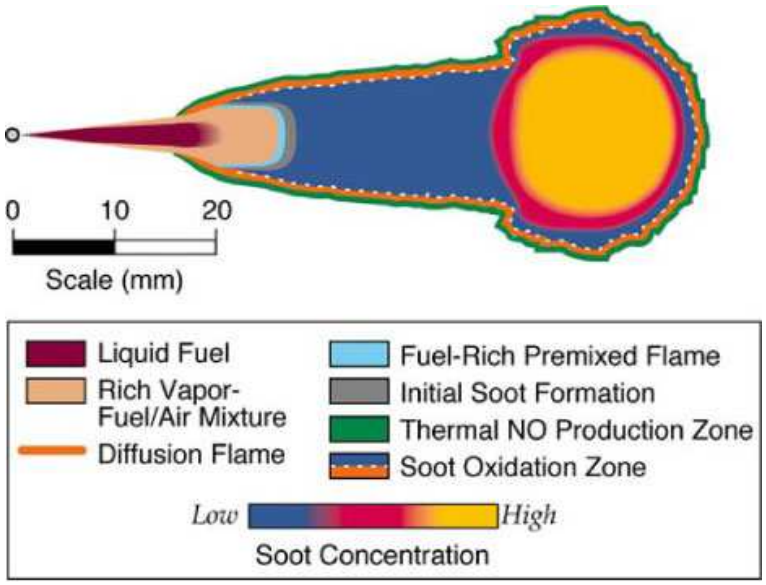

Fig 1.1 Conceptual schematic of conventional Diesel combustion

Due to the conventional Diesel combustion limits, researchers and development engineers have been turning to alternative forms of CI combustion, which mostly rely on the principle of dilute premixed or partially premixed combustion to reduce emissions. This approach is exemplified by a technique commonly known as homogeneous charge compression-ignition (HCCI) [5]. In this combustion strategy, fuel is injected and well premixed with air before ignition, thus avoiding fuel-rich regions leading to reduction of soot emissions. Combustion takes place at the same time in the whole combustion chamber, since lean mixture is used and charge is diluted with exhaust products. Because of the high dilution, combustion temperatures are low, resulting in low NO_X emissions. Because of these advantages, substantial research and development efforts on HCCI are

underway using a variety of fuels, including gasoline, Diesel fuel, ethanol, natural gas, and so on.

On the other hand, since HCCI is triggered by homogenous charge spontaneous ignition during compression, combustion timing and control are not easily manageable (in conventional S.I and C.I engines the control is achieved by spark timing and injection timing, respectively), thus high peaks in the heat release profile can be observed, leading to high pressure gradients, causing intolerable combustion noise, and mechanical stress.

These drawbacks are seen in particular when using Diesel fuel, due to its low volatility and the ease with which it autoignites (high cetane number). Therefore, researchers are pursuing alternative approaches to achieve HCCI-like combustion, commonly referred to as Diesel Low-Temperature combustion (LTC). With Diesel LTC, various techniques are applied to obtain sufficient premixing so that combustion temperature and equivalence ratio combinations that lead to soot and NO_X formation are avoided.

A better understanding of benefits coming from HCCI and LTC can be achieved through the equivalence ratio (Φ)-temperature diagram in Fig. 2.1. The diagram shows contour plots of the Φ-temperature combinations at which soot and NO_X formation occur.

In conventional Diesel combustion, the fuel and air first react in a rich mixture at about $\Phi = 4$, and then combustion goes to completion in a stoichiometric ($\Phi = 1$) diffusion flame. Assuming that the combustion is nearly adiabatic, Fig. 2.1 shows that these combustion zones fall in the soot and NO_X regions, respectively, leading to high levels of emissions. Also shown in Fig. 2 is the HCCI combustion region, which falls outside the soot– and NO_X –formation regions.

However, not only HCCI can avoid both pollutant generation zones; Diesel LTC, for instance, allows combustion to occur anywhere in the gray-shaded region, while trying to insure that most of the fuel is mixed and burned at $\Phi \leq 1$, like in HCCI combustion. Thus, although Diesel LTC combustion is not fully premixed, it uses essentially the same principles as HCCI to obtain low emissions. Current research and development efforts for advanced CI engines are directed at overcoming the difficulties of implementing HCCI and Diesel LTC in practical engines.

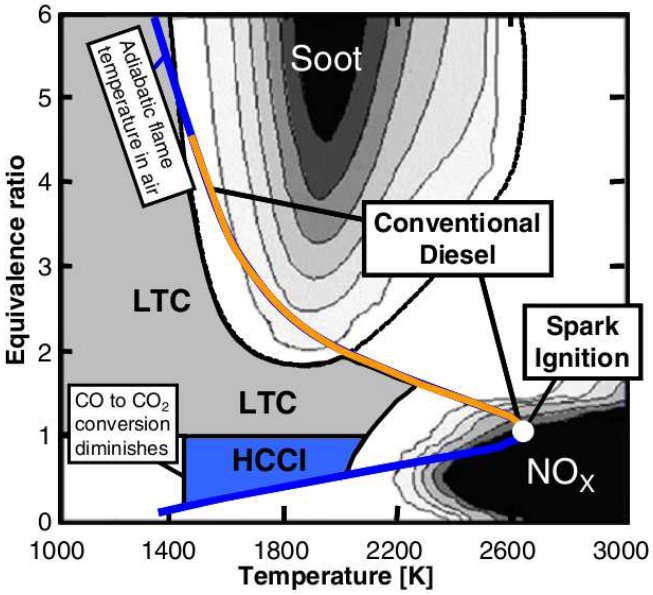

Fig. 1.2. Equivalence Ratio-temperature map for soot and NO_X formation and regions for conventional Diesel, SI, HCCI, and Diesel LTC engines.

Fig. 1.3 shows the huge amount of work that was put into HCCI combustion research during the last decade [6]. The subject of the different research activity span from fuels to mode switching (from conventional to HCCI operation and vice versa), from mixture preparation to boosting, from experimental optical analysis to numerical simulation, and so on.
As of today, HCCI applications remain mostly limited to research labs, except from a few production models, which run in HCCI operation only for a limited range of BMEP and engine speed.
LTC shows similar drawbacks with respect to HCCI, if particular charge stratification techniques or high level of dilution/EGR are not employed. Charge stratification primarily includes stratification of concentration, composition, and temperature, all of which have important influences on ignition, combustion rate, emissions, and load extension.
Fuel design and management can be used to optimize LTC combustion within the full load range and have the potential to control ignition timing and combustion rate, eliminate misfire at light loads and knock problems at heavy loads, and maintain Diesel-like thermal efficiency throughout the full engine operational range. Strategies based on the combination of port injection and in-cylinder direct injection of fuels with different physico-chemical properties can produce in-cylinder mixture stratification, composition stratification, and temperature stratification.

Categories and main contents in SP regarding HCCI (published by SAE from 2001 to 2010).

Research aspects	Paper numbers	Research contents	Main research unit
Gasoline HCCI	78	Residual gas trapping and its control, external EGR, camless HCC engine, load expanding, mode switching, GDI based HCCI, cyclical fluctuation, SCCI, spark-assisted self-ignition	Brunel University, Lund University, University of Birmingham, Ford, GM, Stanford University, University of Cambridge, Jugar, Tsinghua University, AVL, Tianjin University, etc.
Diesel HCCI	45	External EGR, load extension, fuel-supplying strategy, influence of combustion chamber boosting, VVT, VCR, PCCI, mixture preparation	University of Wisconsin Madison; National Traffic Safety and Environment Laboratory, University of Michigan, Sandia National Lab, New ACE, Toyota, Tianjin University, Shanghai Jiao Tong University, Southwest Research Institute, IFP, Lund University, etc.
Alternative fuel HCCI	25	Natural gas, Ethanol, methanol, hydrogen, DME	Shanghai Jiao Tong University, Keio University, Korea Advanced Institute of Science and Technology, Lund University, Tianjin University, University of California Berkeley, etc.
Theoretical study	108	Mixture and temperature distribution, fuel design, closed-loop control, heat transfer of boundary layer, effect of compression ratio, chemical kinetics, VCR, EGR mechanism, Heat management, cyclical fluctuation, gas reforming, analysis of emission components, measurement of in-cylinder temperature and emission formation, measurement and control of combustion process	Shanghai Jiao Tong University, Keio University, Lund University, Lawrence Livermore National Lab, Sandia National Lab, University of Michigan, University of California Berkeley, etc
Optical diagnostic	22	PLIF research on boundary layer reaction, PLF and chemoluminescence, Mixture distribution, ignition mechanism, combustion process, pollutants formation and evolution	Brunel University, Lund University Sandia National Lab, Stanford University, University of Illinois at Urbana-Champaign, etc
Numeric simulation	61	Multi-zone model, Ignition prediction with detail chemical kinetics, multi-dimension CFD coupled with detail chemical kinetics, sequential CFD-multi-zone chemical kinetics, Detail chemical kinetics with gas exchange process, Large eddy simulation, direct numerical simulation	University of Wisconsin Madison, Ricardo, Tianjin University, Brunel University, University of Michigan, Tsinghua University, University of California Berkeley, etc

Fig 1.3 HCCI research activity overview from 2001 to 2010

Therefore, the ignition timing, combustion phasing, and heat release characteristics of the full engine operational range can be adjusted for engine performance and emission optimization.
This strategy is employed in the Reactivity Controlled Compression Ignition system (RCCI). The concept consist in performing in-cylinder fuel blending of two fuels with different reactivity. By using in-cylinder fuel blending, the fuel reactivity can be adjusted on a cycle-to-cycle basis by changing the injected quantities of, for instance, gasoline and Diesel fuel to optimally accommodate engine load and speed changes. Furthermore, reactivity stratification may be beneficial in reducing combustion noise.
Fuel stratification addresses several issues associated with kinetic control of the combustion event, such as lack of combustion phasing control at high engine loads and excessive rates of pressure rise.
Kokjohn et al. [7] proved the RCCI engine to achieve NO_X and soot emissions below latest emissions regulations limits (EURO 6, EPA 2010) for both Light-Duty and Heavy-Duty applications, with gross indicated efficiencies above 50 per cent.

The research activity presented in this thesis, aims at a similar result as the one achieved by the RCCI combustion: developing a EURO 6/EPA 2010 compliant engine, with no need of latest-technology aftertreatment systems.
A new approach for a low emission – high efficiency Diesel combustion was conceived: the basic idea is to control the heat release rate by a gradual supply of an almost homogeneous charge in the combustion chamber, without relying on exhaust gas recirculation or extremely diluted mixtures to moderate the combustion reactions. This new approach was defined Homogenous Charge Progressive Combustion (HCPC).
HCPC is based on the split-cycle principle. The intake and compression phases are performed in a reciprocating external compressor, which drives the air into the combustor cylinder during the combustion process, through a transfer duct. A transfer valve is placed between the compressor cylinder and the transfer duct. The compressor piston has a fixed delay, in terms of crank-angle degrees, with respect to the combustor piston. The combustion takes place after combustor TDC, thus, during the combustion process, the combustor piston moves downwards whereas the compressor piston moves upwards. As a consequence, the air moves from the compressor cylinder to the combustor cylinder. Contemporary with the air transfer, fuel is injected into the transfer duct, evaporates and mixes with the air, bringing about the conditions needed for a nearly homogeneous combustion.
In the next chapters the HCPC concept will be described and validated, both for Light-Duty and Heavy-Duty applications.

Chapter 2

HOMOGENEOUS CHARGE PROGRESSIVE COMBUSTION CONCEPT BACKGROUND

2.1 INTRODUCTION

The HCPC concept consists in forming a pre-compressed homogenous charge outside the cylinder and in gradually admitting the charge into the cylinder during the engine combustion phase, so that combustion control is delegated to the charge transfer process.
In the original concept, the charge was formed during the air transfer to the cylinder from a constant-pressure tank. Thus combustion takes place at virtually constant pressure during the first part of the downward stroke of the piston. Combustion behavior is controlled by the transfer rate and soot emissions can be extremely contained in every operating condition. Therefore it is possible to use EGR only to limit NO_X emissions, which can be reduced to the level typical of the Low-Temperature combustions.
In the first part of the research activity a first analysis was addressed to the feasibility of the concept and subsequently two different realizations were considered. Both these proposed solutions were then compared with a Diesel combustion case in terms of pressure, heat release rate, temperature and emissions production.

2.2 CONCEPT VALIDATION

A first CFD analysis was performed to test the validity of the concept, regardless of which effective solution would be adopted. A single cylinder filled with a perfectly stirred mixture of air and Diesel fuel was considered in the simulation. A constant pressure inlet surface connecting the cylinder with a transfer duct is also modeled. Figure 2.1 shows a conceptual scheme of the HCPC concept [8].

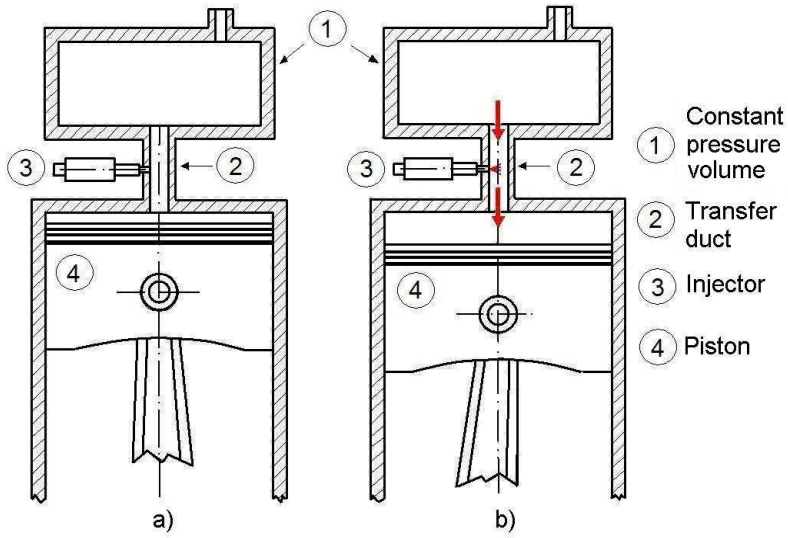

Fig. 2.1. Conceptual HCPC concept scheme

The simulation starts at TDC with initial conditions reported in Tab. 2.1. Transfer and combustion phase occur at the beginning of the downward piston stroke. Cylinder pressure is kept constant thanks to proper transfer flow rate.

Displacement (cm3)	1932
Bore (mm)	135
Stroke (mm)	135
Engine speed (rev/min)	2400
Global equivalence ratio (Full load /1/3 of Max. load)	0.588 / 0.196
Initial P (MPa)	6.8
Initial T (K)	1150

Tab. 2.1. Simulation settings for the concept validation.

In Fig. 2.2 the computational grid of about 20000 cells at TDC is reported. The simulations were performed using AVL FIRE release 8.5 [9]. The turbulence model based on the RANS method is the two-equation K-ε model, very common in computational fluid dynamics, which takes into account the effects of turbulence in the mean flow. Ignition and combustion

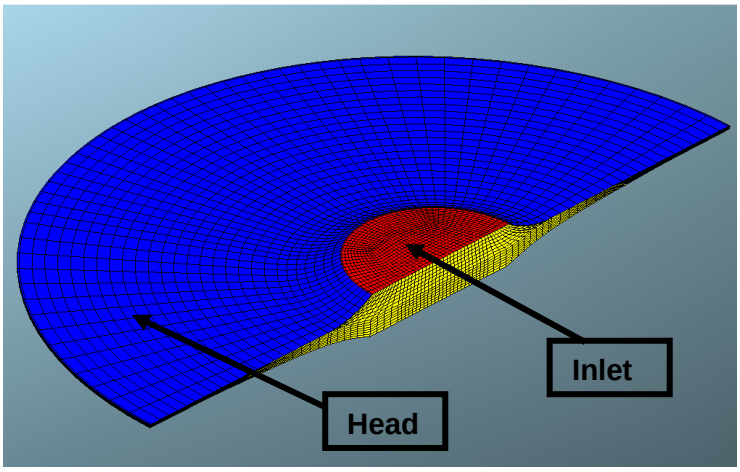

Fig. 2.2. Computational grid with around 20000 cells at TDC.

were simulated using the AVL DIESEL [10] autoignition model coupled with the Eddy Breakup Model.

Only the combustion phase was simulated, starting from TDC while the charge begins entering the cylinder. Initial conditions for pressure and temperature were calculated by a zero-dimensional code.

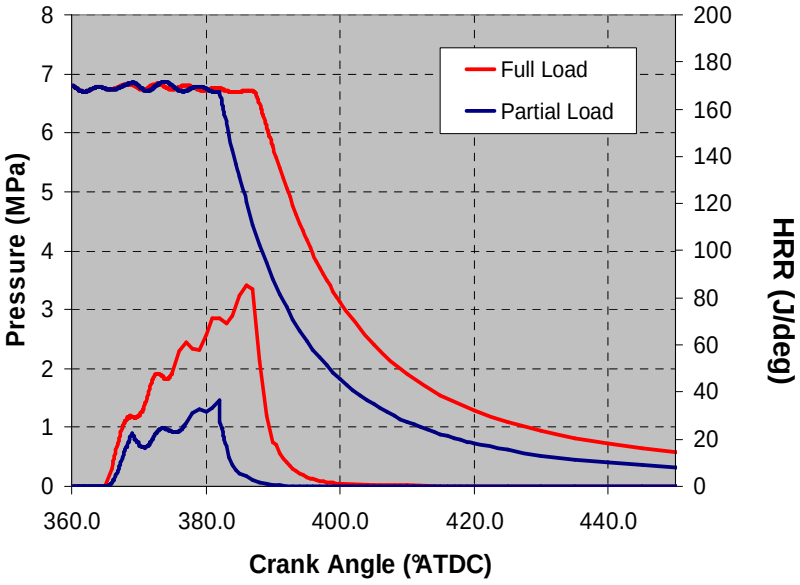

Fig. 2.3. Pressure profile for the different load conditions.

Two different load conditions (full load and 30% of maximum load) were considered. In Fig. 2.3 pressure profile and heat release rate are given for full and partial load conditions. These plots show that combustion occurs with almost constant pressure. The heat is released in a gradual way as

well, as it was expected. The obtaining of almost constant pressure combustion allows using high engine compression ratio and consequent high initial pressure and temperature conditions, satisfying the basic idea of Diesel cycle of obtaining the highest efficiency for a given maximum admissible pressure, as well as noiseless and smooth engine operation.

As in the Diesel ideal cycle, the maximum (constant) pressure part of the thermodynamic cycle, depends on the engine load. In Fig. 2.4 mean temperature distributions are given for full and partial load condition. In Fig. 2.5 NO_X and soot emission results are given. In Figs. 2.6 and 2.7 temperature distributions are reported for the two considered load conditions at two fixed crank angles. It can be observed that local temperatures are fairly low, thanks to homogeneous charge burning in the cylinder.

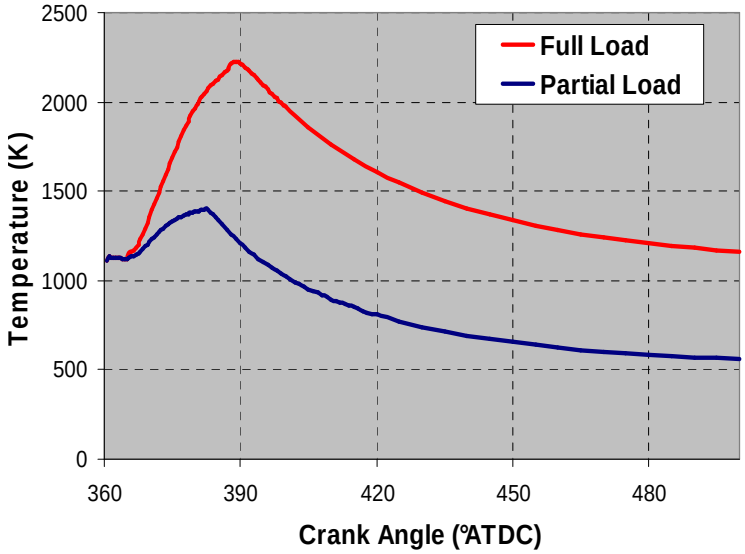

Fig. 2.4. Mean temperature profile.

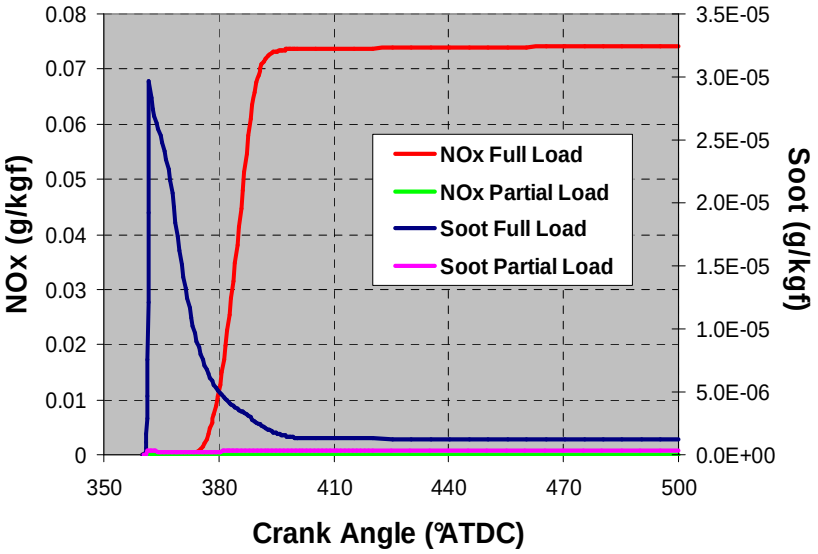

Fig. 2.5. NO_X and soot results for concept validation simulation.

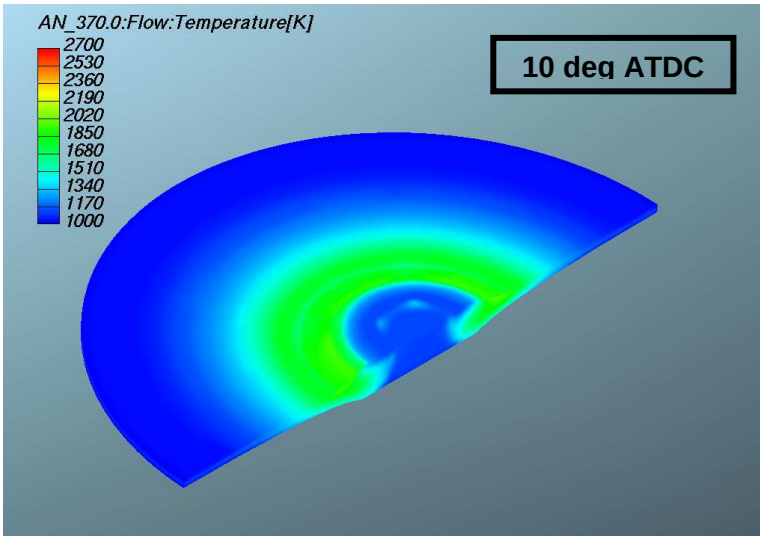

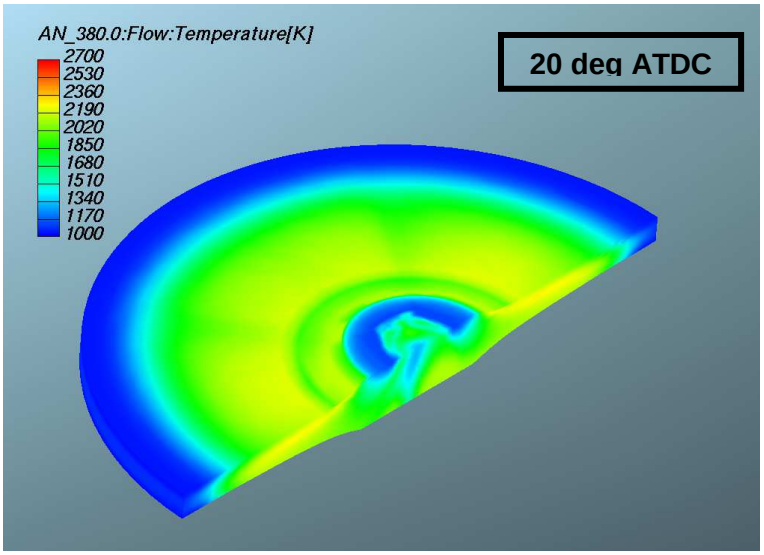

Fig. 2.6. Temperature distribution in full load condition.

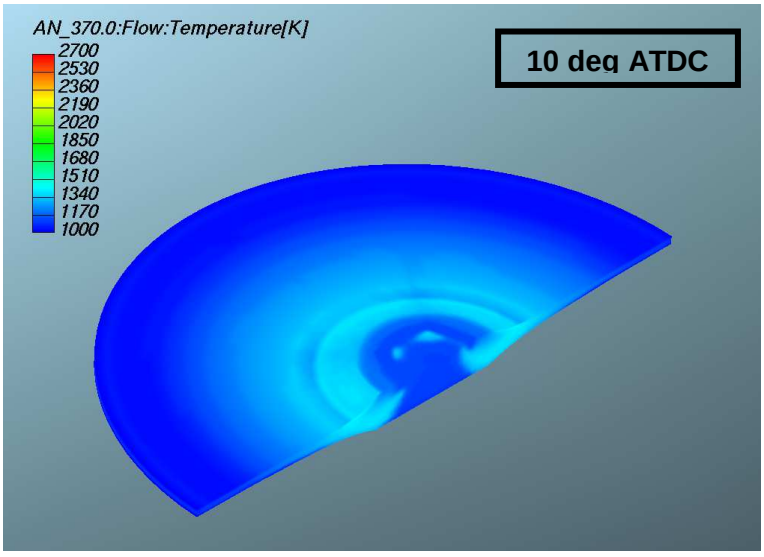

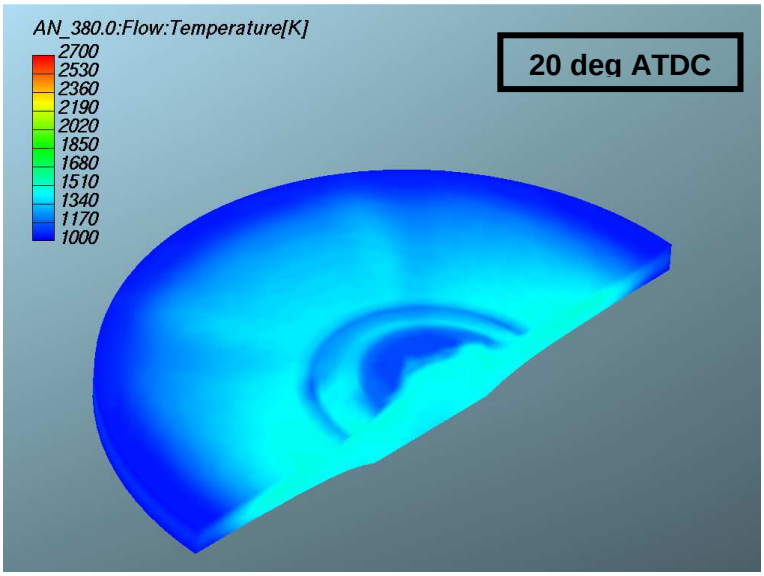

Fig. 2.7. Temperature distribution in partial load condition.

2.3 PROPOSED SOLUTIONS

As previously mentioned, in this preliminary study two different solutions are proposed to achieve the gradual admission of a pre-compressed homogenous charge during combustion in the cylinder. The first one involves the two-stroke cycle, the other the four-stroke one, as the sketches reported on Figs. 2.8 and 2.9 show.

The first solution (Fig. 2.8) is based on the split cycle concept, with intake and compression phases performed outside the cylinder. Compression is realized by an external volumetric compressor which drives the air into a tank, sized to keep pressure nearly constant. The external compressor performs the same compression work, which would be accomplished by a four stroke conventional cylinder, during the compression phase. The compressor displacement, in a first approximation, is the same of the cylinder. The high-temperature compressed air is transferred to the cylinder through an inlet valve during the combustion phase. Contemporary with the air transfer, fuel is injected into the transfer duct, evaporates and mixes with air, bringing about the conditions for homogeneous combustion. Compressor work recovery takes place during the downward piston stroke, due to engine work produced by the transferred air.

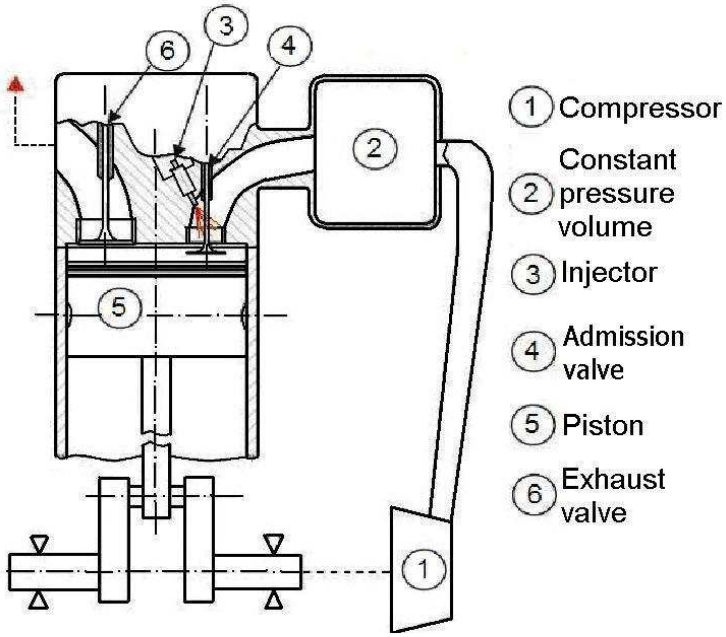

Fig. 2.8. Schematic of the two stroke solution.

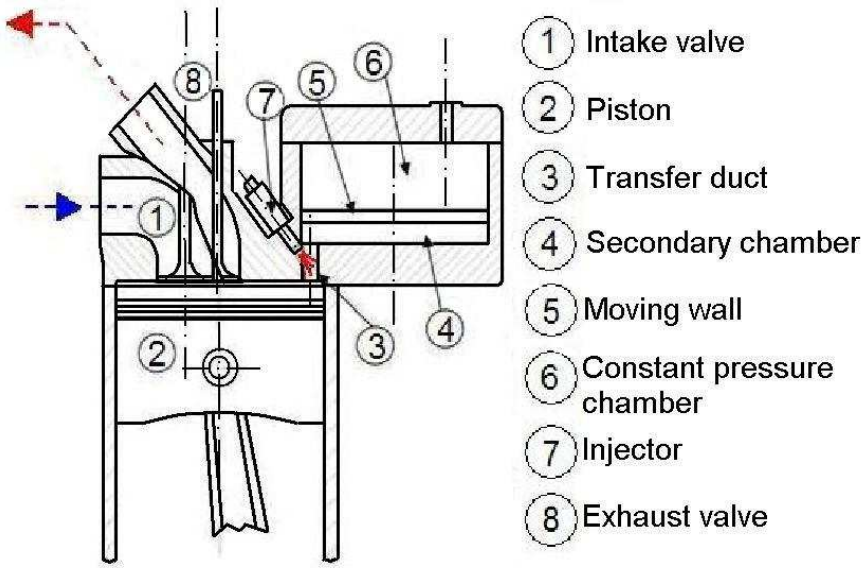

Fig. 2.9. Schematic of the four stroke solution.

In the second solution, based on the four-stroke cycle (Fig. 2.9), the air is directly compressed by the piston during the compression stroke. The maximum pressure is reached before the piston arrives to TDC; then compressed air begins entering a secondary chamber which is in constant communication with the cylinder. The volume of this secondary chamber, theoretically starting from zero, varies keeping the pressure constant during the last part of the compression stroke and the combustion, thanks to a moving wall over which a constant pressure acts (the volume must be large enough to minimize pressure oscillations due to wall movement; a small compressor generates the needed pressure and compensates air leakages). When the piston begins its down-stroke, air is transferred back into the cylinder while fuel is injected, evaporates and mixes with air, bringing about the conditions for homogeneous combustion.
Both solutions allow achieving constant combustion pressure, satisfying the basic idea of Diesel cycle. This allows obtaining the highest efficiency for a given maximum admissible pressure, as well as noiseless and smooth engine operation, because peak pressure is gradually reached during the compression stroke. Mechanical efficiency is also improved due both to the absence of pressure peaks and to the consequent reduction of reciprocating masses.

2.4 PROPOSED SOLUTIONS CFD ANALYSIS

CFD simulations were performed to study both the two-stroke and the four-stroke solutions. Pressure, heat release rate and temperature distribution results are shown. The injection process was taken into account in this part of the study, using the Discrete Droplet Model (DDM) [11] together with the Taylor Analogy Breakup (TAB) model and the Dukowicz evaporation model [12] for the spray behavior prediction. Emissions model as Zeldovich and Kennedy-Hiroyasu-Magnussen [10] were used to predict NO_X and soot production respectively. Ignition and combustion models are the same used in the concept validation part.
Two different load conditions were considered taking injection and mixing processes into account. Differently from the previous case, boundary and initial conditions were calculated using the AVL BOOST release 5.0 [13] one-dimensional code. In Figs. 2.10 and 2.11 the computational grids for the two solutions are shown.
Both grids used in the simulations contained around 40000 cells at TDC. In both the two-stroke and the four-stroke solutions of Figs. 2.8 and 2.9 pressure is supposed to be kept nearly constant in the transfer duct thanks to the constant pressure tank and to the moving wall respectively. Therefore the air transfer is influenced only by the pressure in the

combustion chamber, which allows considering only the combustion chamber and the transfer duct in the computational domain. An inlet surface was placed at the boundary of the duct with a static pressure of 2.8 MPa, as obtained from the one-dimensional simulation.

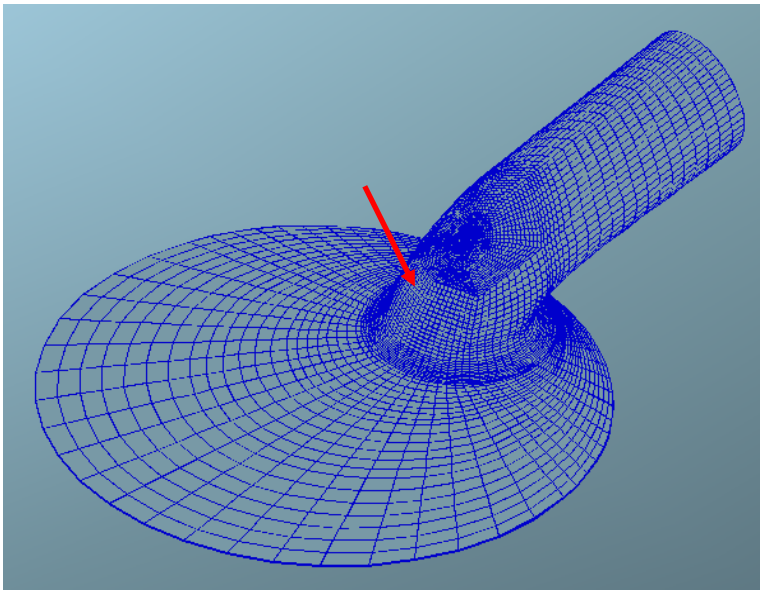

Fig. 2.10. Computational grids of the two-stroke solution

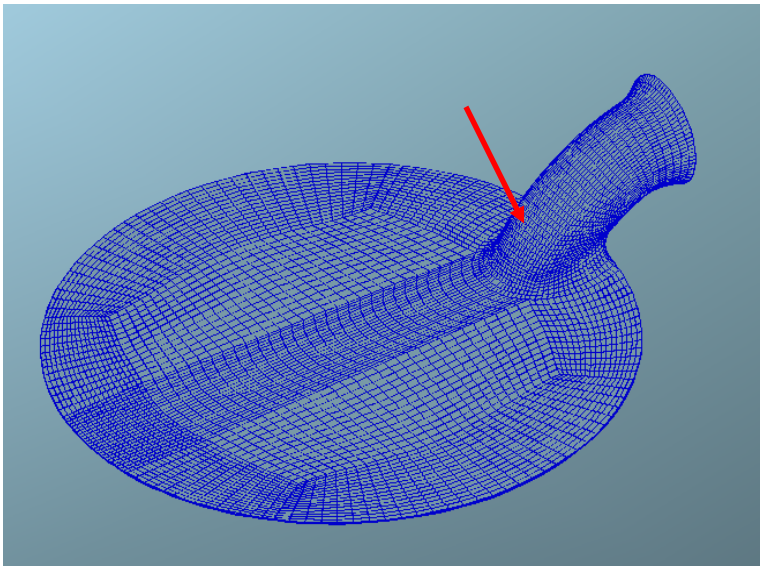

Fig. 2.11. Computational grids of the four-stroke solution

Air transfer and combustion phases only were considered in the simulations, therefore in the four-stroke domain the intake and exhaust valves were not represented. In the two-stroke solution only the transfer valve was considered. The fuel is injected by means of an 8-hole Diesel injector located inside the transfer duct, on its symmetry plane (Figs. 2.10 and 2.11: arrows point out the injection direction). In Fig. 2.12 the fuel injection rate is given. A pre-injection, was performed before TDC to reduce the ignition delay, leading to a smoother heat release. Apart from pressure waves, the air mass enters the cylinder according to the piston velocity. For the main injection rate, a triangular shape was assumed, approximating piston velocity behavior soon after TDC. This approximation is reasonable, since main injection covers only a very short part of the piston stroke. The simulation settings are reported in Table 2.2.

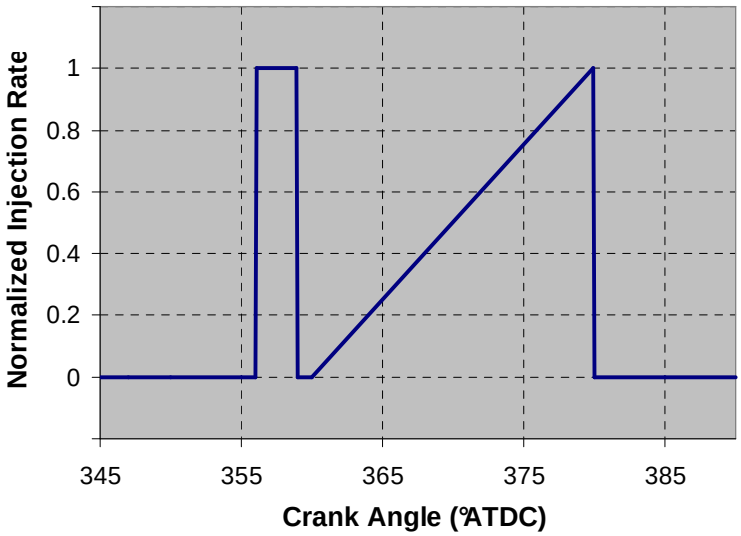

Fig. 2.12. Fuel Injection profile.

In Figs. from 2.13 to 2.16 pressure, heat release rate and mean temperature profiles are given for both the two-stroke and the four-stroke solutions in the different load conditions.
Likewise in the concept validation results, pressure remains almost constant during the combustion phase and heat is released in a gradual way as well. However, bigger pressure oscillations are present at the beginning of air transfer due to pressure losses in the transfer duct, not considered in the concept validation calculations. Comparing the HRR profiles it appears that the Two-Stroke combustion is longer than the Four Stroke one.

Displacement (cm3)	1932
Bore (mm)	135
Stroke (mm)	135
RPM (rev/min)	2400
Inlet P (MPa)	6.8
Injector Type	8 nozzle equally-spaced Multihole injector
Injector pressure (MPa)	150
Included angle (deg)	75
Global equivalence ratio (Full load /1/3 of Max. load)	0.588 / 0.196
Full Load Main Injection duration (DOI) (ca)	20
Main Injection timing (SOI) (ca)	360

Tab. 2.2. Simulation settings for the proposed solutions

This is probably due to the fact that, the injection profile was the same adopted in the Four Stroke case which does not match with the real air flow in the cylinder during the transfer phase.
Temperature distributions for the two solutions in partial load condition are reported in Figs. 2.17 and 2.18 at two different crank angles. These figures show that low combustion temperatures are kept everywhere in the chamber. However, compared with the concept validation results, temperatures are much less homogeneous, proving that injection and mixing processes were not yet optimized.
Even though the presented early results encouraged to proceed the studies on both solutions, the four stroke solution was abandoned in an early stage mainly because of constructive problems (moving wall design and realization) and only the split-cycle solution was considered in the following of the research.

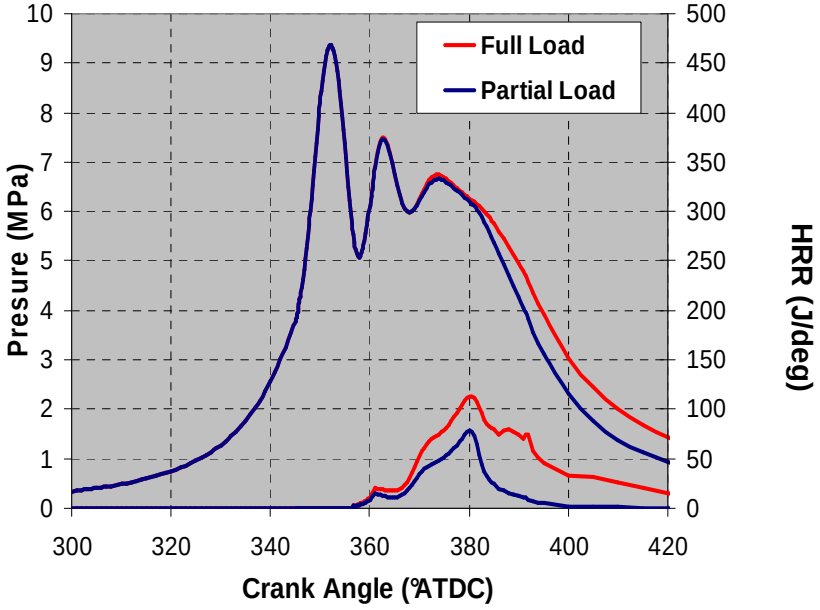

Fig. 2.13. Pressure and HRR for the two stroke solution.

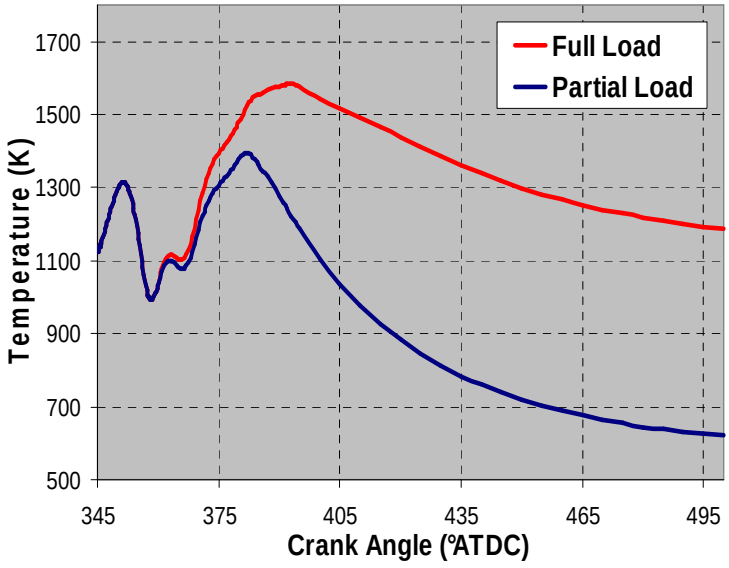

Fig. 2.14. Mean temperature profile for the two stroke solution.

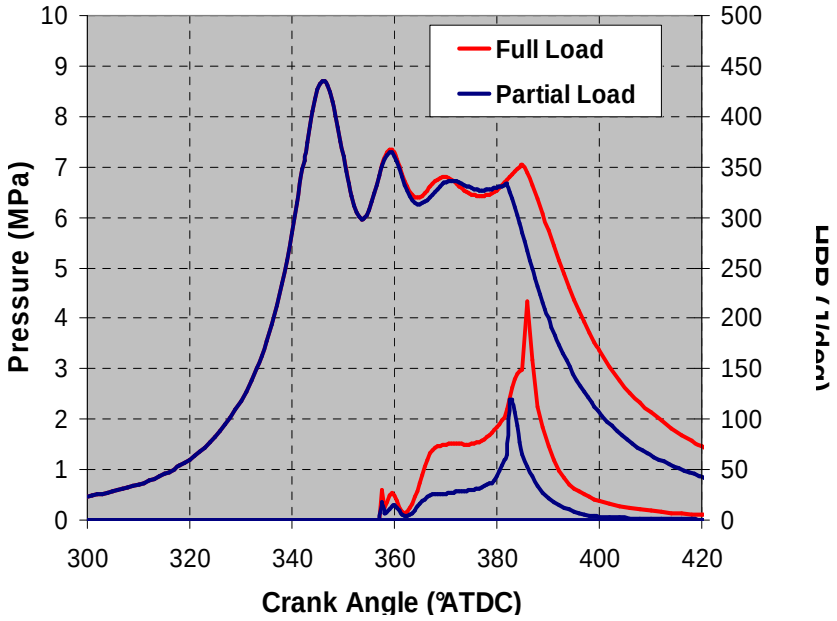

Fig. 2.15. Pressure and HRR for the four stroke solution.

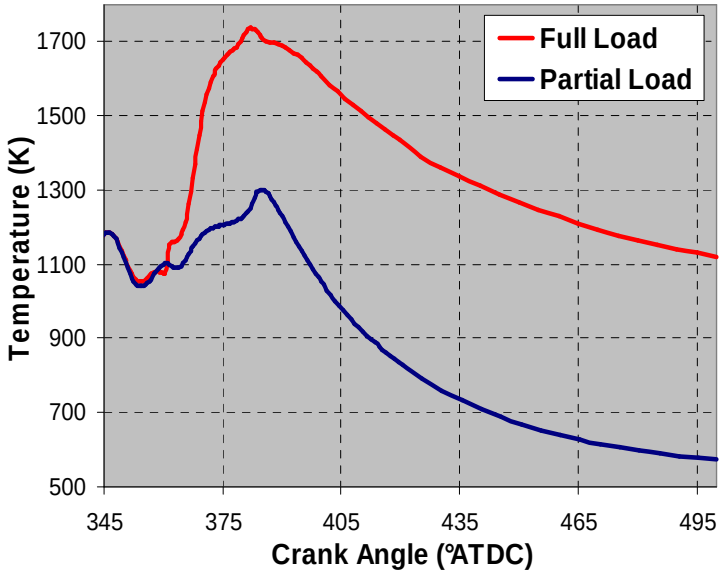

Fig. 2.16. Mean temperature profile for the four stroke solution.

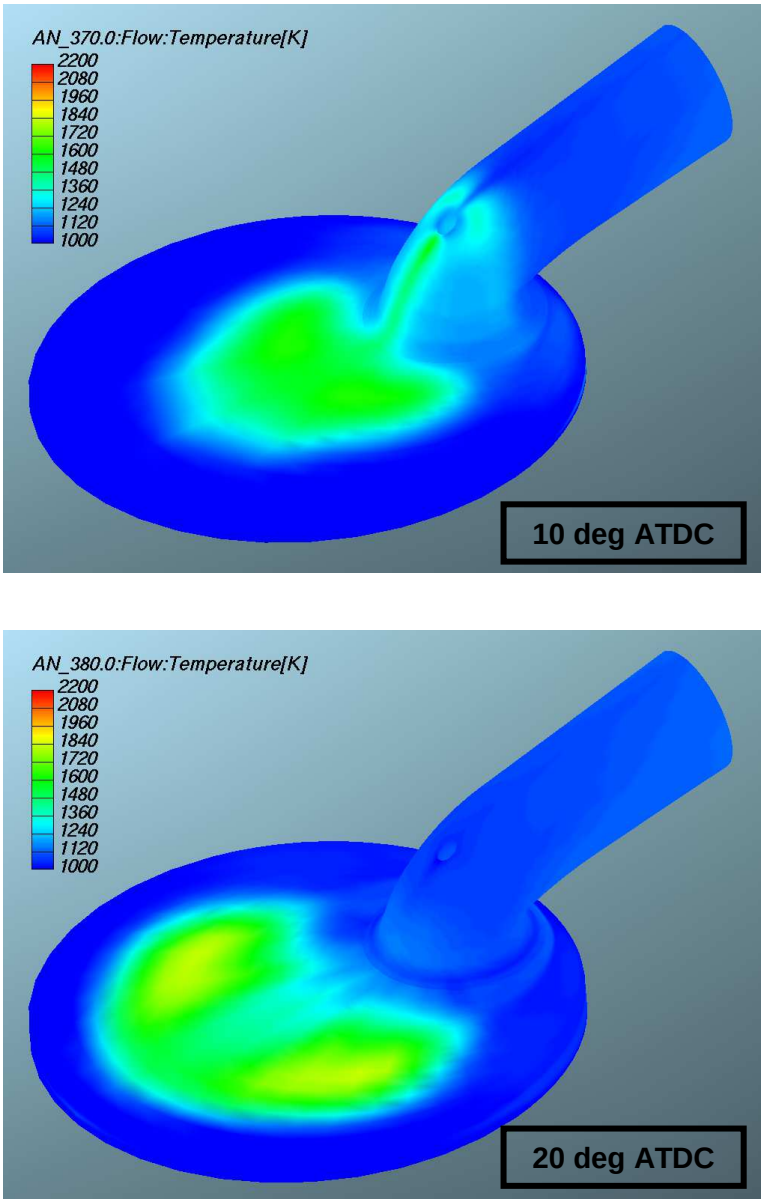

Fig. 2.17. Temperature distribution for the two-stroke solution in partial load condition .

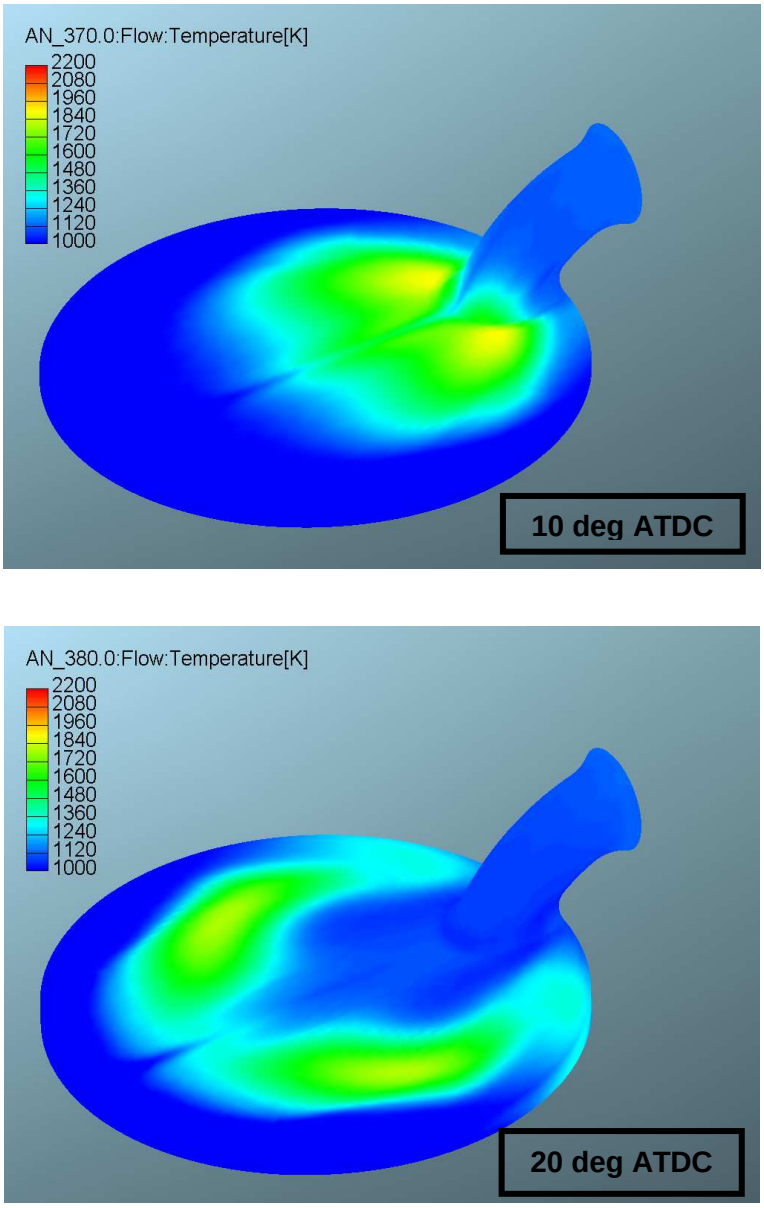

Fig. 2.18. Temperature distribution for the four-stroke solution in partial load condition.

The studies on the split cycle solution were continued [14] with a new computational grid, reported in Figs 2.19 and 2.20 For a better understanding of this new combustion concept the geometries of the intake duct, intake valve, and the combustion chamber were represented in the simplest possible way. For the same reasons a single-hole fuel injector was adopted. As in the previous part of the work, tank and compressor geometries were not considered in the computational domain, due to the assumption of constant pressure in the tank.

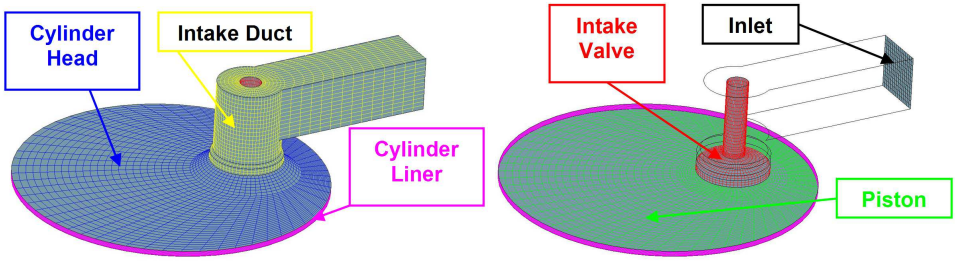

Fig. 2.19 Fluid domain at TDC

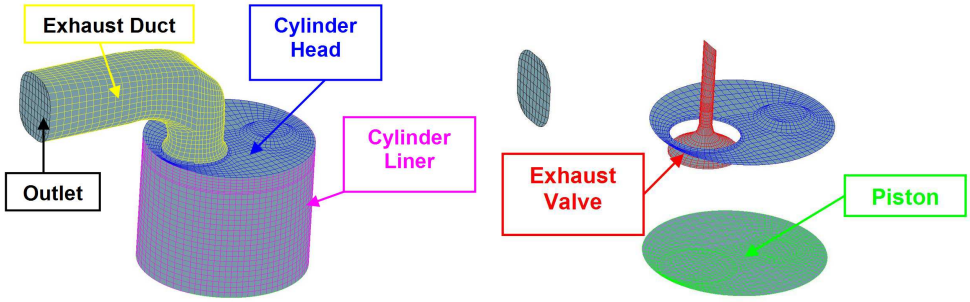

Fig. 2.20 Fluid domain during the exhaust stroke

Displacement	441 cm^3
Bore	86 mm
Stroke	76 mm
Compression ratio	50:1
IVO (CAM 40, CAM 46)	-21°, -23° ATDC
IVO Effective	-5° ATDC
IVC (CAM 40, CAM 46)	51°, 57° ATDC
IVC Effective (CAM 40, CAM 46)	35°, 41° ATDC
EVO	175° ATDC
EVC	-74° ATDC

Tab. 2.3 Specifications of the HCPC combustor

The combustor specifications are summarized in Tab. 2.3. The geometry and the computational grid were generated using the ICEM-CFD software. The grid used in the simulations contained about 40,000 cells at TDC.
An inlet surface was positioned at the boundary of the duct with a static pressure of 7 MPa and a temperature of 1020 K (see Tab. 2.4). Pressure and temperature were determined with zero-dimensional calculation for the boundary inlet condition and with the one-dimensional code AVL BOOST for the initial conditions

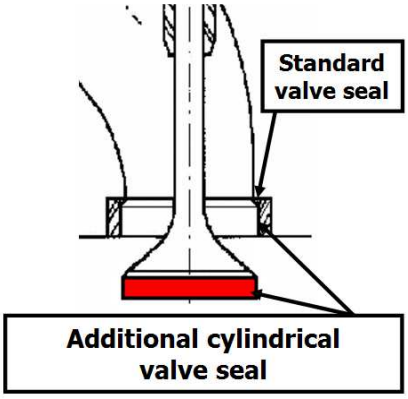

Fig. 2.21 Additional cylindrical seal in the transfer valve

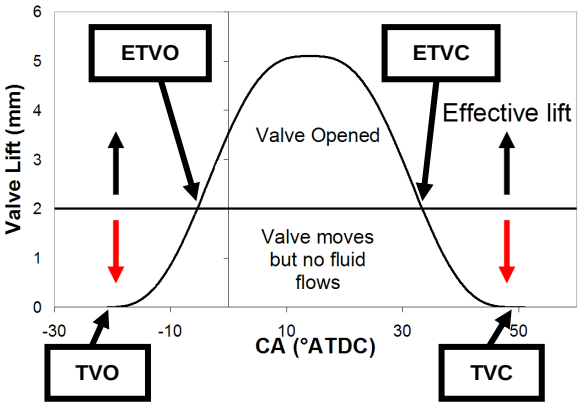

Fig.2.22 Transfer valve lifts

The transfer valve opens and closes in a narrow angular phasing (around 40 CAD). In order to allow wider cam phasing, and therefore feasible valve accelerations, the transfer valve is characterized by an additional cylindrical seal (Figs. 2.21, 2.22). The valve starts moving at TVO and closes at TVC but its effective opening (ETVO) and closing (ETVC) occur when the transfer valve clears and closes the cylindrical seal.
The calculations started at ETVO, when the valve clears its cylindrical seal, and consider the complete cycle of the combustor, namely: intake-combustion, expansion, exhaust, and recompression phases.

Engine Cycle	Two-Stroke
Engine speed	2000 rpm
Inlet T, P	1020 K, 7 MPa
Intake Initial T, P	1020 K, 7 MPa
Combustion Chamber Initial P and T	T: 1630 - 1750 K P: 4.8 - 5.5 MPa
Simulation Start	-5°ATDC
Simulation End	355°ATDC

Tab. 2.4 Boundary condition of the fluid domain considered

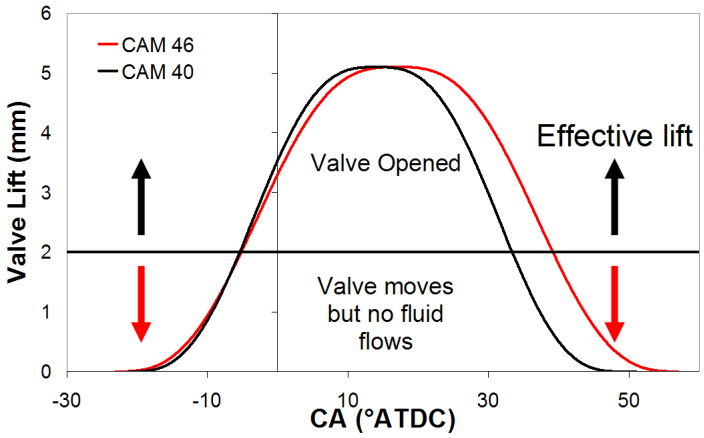

Fig. 2.23. Transfer valve lift curves .

24 cases were considered for the CFD simulations that represent all the combinations of the two valve lift curves considered (CAM 40, 46) (Fig. 2.23), two injection rate profiles (SQUARE, LINEAR) (Fig. 2.24) and six A/F (ALFA 17-45) (Fig. 2.25) for each case. The designation of each case is CAM 40/46, SQUARE/LINEAR INJECTION, ALFA 17–45.

The simulations were performed using AVL FIRE release 8.52. The turbulence model based on the RANS (Reynolds Average Navier Stokes) method is the two-equation K-ζ-f model, which takes into account the effects of turbulence in the mean flow. For the injection process, the Discrete Droplet Model (DDM) was used together with the KH-RT model [15] and the Dukowicz evaporation model. The spray nozzle is located in the intake duct in a vertical orientation, as shown in Fig. 2.26. The spray boundary conditions used in the simulations are summarized in Table 2.5.

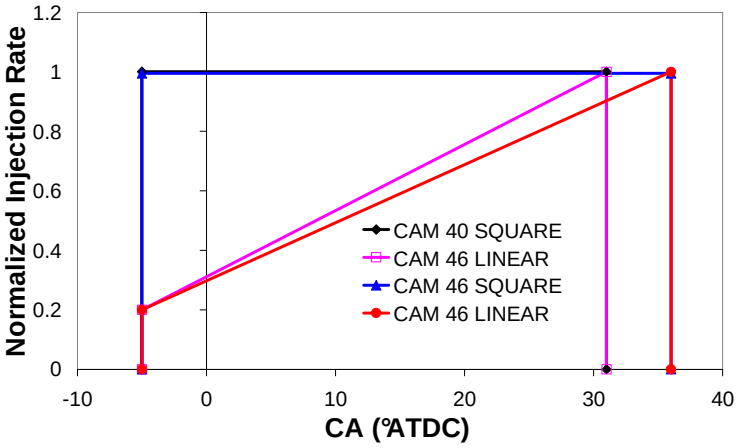

Fig. 2.24 Normalized Injection Rate

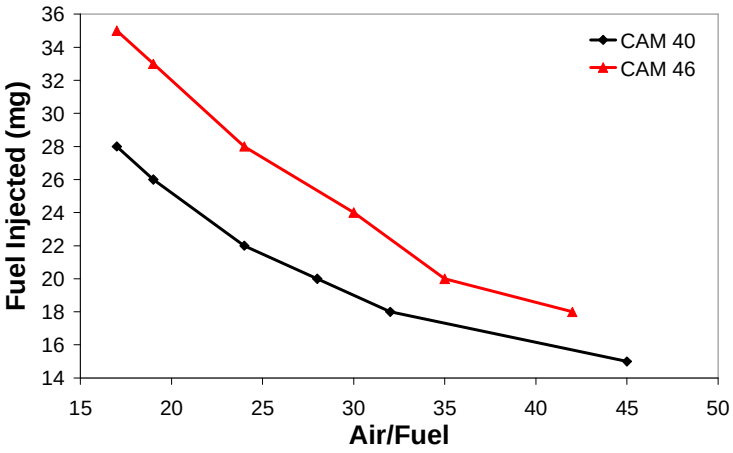

Fig. 2.25 Fuel mass injected

Injection Type	Intake Duct Injection
Fuel	C14H30
Fuel Temperature	363 K
SOI (°ATDC)	-5
Injector	Single-Hole
DOI (CAM 40, CAM 46)	35°CA, 41°CA
Fuel Injected	15-35 mg (see Fig. 15)
Nozzle Diameter	256 µm
Cone Angle	22°
Injection profile	Square, Linear (see Fig.14)

Tab. 2.5 Spray Boundary conditions

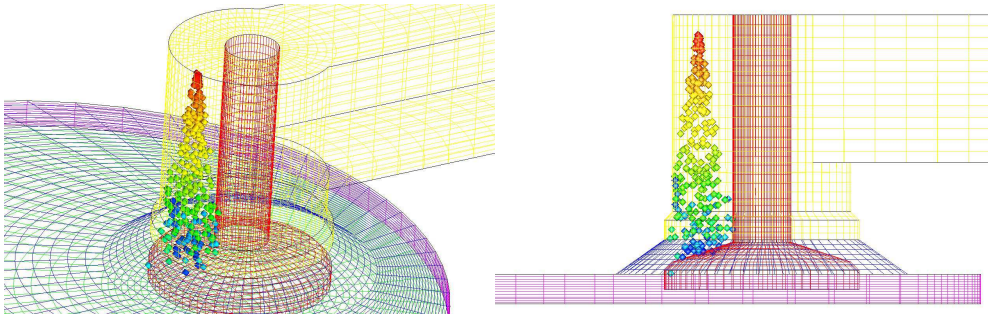

Fig. 2.26 Spray position in the intake duct

2.5 COMBUSTION MODEL

Being HCPC combustion process different both from HCCI/LTC and conventional Diesel, a simulation activity on a test case was performed, to choose the proper combustion model. Three different models were tested on the same case, namely: the Characteristic Timescale Model [16], ECFM-3Z and coupling the chemical kinetics solver Chemkin with the FIRE code. The ERC n-heptane mechanism [17] with 34 species and 74 reactions was used. This mechanism has been widely employed for Diesel combustion calculations because of its similar ignition characteristics of n-heptane to those of conventional Diesel fuel [18].
The simulation results were considered to be very encouraging, being the predicted pressure traces were very similar for the three cases (Fig. 2.27). In particular, the ECFM-3Z and the Chemkin pressure traces are pretty much the same.

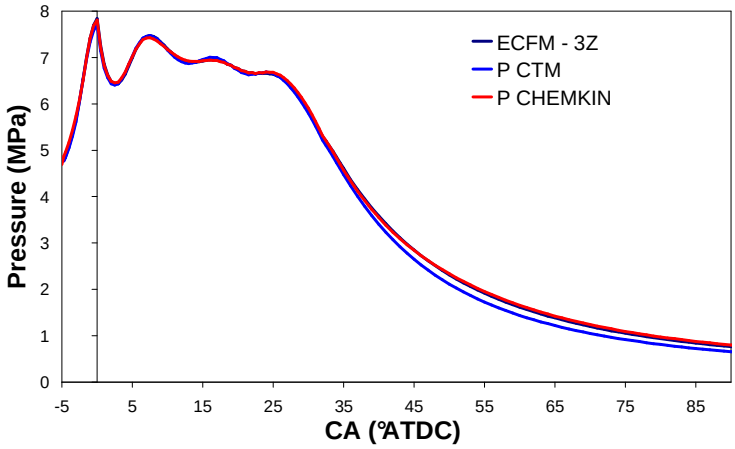

Fig. 2.27 In-cylinder pressure with different combustion models (case ALFA 28 LINEAR INJ)

As far as emissions are concerned, (Tab. 2.6) the very simplified CTM model is unfit to predict NO_X emissions, and needs a complementary NO_X model to do so [19]. Moreover it predicts and a very high CO value, but HC emissions are of the same order of magnitude as in the other models. The Chemkin and ECFM-3Z models are in the closest agreement, apart from NO_X emissions that seem to be underestimated with ECFM-3Z.
Chemkin results were trusted to be more accurate and more reliable. For those reasons the reduced chemical kinetic mechanism was chosen for this part of the HCPC simulation activity, even though the calculation time was almost an order of magnitude longer than that of the other models.

	CHEMKIN	ECFM-3Z	CTM
HC [g/kg-f]	22.7	28.8	34.2
NO_X [g/kg-f]	31.0	7.8	0.0
CO [g/kg-f]	34.8	38.8	485.3

Tab. 2.6 Emissions results with different combustion models

2.6 RESULTS AND DISCUSSION

2.6.1 PERFORMANCE RESULTS

HCPC engine performance was calculated using CFD results for the combustor and by modeling the external compressor considering an adiabatic compression with 90% polytrophic indicated efficiency. The indicated data were derived from the indicated work calculated with:

$$Indicated\_Work = W_{combustor} - W_{compressor}$$

where:

$$W_{combustor} = \oint p_{Fire} dV = \sum_{n=0}^{n} 0.5 \cdot \left[\left(p_n + p_{n-1} \right) \cdot \left(V_n - V_{n-1} \right) \right]$$

$$W_{compressor} = \frac{M_{Fire}}{\eta_{icompresso\ r}} \cdot \frac{nRT_1}{n-1} \left[1 - \left(\frac{P_2}{P_1} \right)^{\frac{n-1}{n}} \right]$$

M_{Fire} : Air mass delivered (calculated with FIRE)

$\eta_{icompresso\ r} = 0.9$: Compressor Polytrophic Indicated efficiency

$T_1 = 303K$: Compressor intake temperature

$n = 1.4$: Polytrophic exponent

$P_2 = 7MPa$: Outlet compressor pressure, Tank Pressure

$P_1 = 0.1MPa$: Inlet compressor pressure

$R = 286.9[J/kgK]$: Specific gas constant for dry air

Figures 2.28, 2.29 and 2.30 show indicated power and efficiency results obtained with the simulation activity. Indicated power decreases increasing A/F ratio, due to the less fuel mass injected. With a wider cam phase angle air mass delivered increases, thus compressor work increases as well. However part of the compressor work is recovered, due to engine work produced by the transferred air in the combustor during the expansion

stroke of the piston. The net effect is an increase of power with a wider cam phase.
Indicated efficiency varies with A/F ratio and reaches a maximum for A/F ratio around 30 for all cases with CAM 40 and at around 35 for the cases with CAM 46. The best results were obtained using the linear injection ramp rate, especially with higher A/F ratios.

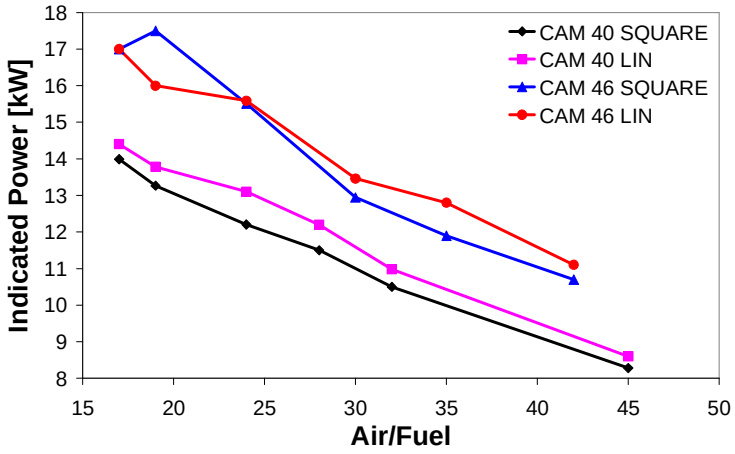

Fig. 2.28 Predicted Indicated Power

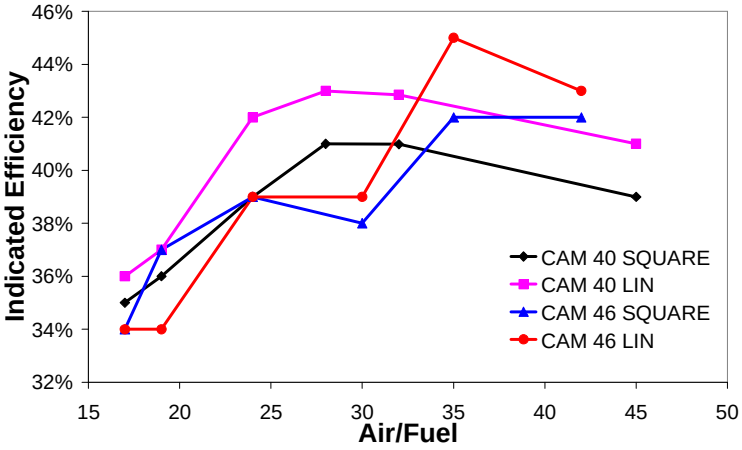

Fig. 2.29 Predicted Indicated Efficiency

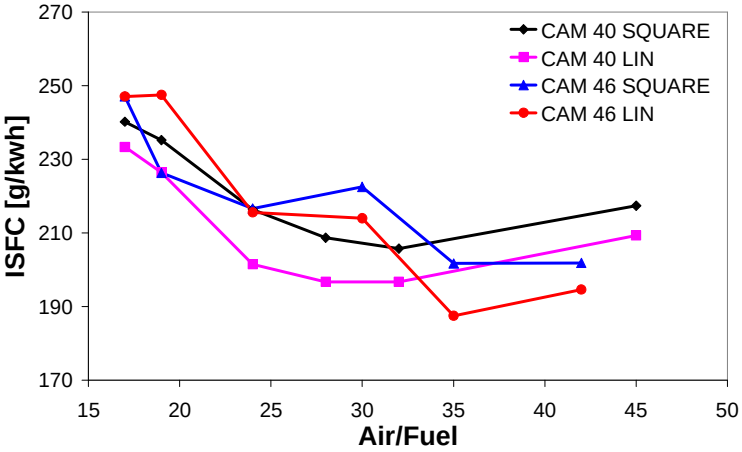

Fig.2. 30 Predicted ISFC

2.6.2 PRESSURE AND HEAT RELEASE RESULTS

Figures 2.31 to 2.33 show cylinder pressure and HRR comparisons for the different cases studied. For all cases the pressure remains almost constant during combustion, proving that the basic idea of the HCPC concept is accomplished. No large pressure gradients are present and the maximum peak pressure rise rate for the worst case is 0.25 MPa per degree, which benefits mechanical efficiency and engine noise compared to other types of HCCI/LTC combustion, and even with standard Diesel combustion.
As mentioned in the previous paragraph the linearly increasing injection rate profile gave better results than the square one in most of the cases.
Figure 2.31 shows Pressure and HRR with different A/F ratios for the case CAM 40 SQUARE INJ. The pressure curves of the case A/F 24 is very close to the case A/F 17 despite the fact that the fuel amount is 25% less with benefits in the efficiency, as shown in Figure 2.29.
From Fig. 2.32 it can be seen that the pressure oscillations have lower amplitude and the heat release rates have a smaller peak around 5°ATDC because less fuel is added in the first part of the combustion. After this peak the HRR and the pressure start to decrease. This happens because there is some back flow and combustion starts to propagate also into the intake port. The air mass flow rate is, in fact, proportional to the piston velocity and inversely proportional to the heat released in the chamber. Therefore, with the linear injection profile there is less back flow combustion, as seen in Fig. 2.34, with consequent advantages in the thermal efficiency, as seen in Fig. 2.29.

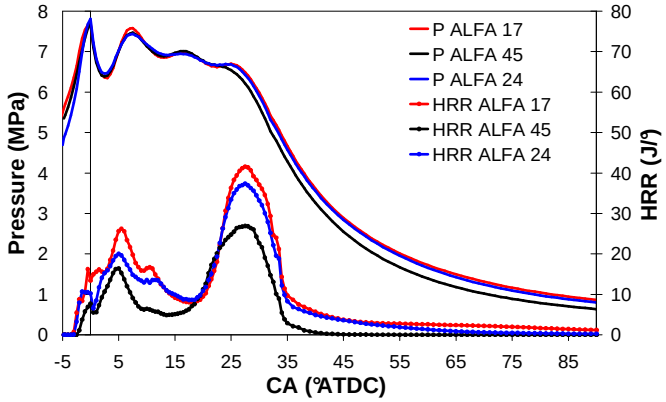

Fig. 2.31 Pressure and HRR with different A/F ratios (case: CAM 40 SQUARE INJ)

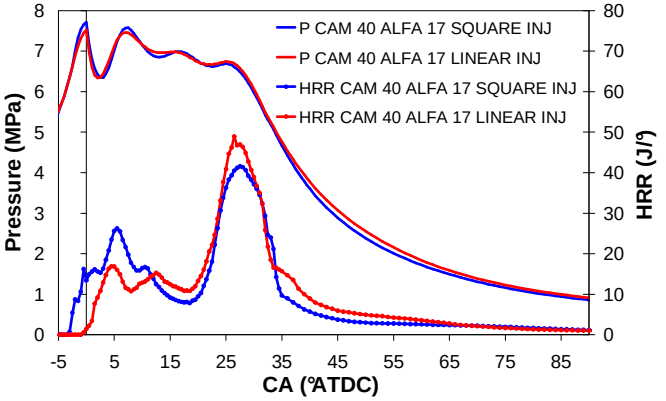

Fig. 2.32 Pressure and HRR comparison between square and linear injection profiles

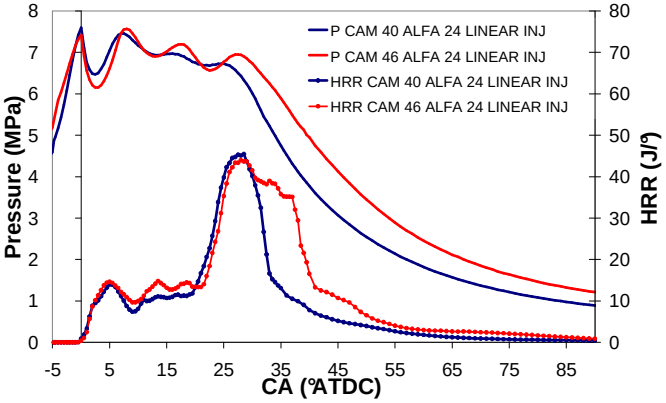

Fig. 2.33 Pressure and HRR with the two intake valve lifts considered (case: ALFA 24 LINEAR INJ)

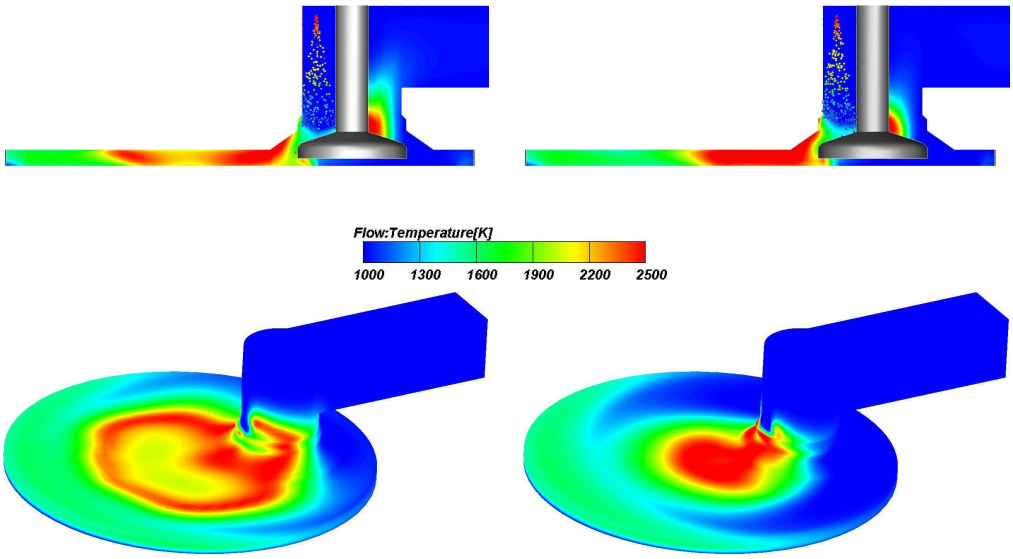

Square Injection Linear Injection

Fig. 2.34 Temperature in a cross-section plane through the valve axis and in the combustion chaber for the two injection profiles considered at 12ºATDC (case: CAM 40 ALFA 24)

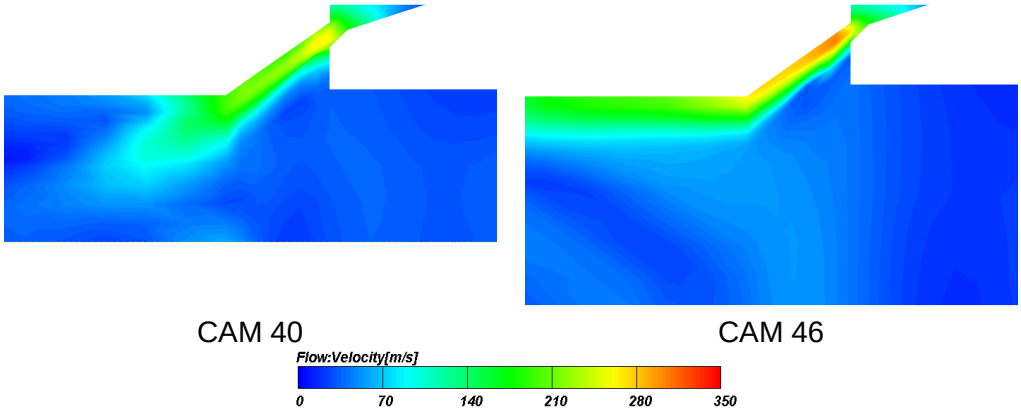

Fig. 2.35 Velocity magnitude at 3° BTVC with the two valve lifts considered (case: ALFA 24 LINEAR INJ)

With the wider transfer valve lift profile pressure remains constant for a longer time (Fig. 2.33) and producing more power. However, efficiency is lower in this case compared with the case with CAM 40 because closing the valve with a higher piston velocity leads to higher flow velocities, as shown in Fig. 2.35, and therefore larger pressure losses.

2.6.3 EMISSIONS RESULTS

In Figs. 2.36 to 2.38 pollutant emissions results in terms of HC, NO_X and CO are reported for all cases considered in the analysis. soot emissions calculated with FIRE-Chemkin were not available because the soot reactions have not yet been implemented in the Chemkin mechanism with FIRE. Therefore, for the soot prediction two approaches were used: in the first one the ECFM-3Z model was used combined with the Kennedy-Hiroyasu-Magnussen model [15]; in the second one qualitative soot emissions analysis was discussed by means of a Φ-T analysis (see next paragraph).
HC emissions were lower with respect to those produced by HCCI/LTC combustion. Moreover, they can be reduced by using a different injection strategy and with a better design of the transfer duct/valve seat, because most of them come from the wall-film on the transfer valve surfaces.
NO_X emissions still needed to be reduced, due to the high combustion temperature reached during combustion. In all the cases NO_X emissions increased increasing oxygen partial pressure, proportional to the A/F ratio.
As regards CO emissions, they increased decreasing A/F ratio. With an A/F ratio of 17 they were one order of magnitude higher than in the cases with A/F ratio greater than 24, indicating that the fuel oxidation was not completely accomplished.
soot emissions predicted with the ECFM-3Z combined with the Kennedy-Hiroyasu-Magnussen model are shown in Fig. 2.39. No noticeable difference was noticed between the two injection profiles. Using A/F ratios lower than 24 soot emissions spiked to be very high values. With A/F = 28 the soot was around 2 g/kg-f and with higher A/F the soot emissions were on the same order of magnitude as the PCCI cases of Opat et al. [17].

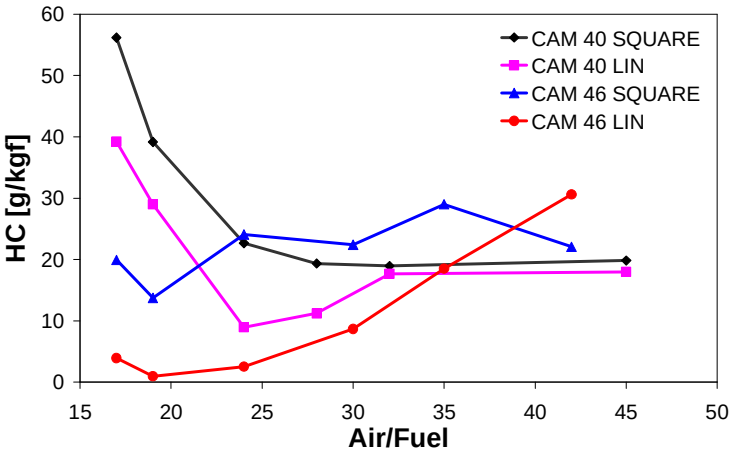

Fig. 2.36 HC emissions for all cases considered

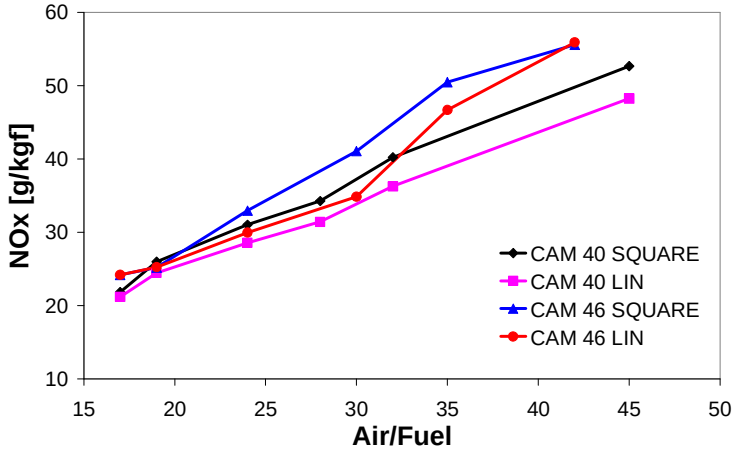

Fig. 2.37 NO_X emissions for all cases considered

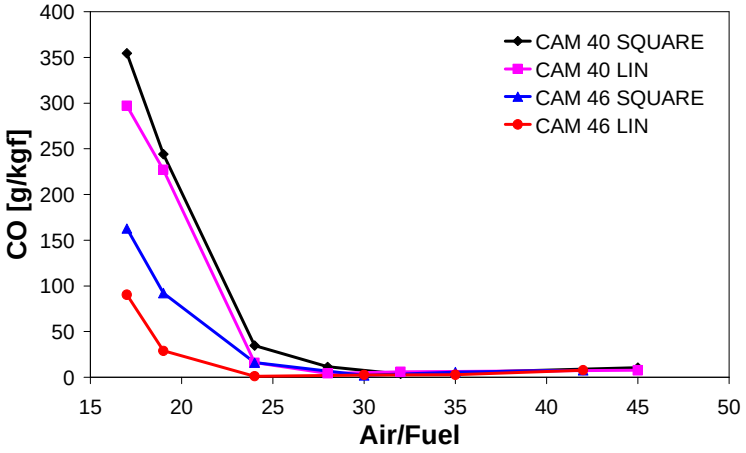

Fig. 2.38 CO emissions for all cases considered

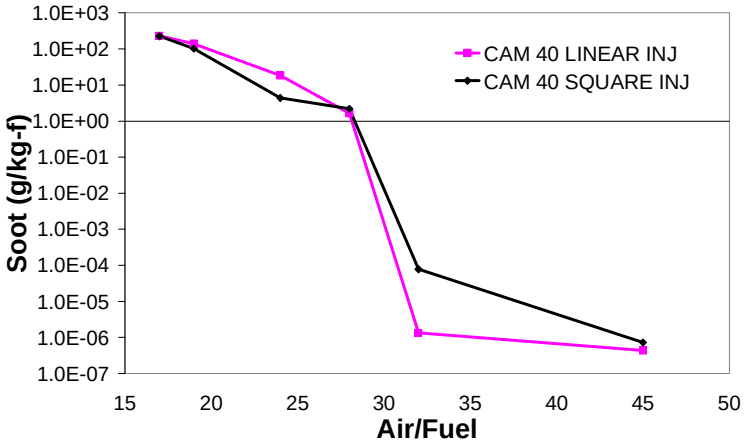

Fig. 2.39 soot emissions for the CAM 40 cases

2.6.4 Φ-T ANALYSIS

Additional analysis was also conducted by plotting the in-cylinder conditions predicted by the 3D-CFD code on the equivalence ratio (Φ) – temperature (T) map, previously described in Chapter 1. The equivalence ratio was defined as [20,21],

$$\Phi = \frac{2 \cdot \sum_{i=1}^{n} C_i^{\#} + \frac{1}{2} \cdot \sum_{i=1}^{n} H_i^{\#}}{\sum_{i=1}^{n} O_i^{\#}}$$

Where $C_i^{\#}$, $H_i^{\#}$, $O_i^{\#}$ are the numbers of atoms of the ith species and n is the total number of species in the calculation domain.
Two cases were chosen for the analysis depending on NO_X emissions. The first one (CAM 40 SQUARE INJECTION ALFA 17) had the lowest NO_X emissions, while the second one (CAM 40 SQUARE ALFA 45) had the highest NO_X emissions.
Figures 2.40 and 2.41 show that Φ-T maps look significantly different from both conventional Diesel and PCCI combustion maps. In Diesel and PCCI combustion the Φ-T points are located mainly around the adiabatic flame temperature curve [20]. In this early stage of HCPC research the Φ-T values were more spread in the Φ-T plane, especially in the final part of combustion (30° ATDC).

In both cases considered in the analysis the NO region was reached due to very high local combustion temperatures (around 2700 K). In the first case produced NO_X was 22 g/kgf compared to 53 g/kgf in the second case due to higher local equivalence ratios. As regards soot emissions in both cases the results were below the conventional Diesel combustion line, and in the case with A/F 45 the soot region was touched only between 10° and 20°ATDC.

Figs. 2.42 to 2.45 show temperature and equivalence ratio maps in the combustion chamber. The differences in the equivalence ratio between the two cases produce differences in the combustion propagation. In the case with an A/F ratio of 17, diffusion flame combustion can be noticed at the periphery of rich regions in the chamber. In the case with an A/F ratio of 45, diffusion flame propagation was still observed, even though combustion took place mainly where the equivalence ratio is higher, generating a volumetric heat release characteristic. The results achieved during this stage of the research activity, encouraged carrying on with new studies, including in the computational domain the compressor cylinder. In the following stages of the research activity different engine sizings were analyzed both for Light Duty and Heavy Duty applications.

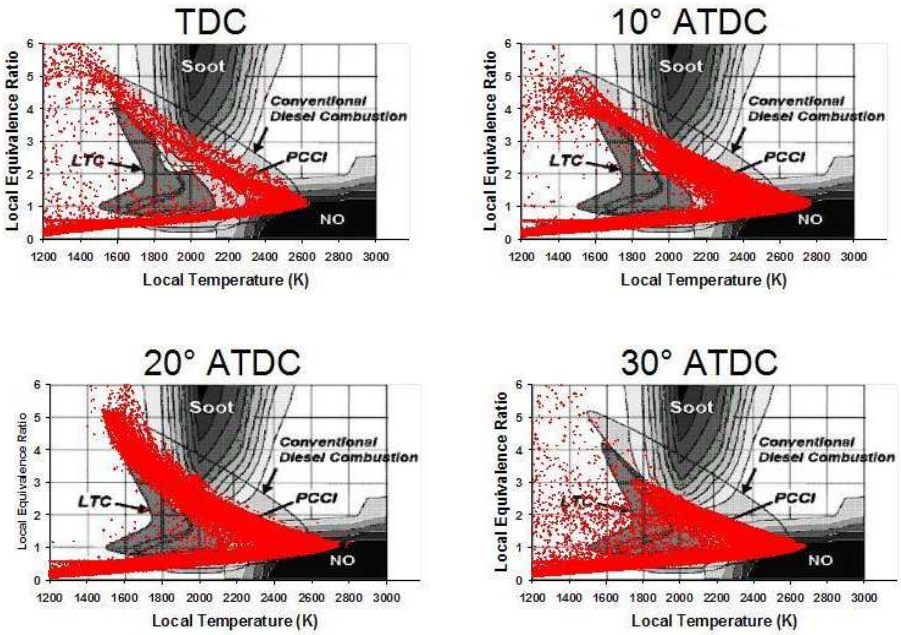

Fig. 2.40 Φ-T maps of the case CAM 40 SQUARE INJECTION ALFA 17

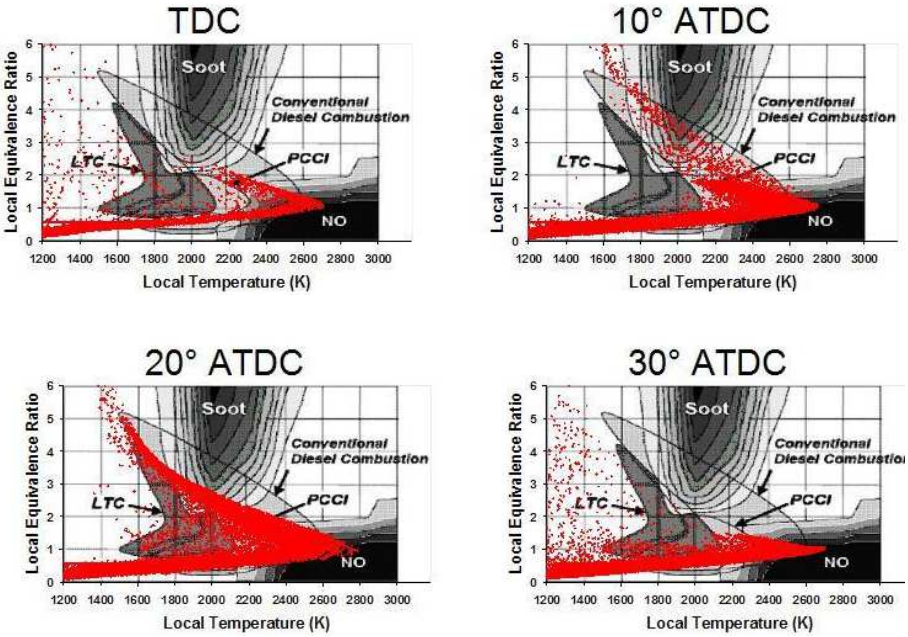

Fig. 2.41 Φ-T maps of the case CAM 40 SQUARE INJECTION ALFA 45

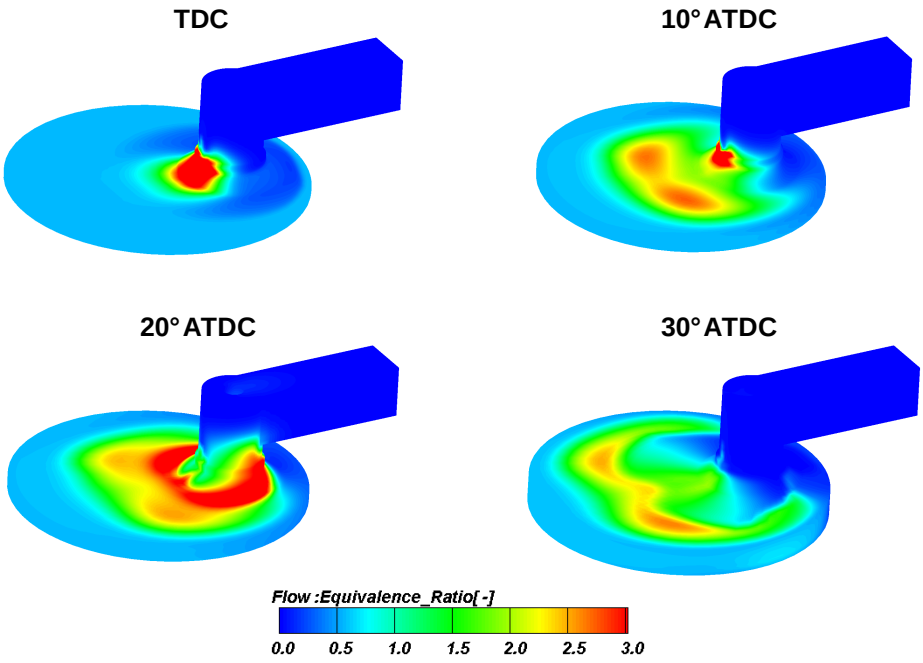

Fig. 2.42 Equivalence ratio in the combustion chamber for the case CAM 40 SQUARE INJECTION ALFA 17

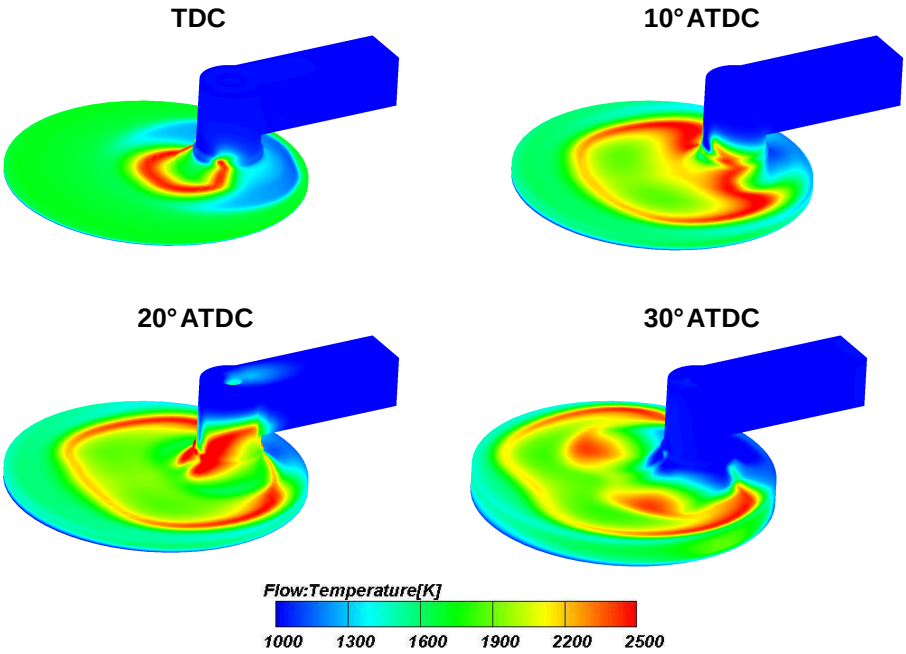

Fig. 2.43 Temperature in the combustion chamber for the case CAM 40 SQUARE INJECTION ALFA 17

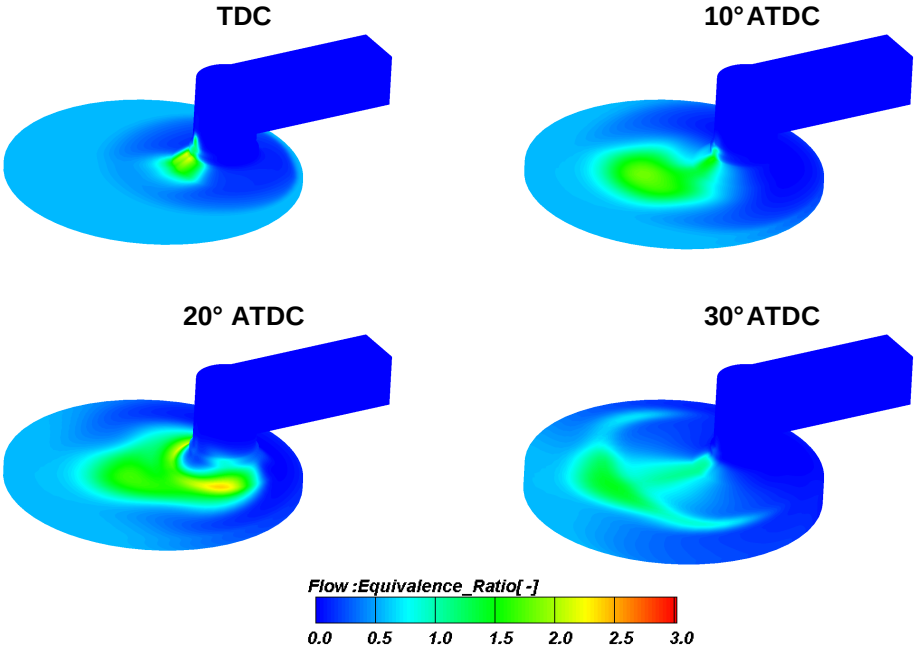

Fig. 2.44 Equivalence ratio in the combustion chamber for the case CAM 40 SQUARE INJECTION ALFA 45

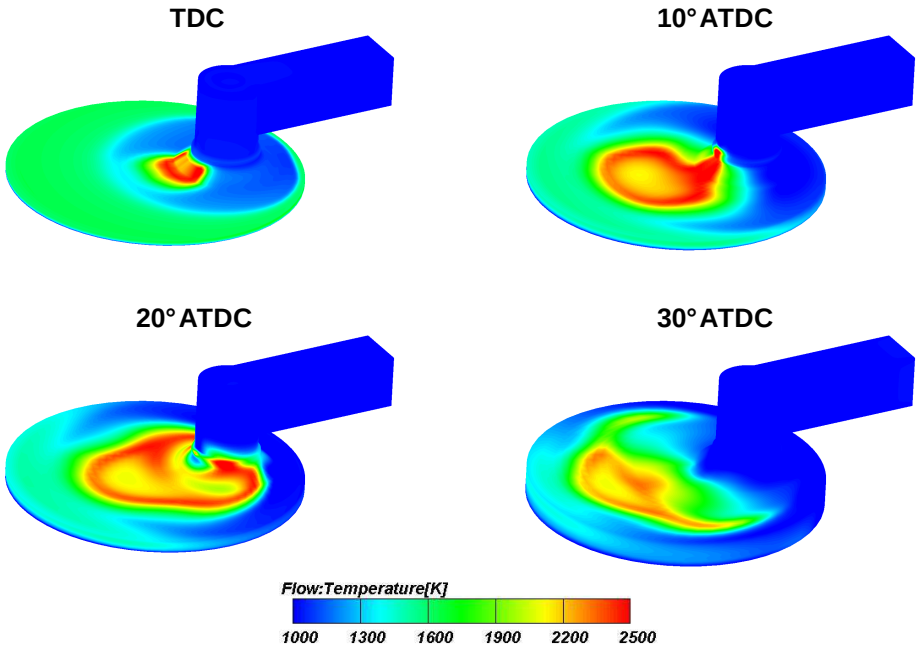

Fig. 2.45 Temperature in the combustion chamber for the case CAM 40 SQUARE INJECTION ALFA 45

Chapter 3

LIGHT DUTY HCPC ENGINE

3.1 A NEW SPLIT-CYCLE ARCHITECTURE

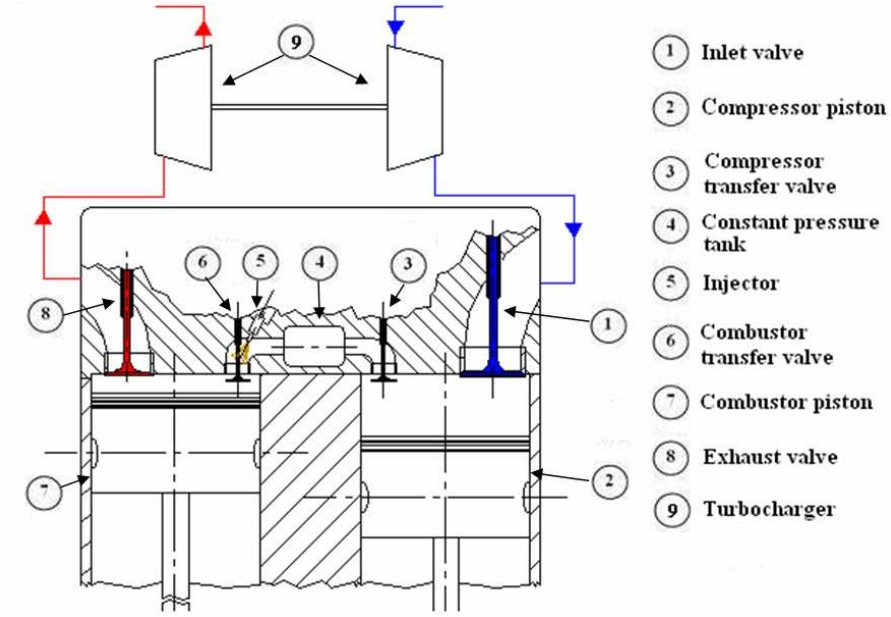

Fig. 3.1 First scheme of the Split-Cycle solution

The first HCPC engine scheme based on the split cycle concept, is shown in Fig. 3.1.
In the original concept the high-temperature compressed air is transferred to combustor cylinder during the engine combustion phase, from a properly sized tank. The pressure in the tank must remain almost constant during the cycle, thus two transfer valves are needed, to isolate it from the two cylinders during the low pressure engine phases. Both transfer valves have to open and close in a small angular phasing (around 40 CAD).
Constant pressure combustion allowed realizing a thermodynamic cycle which was close to the Diesel Cycle, therefore highest efficiency for a given maximum admissible pressure could be achieved, as stated in the previous chapter. Unfortunately, the first simulations realized considering the whole

model (compressor cylinder, constant-pressure tank, combustor cylinder), worsened the results achieved during the preliminary analysis. This result was due to the constant pressure condition, which led to considerable pressure losses during the air transfer phase, especially during the opening and closing phases of transfer valves. In Fig. 3.2 the pressure difference at the effective opening and closing phases of the combustor-side transfer valve are shown. In particular, the pressure drop during the closing phase was very high (15 bar), due to the high mass flow rate induced by the high piston velocity, with a strong negative impact on engine thermal efficiency [22, 23].

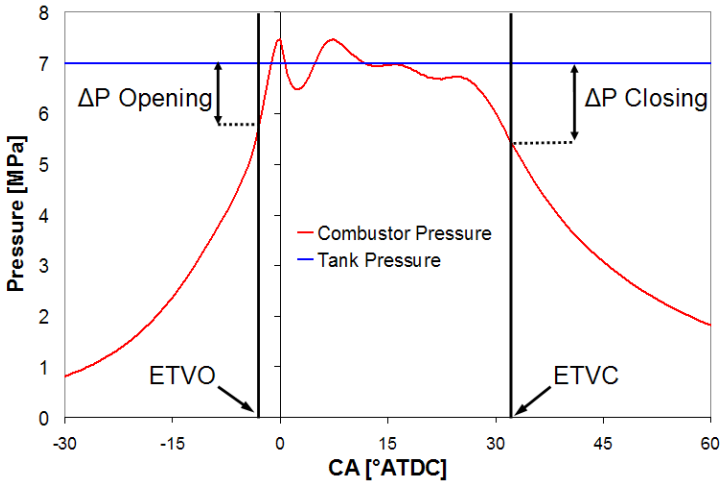

Fig. 3.2 Pressure traces during combustion

Therefore it was decided to remove the constant pressure condition, thus eliminating the need of two transfer valves as well, with the result of getting almost equal pressure in the two cylinders during the transfer process, apart from the transfer-valve opening phase, nearly eliminating the pressure losses at the transfer valve closing that penalized the HCPC engine with constant combustion pressure.

To reduce also the pressure difference between the two cylinders when the transfer-valve opens, the effective valve opening was advanced to 30° BTDC (from 5° BTDC), so that it occurs when pressure is r easonably low in both cylinders. Moreover, increasing the opening duration of transfer valve, its acceleration decreases, limiting the feasibility concerns which were feared in the original engine concept.

Thanks to these improvements an increase of around 10-15% in terms of thermal efficiency, predicted with the complete CFD model, was achieved. Two possible solutions, one with the transfer valve on the compressor side and the other on the combustor side were tested, despite the high valve temperature present in the last solution. Indeed the solution with the

transfer valve on the combustor side delivered higher predicted thermal efficiency, due to the larger expansion ratio and induced to study a moving cylindrical surface to replace the valve avoiding its temperature problems. However after some tuning work done with a one-dimensional code the benefits of the combustor-side valve in terms of efficiency turned out to be reduced and the solution with the transfer valve on the compressor side was preferred mainly for feasibility reasons. Placing the valve on the compressor side, allows in fact using a conventional poppet valve (additional cylindrical seal aside), because valve temperature is much lower since combustion does not reach the compressor side.

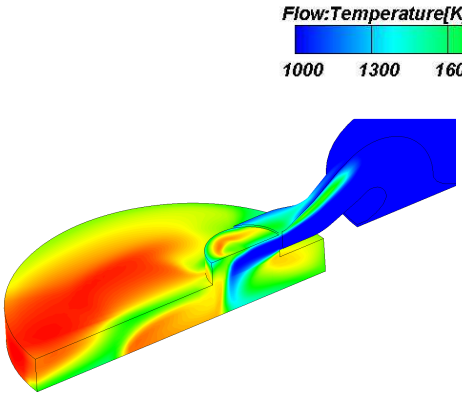

Fig. 3.3 Single transfer valve solution with the valve on the combustor side 30°ATDC

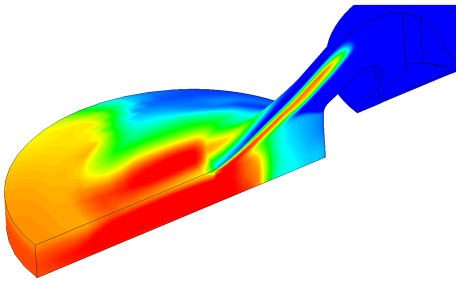

Fig. 3.4 Single transfer valve solution with the valve on the compressor side 30°ATDC

This decision of removing one of the transfer valves also led to a new split cycle engine concept (patent pending [31]). The split-cycle idea is being studied for more than a century: as a matter of facts, Backus Water Motor Company of Newark, NJ, was producing a split-cycle engine in 1891 [24] and the Koenig split-cycle engine was patented in 1914 [25]. In recent times, the split-cycle concept has been reconsidered for Diesel engines [26, 27, 28], for S.I. engines [29] as well as for large power-plant gas engines [30].

In all of the previously conceived split-cycle engines, the thermodynamic cycle is accomplished by means of three different environments:

- Compression volume
- Passage/transfer volume
- Expansion/combustion volume

In the HCPC engine on the other hand, the transfer duct is actually part of the combustion chamber, therefore only two environments are present, a compressor cylinder and a combustor cylinder, in which both combustion

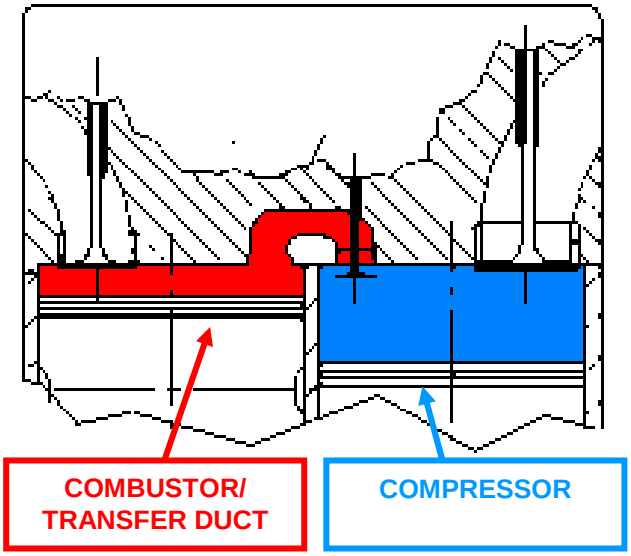

Fig. 3.5 New Split-Cycle architecture

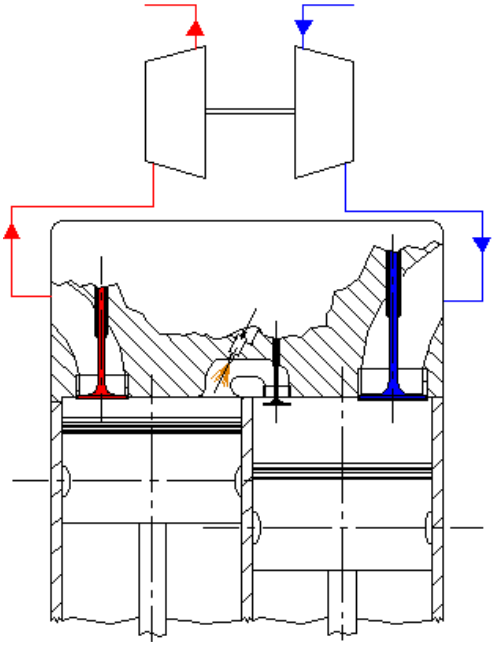

Fig. 3.6 Final HCPC engine scheme

and expansion phases are accomplished, and is at every time connected to the transfer duct (Fig. 3.5). The two environments (compressor and combustor) are connected only during the air transfer phase and the combustion. The split-cycle concept also allows separating the intake and

compression phases from the combustion, expansion and exhaust phases. By so doing it is possible to specialize the two cylinders respectively as a compressor and a combustor/expander, realizing a Miller cycle, with higher expansion ratio than compression ratio, thus the thermodynamic cycle can allow higher indicated efficiency with respect to a conventional Diesel cycle. Based on this considerations a final HCPC engine conceptual scheme was defined (Fig. 3.6) [22, 31], and an intense CFD simulation activity on a light duty application of the engine itself was started.
The following paragraphs show the studies that were performed along the research, regarding the engine head, piston and transfer duct design, the use of turbocharging, the possibility of recirculating exhaust gas to reduce NO_X emissions, as well as the possibility of insulating engine walls to improve thermal indicated efficiency.

3.2 BASELINE ENGINE

3.2.1 GEOMETRY

Once defined the final engine scheme, a geometrical model and a computational grid (Fig.3.7) were defined [22].

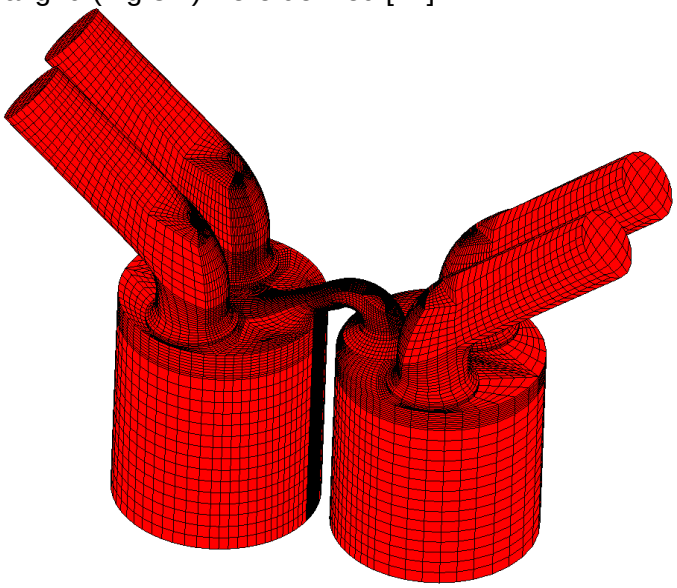

Fig. 3.7 Baseline engine computational grid(85000 cells at TDC, half-model)

From the pictures some design features of the HCPC engine can be seen. The intake and exhaust valve (2 valves of 38 mm for both the 86 mm cylinder bore) are much bigger than the ones of a similar displacement engine with advantages in volumetric efficiency. The transfer duct (Fig. 3.8) has instead a very small volume (around 9 cm^3) because of high air density

during the transfer phase. In Tabs. 3.1 and 3.2 compressor and combustor cylinder specifications are reported, as well as valve timings. As concerns valve timing the same kind of double-seal valve presented in Chapter 2.

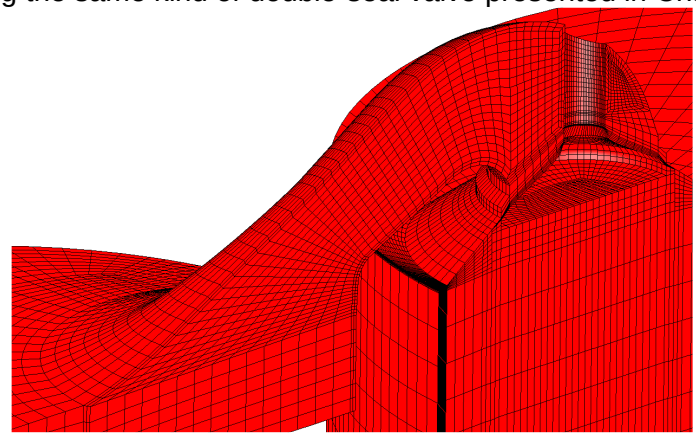

Fig. 3.8 transfer duct geometry detail

	Compressor	Combustor
Displacement	499 cm^3	598 cm^3
Bore	86 mm	86 mm
Stroke	86 mm	103 mm
Geometric Compression ratio	90:1	47:1

Tab. 3.1 Compressor and Combustor specification

IVO	57°ATDC
IVO Effective	85°ATDC
IVC	-98°ATDC
IVC Effective	-126°ATDC
TVO	-30°ATDC
TVO Effective	-47°ATDC
TVC	60 ATDC
TVC Effective	77 ATDC
EVO	148°ATDC
EVO Effective	175°ATDC
EVC	-36°ATDC
EVC Effective	-9°ATDC

Tab. 3.2 Valve timings

3.2.2 CFD SIMULATION SETUP

For the CFD analysis conducted during the whole research the following computational tools were used:

- Geometry definition: Pro-Engineer Wildfire 4
- Preprocessing (Computational Grids): Ansys ICEM CFD (versions 10 to 12 due to periodic software updates)
- One dimensional analysis: AVL BOOST (versions 5.0 to 2011 due to periodic software updates)
- Three dimensional CFD analysis: AVL FIRE (Versions 8.52 to 2011 due to periodic software updates)

Different models where used during the three dimensional CFD analysis, which are integrated in AVL FIRE. Unless differently reported, the models used were:

- Turbulence: RANS (Reynolds Average Navier Stokes) method, with the two-equation K-ζ-f model
- Combustion: ECFM-3Z
- Injection process: Discrete Droplet Model (DDM) was used together with the KH-RT model and the Dukowicz evaporation model
- NO_X emissions: Extended Zeldovich
- soot emissions: Kennedy-Hiroyasu-Magnussen

Pressure is assumed to be kept constant at the inlet and the outlet of the fluid domain. The initial conditions were calculated by means of the one-dimensional model shown in Fig. 3.9. The same code was used to define various parameters as the intake, transfer and exhaust valve lift and timing, the intake and exhaust duct length and the cylinder-compressor crank-angle phasing. The valve lift curves are shown in Fig. 3.10. (CA is always referred to the combustor TDC). The aforementioned additional cylindrical seal clearance, is 2 mm for intake and exhaust valves and 1 mm for the transfer valve.
3D calculations started at Effective TVO, when the transfer valve clears its cylindrical seal, and consider the combustor and compressor complete cycle. Two complete cycles were calculated in order to reduce the dependency of the results from the initial conditions (see next paragraph).
4 A/F ratios were considered in the simulations: 23, 27, 32, 38. The initial conditions are summarized in Tab. 3.3. The injection rate profile is shown in Fig. 3.11: pilot injection was used to achieve stable ignition timing. The main injection profile has a triangular shape, in order to follow, roughly, the air transfer flow rate from the compressor to the combustor. The injector is located in the transfer duct as shown in Fig. 3.12. The spray boundary conditions used in the simulations are summarized in Table 3.4.

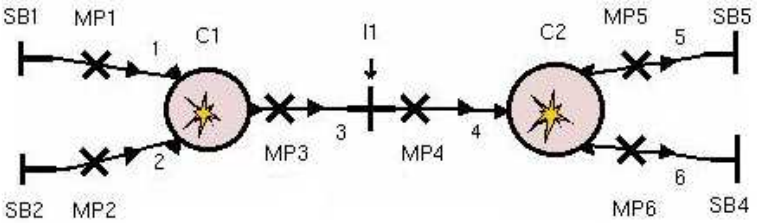

Fig. 3.9 One dimensional model

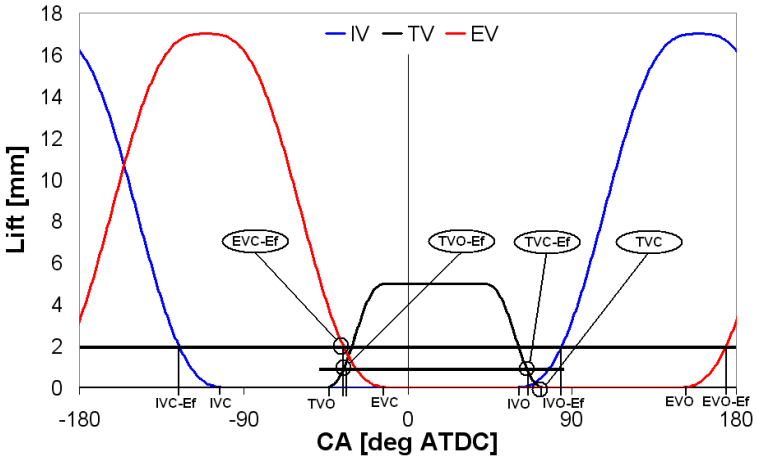

Fig. 3.10 Valve lift curves

Engine speed	2000 rpm
Inlet T, P	363 K, 300 kPa
Outlet P	270 kPa
Combustor Initial T, P	745-900 K, 520-550 kPa
Compressor Initial T, P	560-570 K, 1400-1510 kPa
Simulation Start	-30° ATDC
Simulation End	690° ATDC (2℃ycle)

Tab. 3.3 Initial and boundary condition

Injection Type	Transfer Duct Injection
Fuel	C14H30
Fuel Temperature	363 K
SOI (Pilot injection)	-6°ATDC
EOI (Pilot injection)	-4°ATDC
SOI (Main injection)	-2°ATDC
EOI (Pilot injection)	28°ATDC
Injector	Single-Hole
Fuel Injected	26-40 mg
Nozzle Diameter	256 μm
Cone Angle	22°
Injection rate	Fig. 3.11

Tab. 3.4 Injection boundary condition

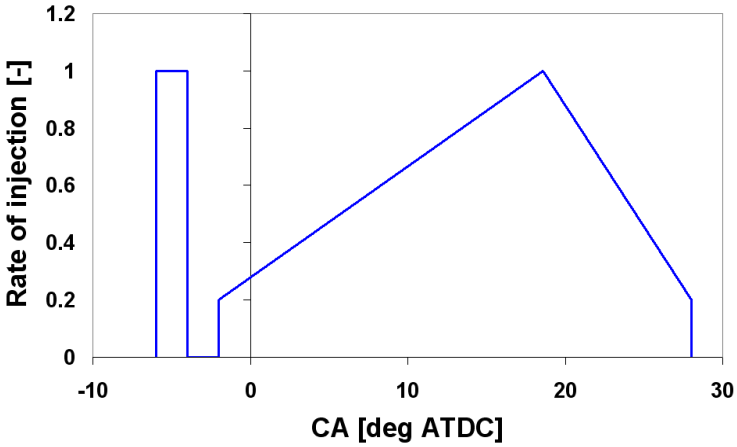

Fig. 3.11 Normalized Injection rate

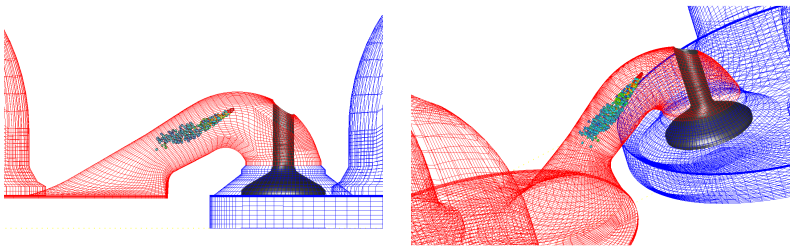

Fig. 3.12 Spray position in the transfer duct

3.2.3RESULTS AND DISCUSSION

In the first simulation runs four cycles were simulated in order to verify the influence of the initial conditions on the results accuracy. Compressor and combustor pressure traces (Fig. 3.13) exhibit a significant difference between the first and the second cycle (almost 1 MPa on the peak pressure value), whereas after the second cycle, no cycle-to-cycle variations were noticed. Therefore the second cycle (from 330° to 690° ATDC) was chosen to analyze simulation results.
Comparison between 1D and 3D simulations are shown in Fig. 3.14. Even if a quite good agreement in terms of pressure traces was obtained, some differences are noticeable, especially during the high pressure engine phases.

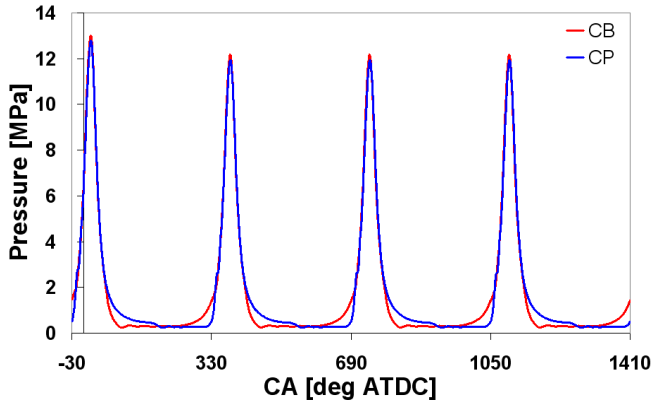

Fig. 3.13 Combustor and compressor pressure traces: effect of the initial conditions

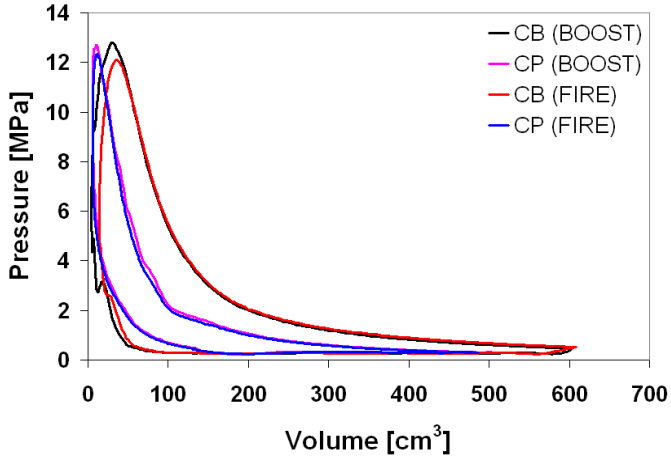

Fig. 3.14 Comparison between 1D and 3D simulation

The performance indicated data were derived from the indicated work (Fig. 3.15) calculated with Equation 1. The combustor and compressor work were obtained integrating the CFD pressure using the following equations:

$$Indicated\_Work = W_{CB} + W_{CP}$$

Where:

$$W_{CB} = \oint p_{CB} dV \approx \sum_{n=0}^{Ncells} 0.5 \cdot \left[\left(p_{n_{CB}} + p_{n-1_{CB}} \right) \cdot \left(V_{n_{CB}} - V_{n-1_{CB}} \right) \right]$$

$$W_{CP} = \oint p_{CP} dV \approx \sum_{n=0}^{Ncells} 0.5 \cdot \left[\left(p_{n_{CP}} + p_{n-1_{CP}} \right) \cdot \left(V_{n_{CP}} - V_{n-1_{CP}} \right) \right]$$

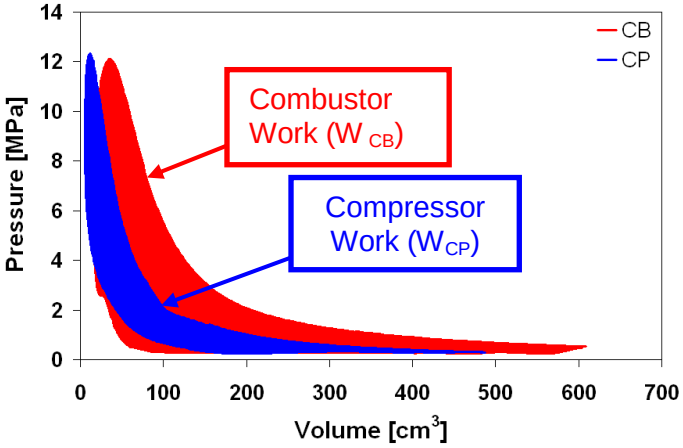

Fig. 3.15 Compressor and combustor indicated work

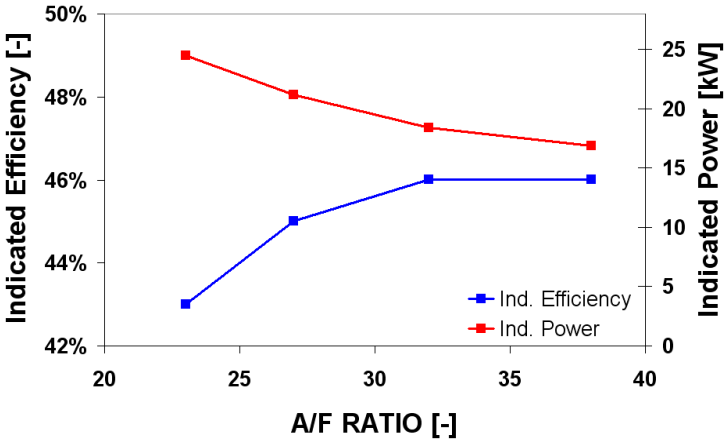

Fig. 3.16 Performance indicated results: efficiency and power

In Fig. 3.16 indicated power and efficiency are given for all the cases considered. Power density and efficiency are predicted to be very promising. Moreover, the indicated efficiency is scarcely dependent on the A/F ratio, reaching 46 % for A/F ratio greater than 32.

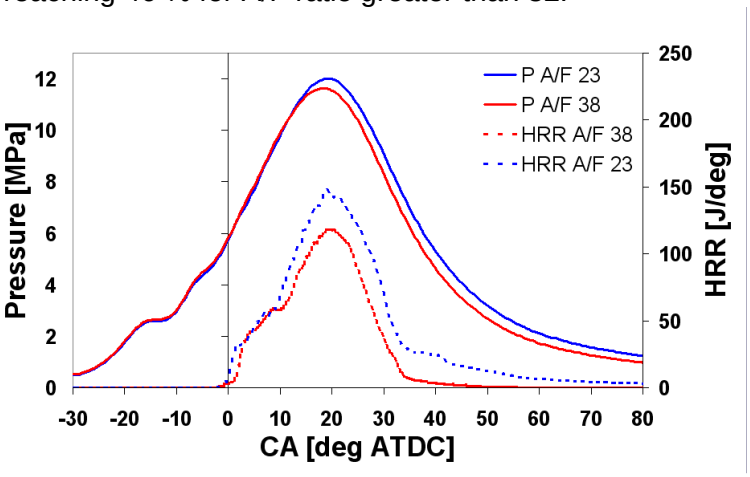

Fig. 3.17 Pressure and HRR for the two extreme cases (A/F 23, 28)

Pressure traces and HRR are shown in Fig. 3.17: the smoothness of the pressure rise, which occurs almost linearly, can be noticed. The HRR behavior follows the injection rate curve reaching the peak at about 20° ATDC.

As regards emission productions (Fig. 3.18), they are not really influenced from the A/F ratio, with the exception of soot, whose emissions decrease increasing the A/F ratio and almost vanish with A/F ratio greater than 27.

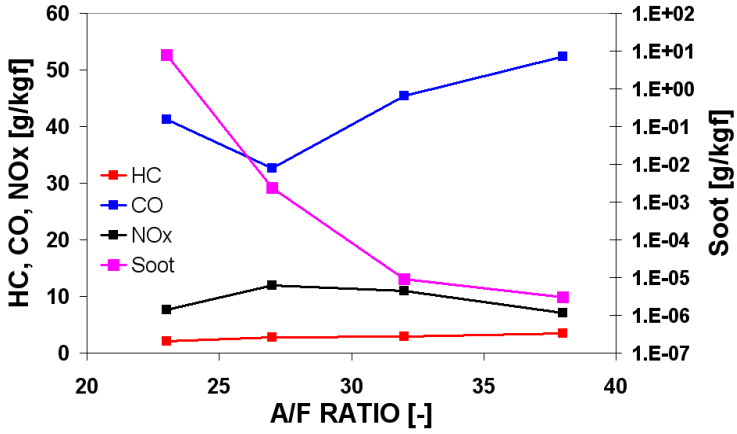

Fig. 3.18 Emission production of the HCPC engine

To gain better insight on the HCPC combustion process, a comparison with conventional Diesel engine was performed, maintaining the same A/F ratio (A/F 27) without EGR. The light duty Diesel engine tested by Musu et Al. [14], was investigated by means of the same spray, combustion, turbulence, evaporation and emission models used for the previously described activity.

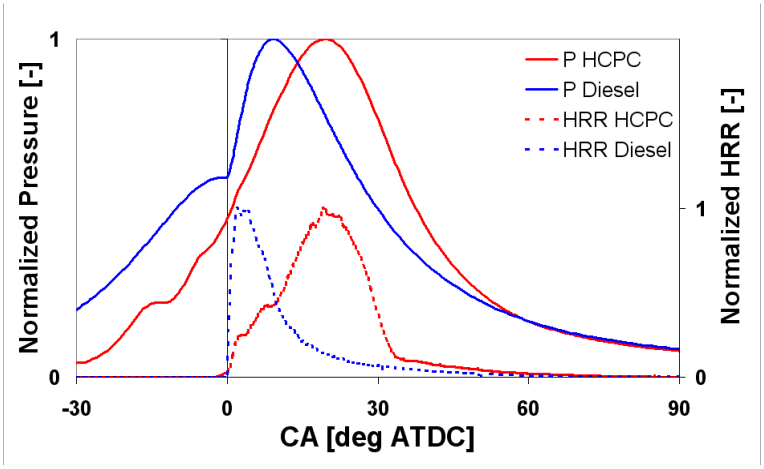

Fig. 3.19 Normalized HRR for the HCPC and Diesel combustion

Heat Release Rate and pressure results (Fig. 3.19) show the differences in combustion regimes between the two cases. In Diesel combustion a significant part of the heat is released (about 30%) during the premixed combustion phase and the remaining part in the mixed-controlled diffusion combustion phase.
In the HCPC, the premixed combustion phase is almost absent, therefore maximum PRR is very small (0.3 MPa/deg) with benefits for engine noise and vibrations. CFD results for equivalence ratio and temperature during combustion (Fig. 3.20), confirm the results obtained in Chapter 2, showing that diffusion flames are limited and most of the combustion takes place mainly where the equivalence ratio is higher, generating volumetric heat release characteristics instead of diffusion flames. Therefore the combustion takes place progressively in almost homogenous charge condition while the charge is admitted into the combustor chamber.
As a consequence the HCPC soot emission production is in the same order of magnitude of the PCCI combustion [18] and 4 orders of magnitude less of the Diesel case considered in the study (Tab. 3.5), while HC, CO and NO_X are in the same order of magnitude of the Diesel case. NO_X emission could be considerably reduced improving the mixing process and using EGR. Moreover higher EGR level than those commonly used in

conventional Diesel engines can be employed, due to the intrinsic low-soot operation typical of HCPC combustion.

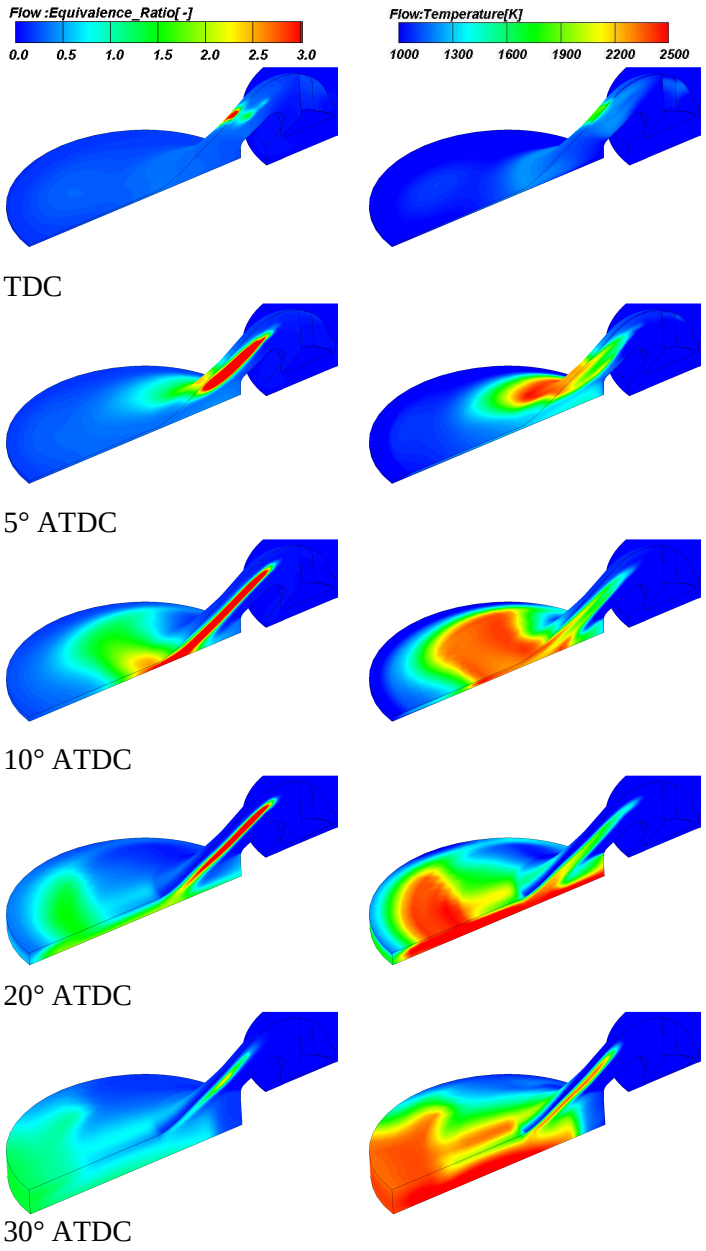

Fig. 3.20 Equivalence Ratio and Temperature maps for the HCPC

	HCPC	Diesel
HC [g/kgf]	3	3
CO [g/kgf]	33	47
NO_X [g/kgf]	12	24
soot [g/kgf]	0.002	39

Tab. 3.5 HCPC-Diesel emission comparison

3.3 IMPROVED GEOMETRY

As stated in the previous paragraph, baseline engine geometry can be largely improved, with benefits for engine indicated thermal efficiency and pollutant emissions. Thus in the following stages of the research a design activity was performed, to improve transfer duct shape and reducing its volume. Once an improved geometry was defined, many CFD analysis were carried out, to confirm its validity and explore the influence of other parameters on the HCPC engine, as for example EGR, engine speed and wall heat transfer. [32]

3.3.1 TRANSFER DUCT GEOMETRY STUDY

In Fig. 3.21 the three transfer duct geometries considered in the study are shown. Starting from the Baseline engine of paragraph 3.2 (Geometry 1), the transfer duct volume was reduced from 9.1 cm^3 to 6.6 cm^3 of geometry 2 and 4.8 cm^3 of geometry 3. In geometry 3 the transfer valve was tilted of 25° and the compressor dead volume was lowered with a specifically designed piston. Decreasing the compressor dead volume the compressor expansion is performed in a shorter crank angle phase therefore the inlet valves can be opened earlier increasing the air trapped mass and therefore the specific power.
The simulations were made at 2000 rpm starting from the transfer valve opening (TVO) to the EVO, therefore calculation domain does not include intake and exhaust ports (Tab. 3.6). Two cases with different fuel amount (16 and 22 mg), tested, performing injection with a single hole injector. Injection boundary conditions are summarized in Tab. 3.7, for other geometrical details and parameters see next paragraph.
Emission results in Figs 23 and 24 prove that the reduction of transfer duct volume lead to a sensible reduction in terms of CO and soot emission. Temperature maps in Fig. 3.25 shows that lowering the transfer duct volume combustion tends to propagate in the entire combustion chamber. Figure 3.26 shows in fact, that a significant part of the oxygen is not used with geometries 1 and 2, due to an undesirable charge stratification. In geometry 3 instead the oxygen concentration is much more uniform leading

to a better soot and CO oxidation. The third geometry was therefore chosen for continuing with the research activity.

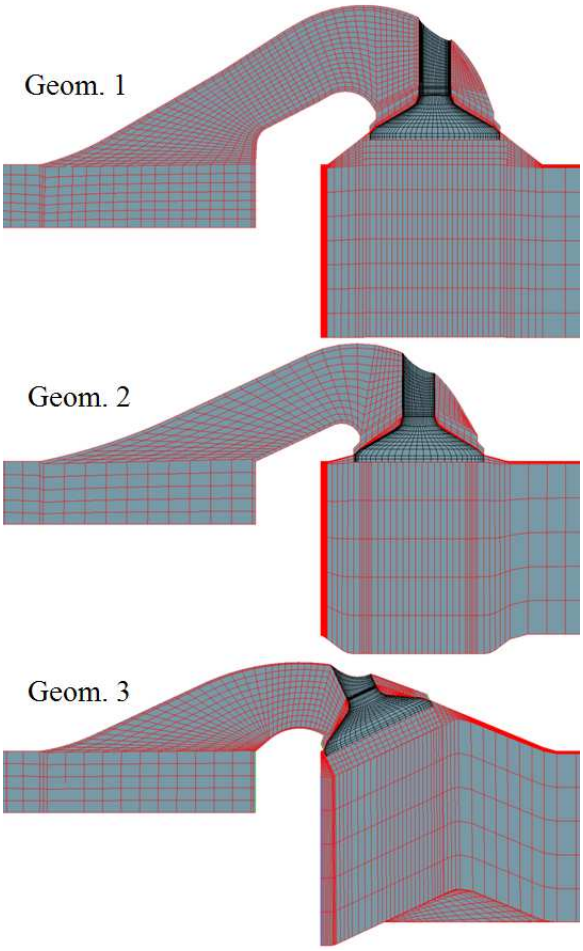

Fig. 3.21 Transfer duct geometries considered in the study

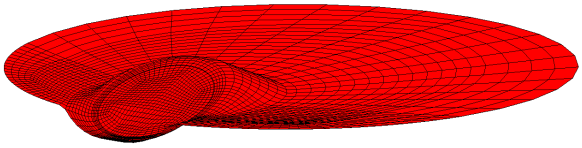

Fig. 3.22 compressor piston of geometry 3

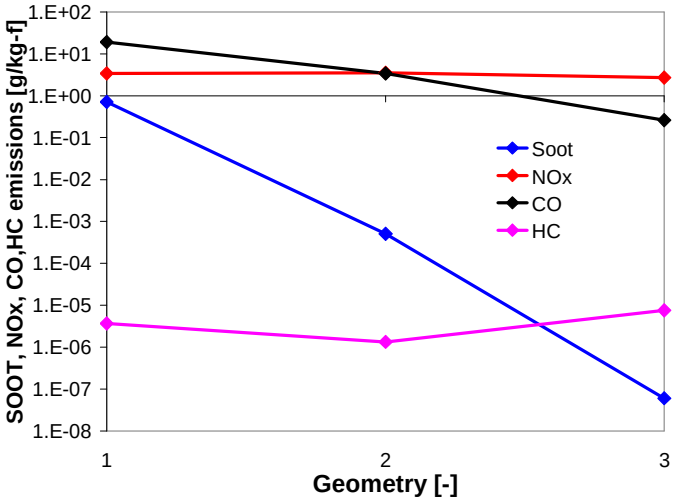

Fig. 3.23 Emission results for the different geometries for the case 16mg

Engine speed	2000 rpm
Combustor Initial T, P	820 K, 350 kPa
Compressor Initial T, P	520 K, 500 kPa
Simulation Start (TVO)	330°ATDC
Simulation End (EVO)	525°ATDC

Tab. 3.6 simulation parameters

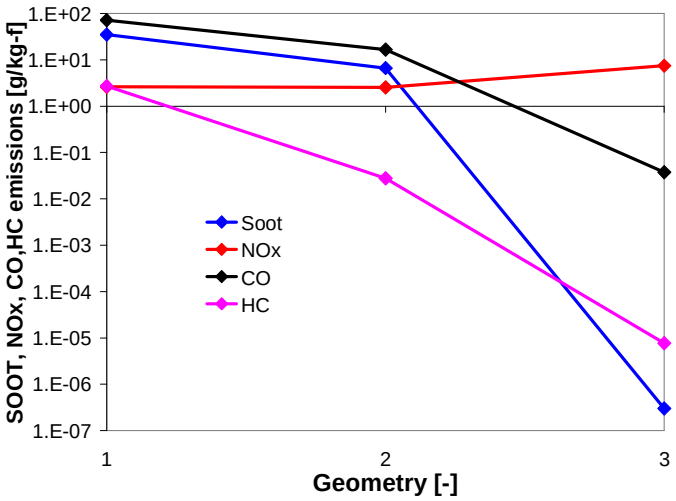

Fig. 3.24 Emission results for the different geometries for the case 22mg

Injection Type	Transfer Duct Injection
Fuel	C14H30
Fuel Temperature	363 K
SOI (Pilot injection)	-8°ATDC
EOI (Pilot injection)	-6°ATDC
SOI (Main injection)	0°ATDC
EOI (Pilot injection)	20°ATDC
Injector	Single-Hole
Fuel Injected	16, 22 mg
Nozzle Diameter	257 μm
Cone Angle	22°
Injection rate	Square profile

Tab. 3.7 Injection boundary condition

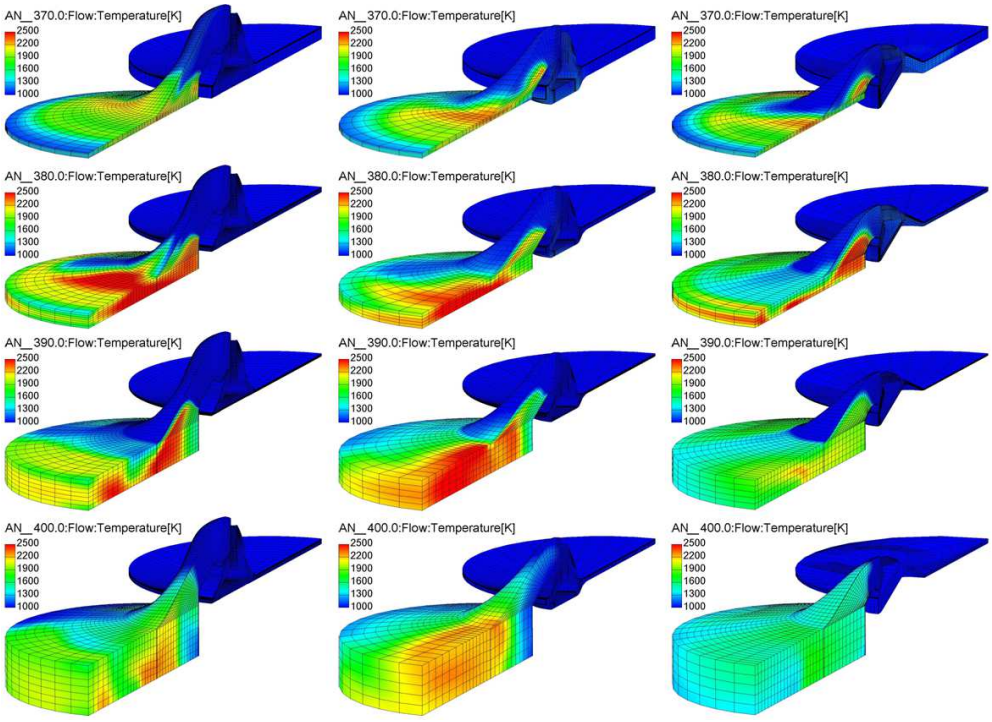

Fig. 3.25 Temperature maps during combustion for Geom. 1 (left), Geom. 2 (middle) Geom. 3 (right)

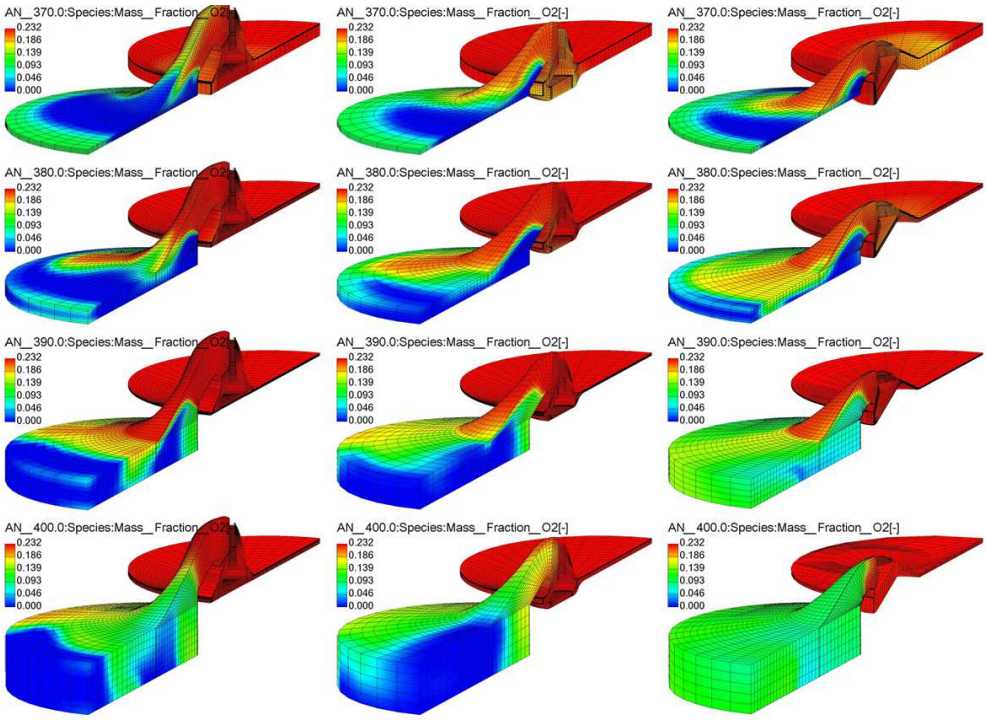

Fig. 3.26 Oxygen concentration maps during combustion for Geom. 1 (left), Geom. 2 (middle) Geom. 3 (right)

3.3.1 RESULTS AT 2000 RPM

In this paragraph results of the complete cycle simulation are presented, similarly to what was done on the baseline geometry. The same software, workflow and models were used.

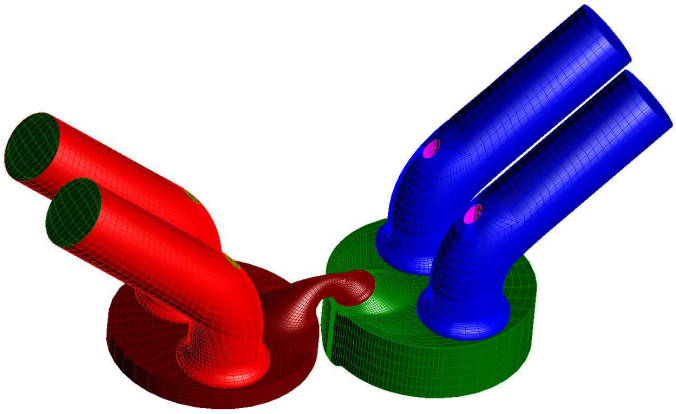

Fig. 3.27 HCPC fluid domain at TVO (85000 cells at TDC)

	Compressor	Combustor
Displacement	499 cm^3	598 cm^3
Bore	86 mm	86 mm
Stroke	86 mm	103 mm
Geometric Compression ratio	117:1	85:1

Tab. 3.8 Compressor and Combustor specification

The new computational domain is shown in Fig. 3.27, and the two cylinder specifications are reported in Tab.3.8: bore and stroke of the two cylinders were maintained unchanged, whereas geometric compression ratios changed due to the new geometry of transfer duct and compressor piston. Valve timings are reported in Tab. 3.9 and valve curves in Fig. 3.28: the new geometry allows anticipating intake valve opening, as aforementioned. Transfer valve phasing was also modified.
Six equivalence ratio from 0.4 to 0.96 where considered injecting 16 to 27 mg each cycle. The initial conditions are summarized in Tab. 3.10. Pilot injection was used to achieve stable ignition timing, and a new 7 holes injector located in the transfer duct (Fig. 3.29) was used. The spray boundary conditions used in the simulations are summarized in Tab. 3.11. Differently from the baseline engine analysis, in this part of the research a naturally aspirated engine was considered.

IVO	35°ATDC
IVO Effective	60°ATDC
IVC	-101°ATDC
IVC Effective	-126°ATDC
TVO	-30°ATDC
TVO Effective	-47°ATDC
TVC	35 ATDC
TVC Effective	52 ATDC
EVO	138°ATDC
EVO Effective	165°ATDC
EVC	-36°ATDC
EVC Effective	-9°ATDC

Tab. 3.9 Valve Timings

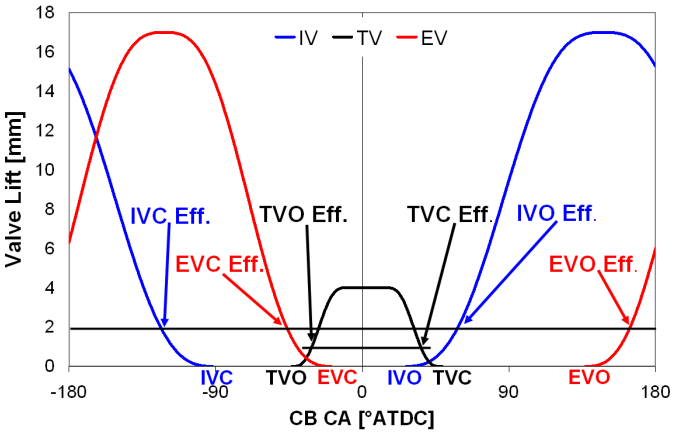

Fig. 3.28 Valve lift curves

Engine speed	2000rpm
Inlet T, P	323 K, 100kpa
Outlet P	100kpa
Combustor Initial T, P	750-850 K, 280-350 kPa
Compressor Initial T, P	480-530 K, 480-520 kPa
Simulation Start	330℃ATDC
Simulation End	1050°ATDC (2℃ycle)

Tab. 3.10 Initial and boundary condition

Injection Type	Transfer Duct Injection
Fuel	C14H30
Fuel Temperature	363 K
SOI (Pilot injection)	-8°ATDC
EOI (Pilot injection)	-6°ATDC
SOI (Main injection)	0°ATDC
EOI (Pilot injection)	20°ATDC
Injector	7-Hole
Fuel Injected	12-27 mg
Nozzle Diameter	140 μm
Cone Angle	12°
Injection rate	Square profile

Tab. 3.11 Injection boundary condition

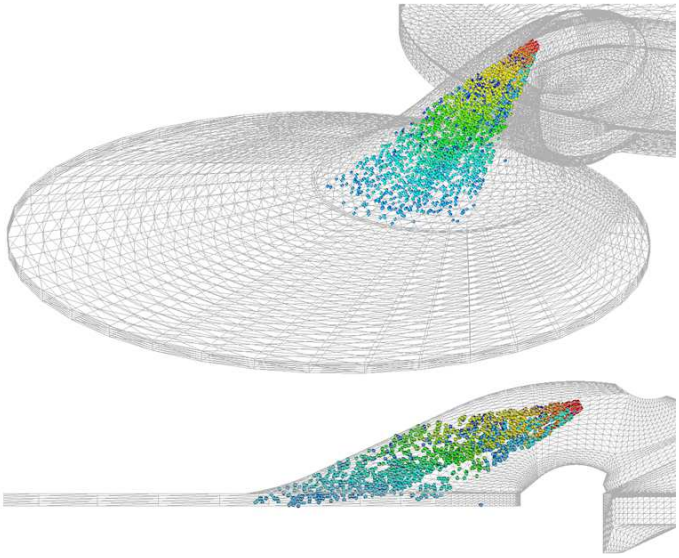

Fig. 3.29 Injector position

In Fig. 3.30 indicated power and efficiency vs. equivalence ratio are given. Thermal indicated efficiency was predicted to be very promising, reaching 46% between an equivalence ratio of 0.55 and 0.85. The naturally aspirated HCPC unit composed by a 600cc combustor and a 500 cc compressor produces more than 16kW at 2000 RPM leading to an IMEP of 1.9 MPa referred to the combustor displacement. Further benefits in terms of efficiency can be obtained using a turbocharged. NO_X emissions are in the same order of magnitude of those produced by a conventional Diesel engine and decrease with decreasing oxygen partial pressure, which is

inversely proportional to the equivalence ratio (Fig 3.31). soot (3.31), HC and CO (Fig. 3.32) emissions are very low up to equivalence ratio of 0.85, and they increase of orders of magnitude from 0.85 to 0.96.
Pressure traces and HRR are shown in Fig. 3.33: as stated in the previous paragraph, the pressure rise occurs almost linearly without high gradients with a PPRR of about 0.3 MPa per degree with benefits for engine noise and vibrations.
CFD maps reported in Fig. 3.34 show how combustion takes place progressively in almost homogenous charge condition while the charge is admitted into the combustor chamber, confirming the results obtained in the previous stages of the research activity.

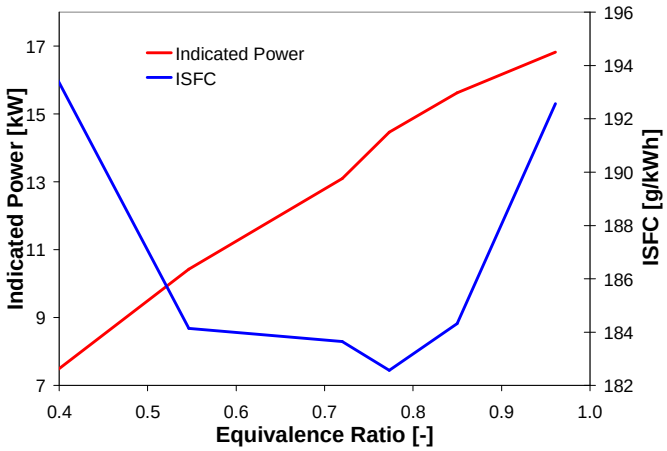

Fig. 3.30 Indicated power and ISFC vs. equivalence ratio

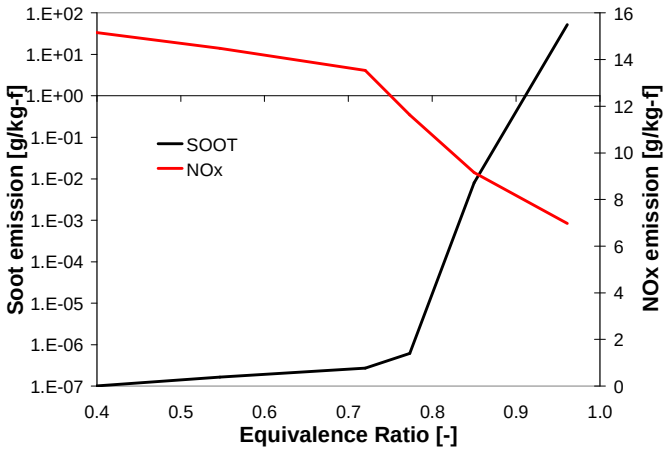

Fig. 3.31 soot and NO_X emissions vs. equivalence ratio

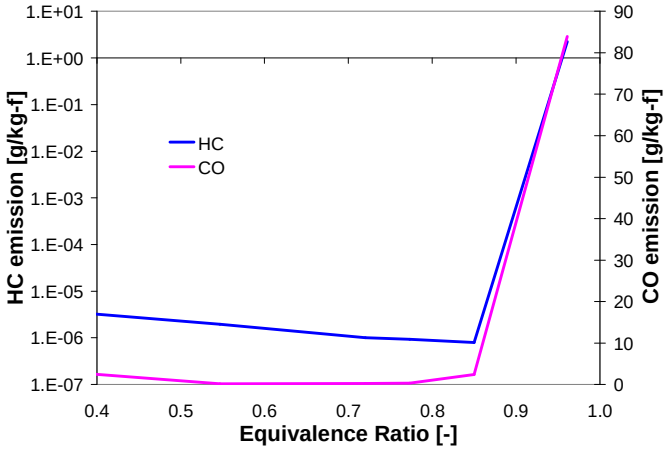

Fig. 3.32 HC and CO emissions vs. equivalence ratio

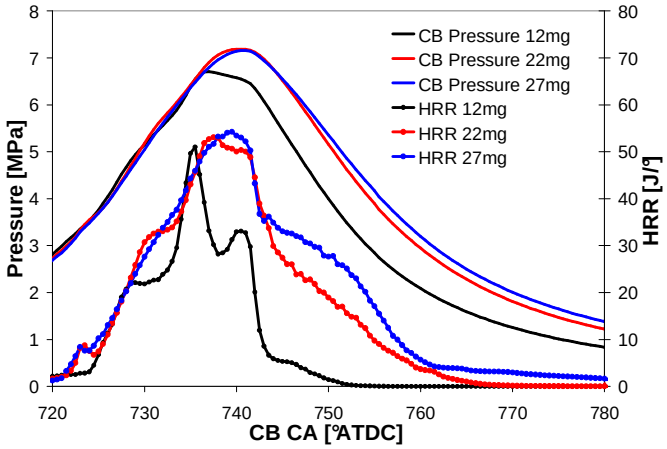

Fig. 3.33 Pressure and HRR for different fuel amounts injected

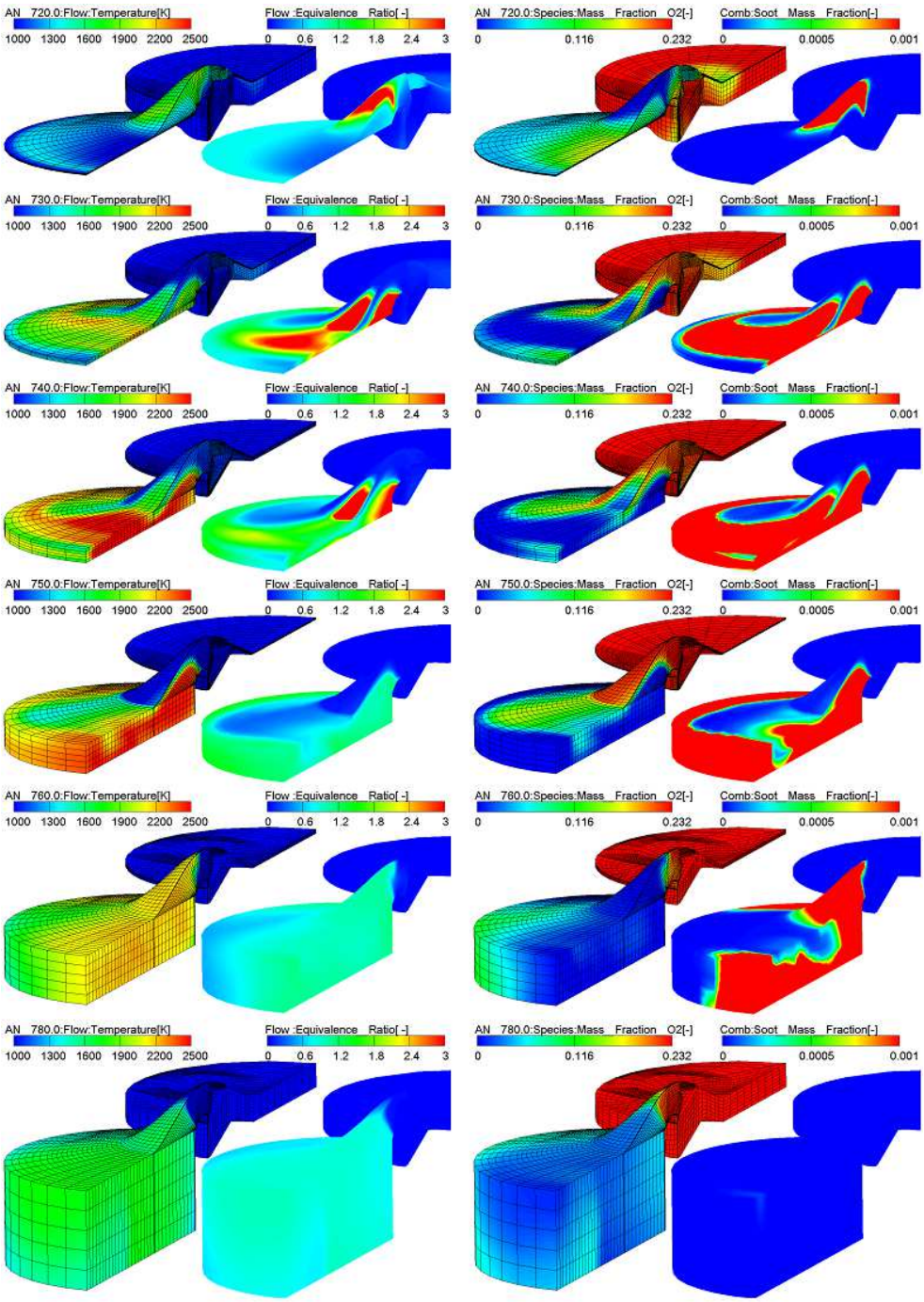

Fig. 3.34 Temperature, equivalence ratio, oxygen and soot mass fractions maps from TDC to 60ºATDC for the case 22 mg

3.3.2 ENGINE SPEED

HCPC combustion quality is not worsened by engine speed, unlike in conventional Diesel engines. In this paragraph HCPC results at full load (equivalence ratio around 0.85) for different engine speeds are presented. The same injection rate and timing were used increasing injection pressure up to 190 MPa at 4000 RPM. Simulation results show that, changing engine speed, emissions remain in the same order of magnitude, but ISFC increases from 184 at 2000 RPM to 205 g/kWh at 4000 RPM (Fig. 3.35). Pressure traces in Fig. 3.36 show a noticeable increment of the compressor pressure during combustion. This effect is caused by the much higher pressure losses during the air transfer from the compressor to the combustor, as Fig. 3.37 proves, incrementing the transfer work. Fig. 3.38 shows that the flow field is almost unchanged, even though the velocity magnitude is over 500 m/s in the throat section of the transfer duct. These results suggest that the transfer duct geometry is still to be improved to reduce pressure loss, in order to keep the typical ISFC of Diesel engines at engine speeds that are typical of SI engines for passenger cars. Moreover, this results were the motivation for the following steps in the research activity, which consisted, as reported in paragraph 3.4, in reducing the compressor displacement and coupling the engine with an external turbocharger. Thanks to this idea the transfer work can be reduced, due to the increases air density, obtained by turbocharging.

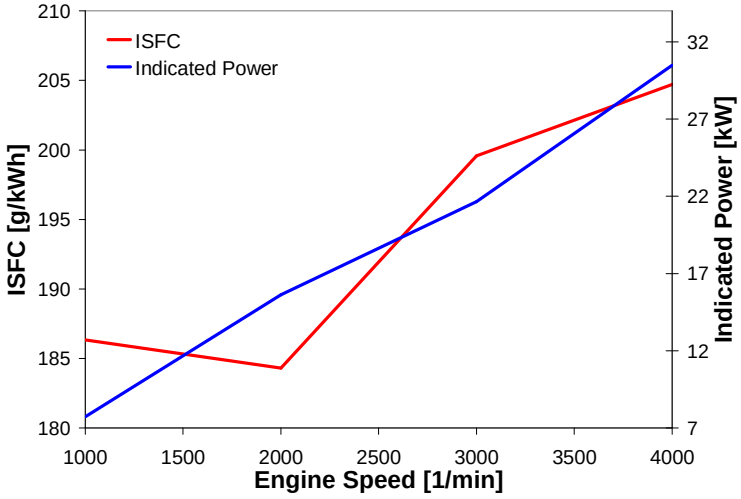

Fig. 3.35 ISFC and indicated power vs. engine speed

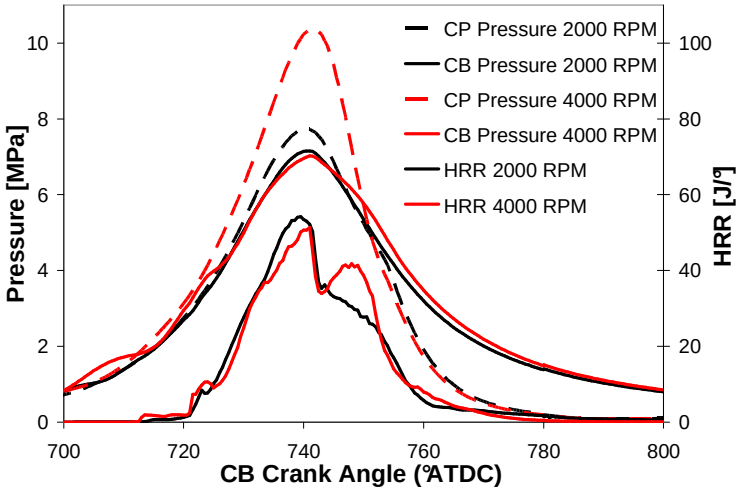

Fig. 3.36 Compressor and combustor pressures and HRR during combustion at 2000 and 4000 RPM

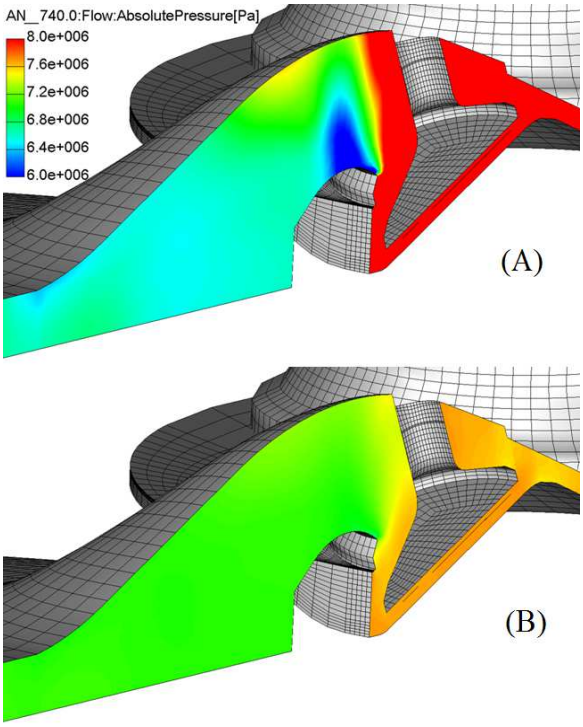

Fig. 3.37Pressure in the symmetry plane at 4000 RPM (A) and 2000 RPM (B) 20 CAD ATDC

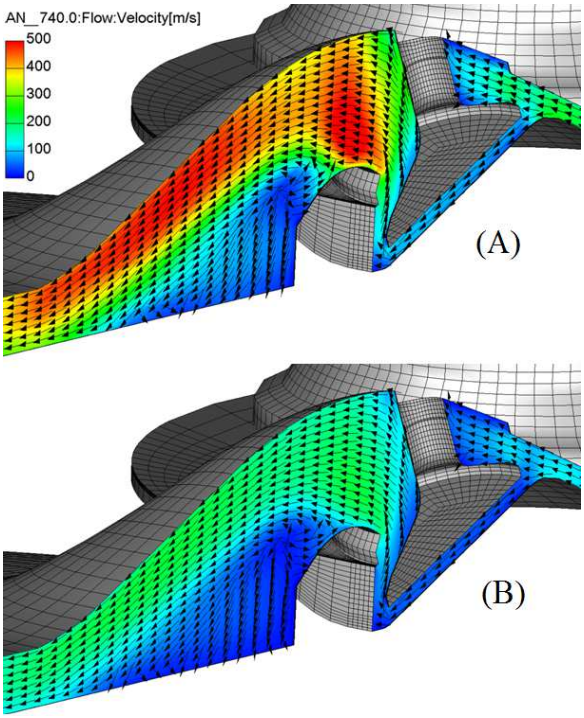

Fig. 3.37 Velocity in the symmetry plane at 4000 RPM (A) and 2000 RPM (B) 20 CAD ATDC

3.3.3 EGR STUDY

Results in paragraph 3.3.1 show that HCPC engine NO_X emissions are in the same order of magnitude of those produced by a Diesel engine, around 10 g/kgf , even though it is possible to reach global equivalence ratios up to 0.85 with almost zero soot emission. Therefore HCPC engine can tolerate much more EGR than a Diesel one without producing soot. In order to decrease NO_X emission as well, the use of external cooled EGR was investigated. Two different fuel amounts, 16 and 20 mg, were used in the study with different levels of EGR. The inlet temperature was assumed to be 363K for all the cases with EGR. As expected, results show that, increasing the amount of EGR, NO_X emissions decrease and soot emissions increase. NO_X decreases because the oxygen concentration decreases and the peak temperatures are lower. Figs. 3.38 and 3.39 prove that peak temperature is much lower using EGR. Combustor and compressor pressures decrease increasing EGR and combustion becomes slower (Fig. 3.40) leading to a reduction of indicated power and to an increment of ISFC (Fig. 3.41). soot production is increased and the lower oxygen concentration makes soot oxidation more difficult as proved by Figs

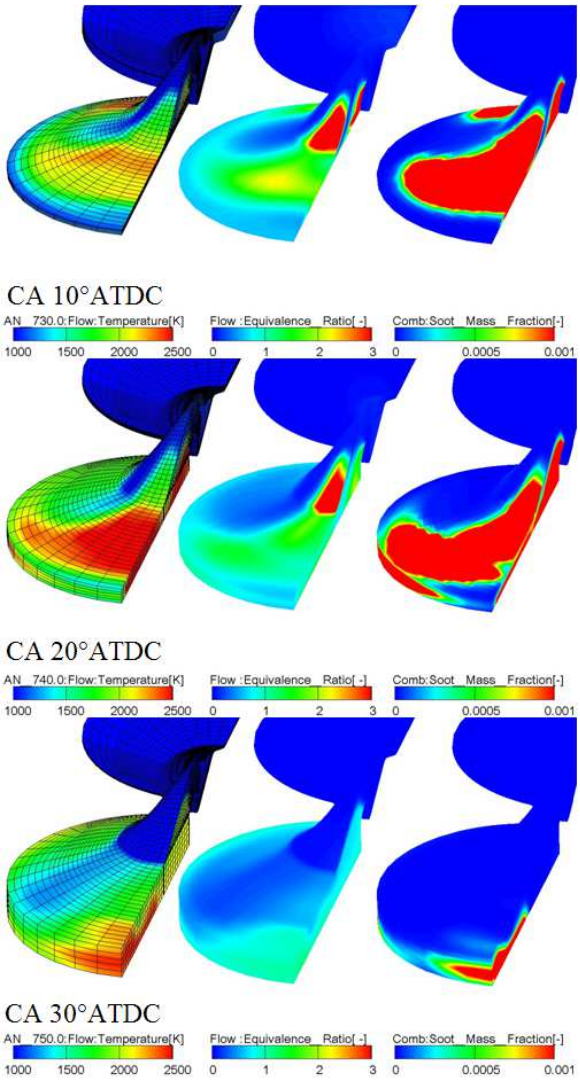

Fig. 3.38 Temperature, Equivalence ratio and soot mass fraction mass maps during combustion of the case 16 mg without EGR

3.39 and 3.42. However, as Fig. 3.43 attests, soot emissions remain almost zero for equivalence ratios below 0.85 (roughly). This value corresponds to 30% EGR for the 16mg case and to 15% EGR for the 20mg case: with those EGR amounts NO_X emissions are respectively reduced by 3 and 1 orders of magnitude with respect to the equivalent cases without EGR. An ultra clean combustion is therefore reached with the HCPC engine. The 16 mg case with 30% EGR has 0.02 g/kgf NO_X and virtually zero soot emission ($3.5e^{-5}$ g/kgf). Such level of NO_X emission is typical of

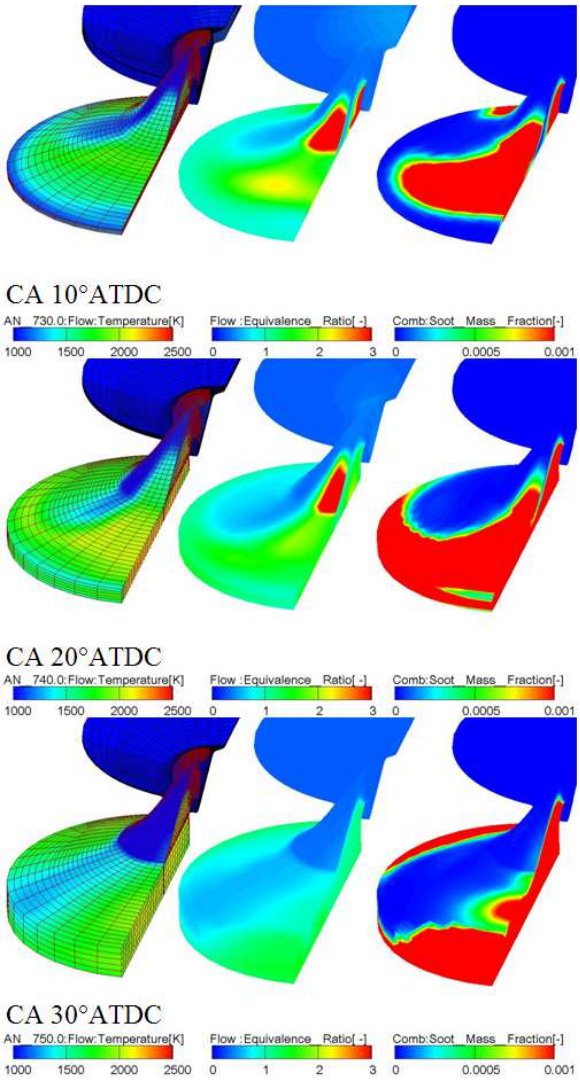

Fig. 3.39Temperature, Equivalence ratio and soot mass fraction mass maps during combustion of the case 16 mg with 30% EGR

low-temperature combustion types such as PCCI [18] and TSC [33, 34]. At 22 mg and 15 % of EGR NO_X emission is one order of magnitude lower than a Diesel engine. To reach the same power density of the last paragraph at higher loads, instead of external EGR, water injection can be used to decrease NO_X. In the HCPC engine the water can be easily injected in the compressor during compression. In this case the compression can even approach an isotherm process [35], decreasing compression work decreases, thus improving engine thermal efficiency.

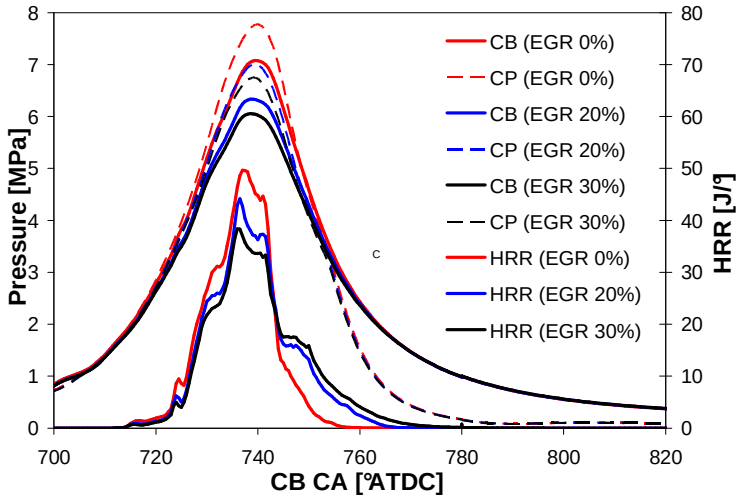

Fig. 3.40 Pressure and HRR traces with different EGR levels

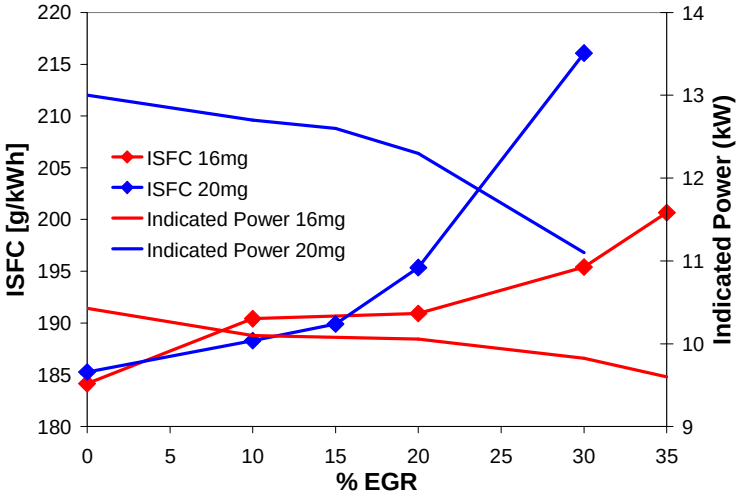

Fig. 3.41 ISFC and indicated power with different EGR levels

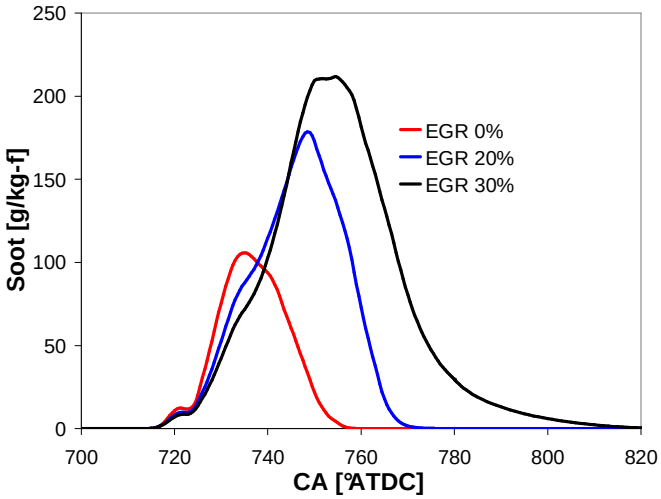

Fig. 3.42 soot concentration during combustion with different EGR levels

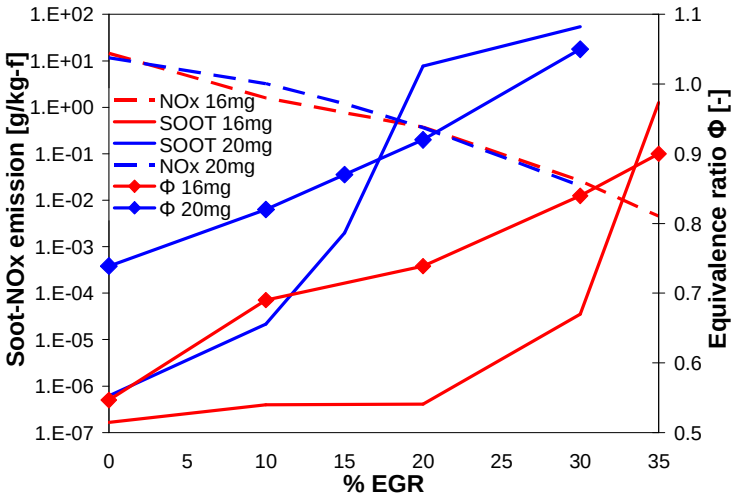

Fig. 3.43 soot and NO_X emission and global equivalence ratio with different EGR levels

3.3.4 WALL HEAT LOSSES

The high velocity air transfer from the compressor to the combustor during combustion produces higher heat losses than a conventional Diesel engine. In order to quantify those losses and identify the critical walls to be insulated in the future engine prototype, a CFD study on the wall heat transfer was conducted. The two heads and pistons and the transfer duct

	CB Piston	CB Head	Transfer duct	CP Head	CP Piston
Case 1	T=550 K	T=550K	T=550 K	T=500	Heat flux = 0
Case 2	T=550 K	T=550 K	T=550 K	Heat flux = 0	Heat flux = 0
Case 3	Heat flux = 0	T=550 K	T=550 K	T=500	Heat flux = 0
Case 4	T=550 K	Heat flux = 0	Heat flux = 0	Heat flux = 0	Heat flux = 0
Case 5	Heat flux = 0	Heat flux = 0	Heat flux = 0	Heat flux = 0	Heat flux = 0

Tab. 3.12 Cases considered for the wall heat losses study

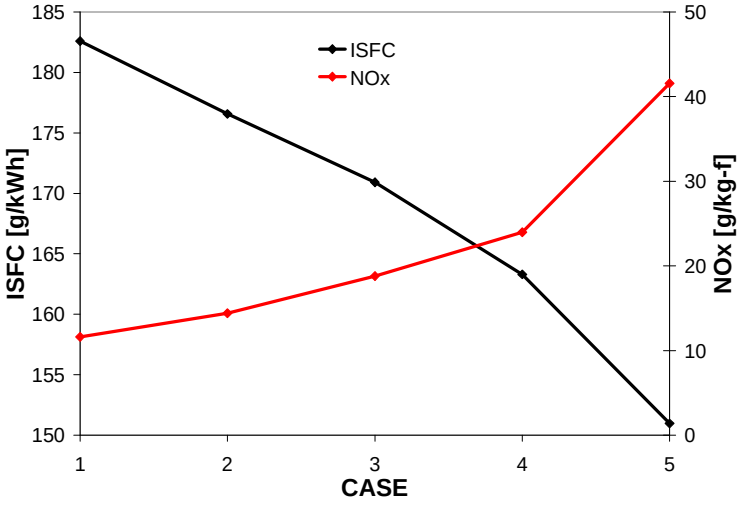

Fig. 3.44 ISFC and NO_X emission insulating different engine walls

surface where selectively considered adiabatic in the calculations leading to the set of cases in Tab. 3.12.

Results in Fig. 3.44 show that insulating the engine walls it is possible to increase indicated thermal efficiency up to ideally 56 % (ISFC 151 g/kWh) when all the combustor and compressor walls except the cylinder liners are considered adiabatic. As far as the emission are concerned soot CO and HC emission remains extremely low and almost unchanged. NO_X emissions are instead increased due to the higher temperature during combustion. This effect can be compensated at low and medium load by using external EGR and by water injection in the compressor at high load increasing furthermore thermal efficiency.

3.4 LIGHT DUTY HCPC ENGINE WITH A SMALLER COMPRESSOR

In this part of the research activity the influence of turbocharging was investigated. A new turbocharged HCPC engine with a smaller-displacement compressor cylinder was considered and studied by means of CFD simulations. The engine specifications are summarized in Tab. 3.13. Valve lifts and timings used were the same described in Tab.3.9

	Compressor	Combustor
Displacement	250 cm^3	598 cm^3
Bore	68.3 mm	86 mm
Stroke	68.3 mm	103 mm
Geometric Compression ratio	79:1	85:1

Tab. 3.13 Compressor and Combustor specification

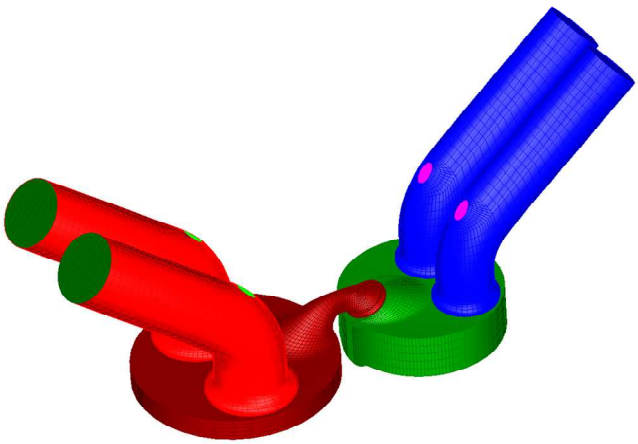

Fig. 3.45 Turbocharged HCPC fluid domain at TVO (85000 cells at TDC)

Initial conditions are summarized in Tab. 3.14. For the inlet and outlet pressure a turbocharging system with overall efficiency of 50% was considered. A pilot injection was used to achieve stable ignition timing. A 7 holes injector was used, located in the transfer duct as shown in Fig. 3.29. Spray boundary conditions used in the simulations are summarized in Tab. 3.15.

Engine speed	2000 - 6000 rpm
Inlet T, P	323 - 413 K, 100 - 300 kPa
Outlet P	100 - 270 kPa
Combustor Initial T, P	845 - 1120 K , 0.35 - 1.38 MPa
Compressor Initial T, P	570 K 0.51 - 2.00 MPa
Simulation Start	330°ATDC
Simulation End	1050° ATDC (2°cycle)

Tab. 3.14 Initial and boundary condition

Injection Type	Transfer Duct Injection
Fuel	N-Tetradecane
Fuel Temperature	363 K
SOI (Pilot injection)	-8° ATDC
EOI (Pilot injection)	-6° ATDC
SOI (Main injection)	0° ATDC
EOI (Pilot injection)	20° ATDC
Injector	7 - Hole
Fuel Injected	7 - 45 mg/cycle
Nozzle Diameter	140 μm
Cone Angle	12°
Injection rate	Square profile

Tab. 3.15 Injection boundary condition

3.4.1 CFD RESULTS

In Fig 3.46 indicated power and ISFC vs. intake pressure at 2000 rpm are shown. The results were obtained with an intake pressure of 100, 200 and 300 kPa which correspond to 100, 190, and 270 kPa respectively. Accordingly, the fuel mass injected was increased to maintain the global equivalence ratio at 0.75. Using a smaller compressor, thermal indicated efficiency increases from 46% of the naturally aspirated engine to 48% with 300kPa intake pressure, whereas maximum indicated power reaches 23 kW.

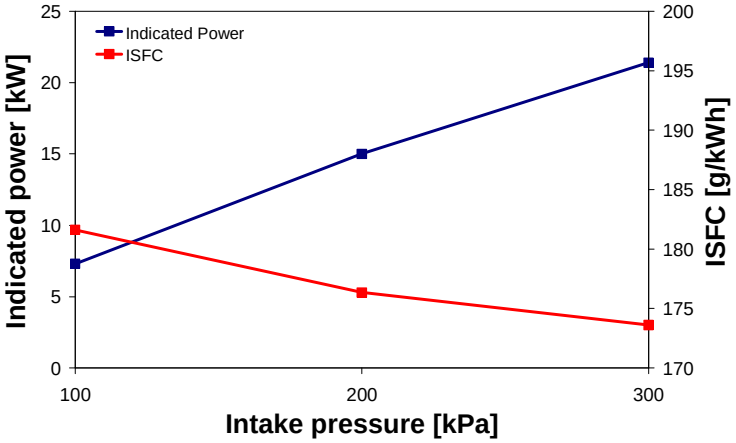

Fig. 3.46 Indicated power and ISFC vs IMEP at 2000 rpm (P_{in}: 100kPa, 200kPa, 300kPa, P_{ex} 100kPa, 190, 270kPa respectively)

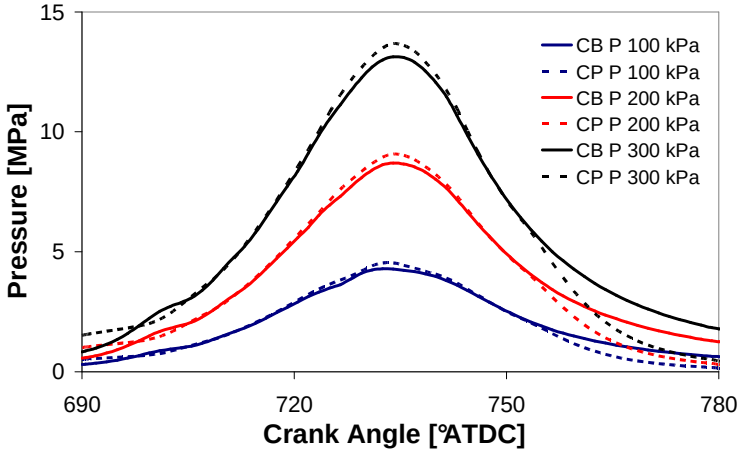

Fig. 3.47 Combustor (CB) and compressor (CP) pressure traces with different turbocharging levels

In Figure 3.47 the influence of boost pressure on the compressor and combustor pressure traces is shown: since pressure losses due to the transfer phase are almost independent from boost pressure, higher boost pressure allows gathering more power with better indicated efficiency.
A study on the influence of engine speed on performance and pollutant emissions was also performed for the new engine configuration.

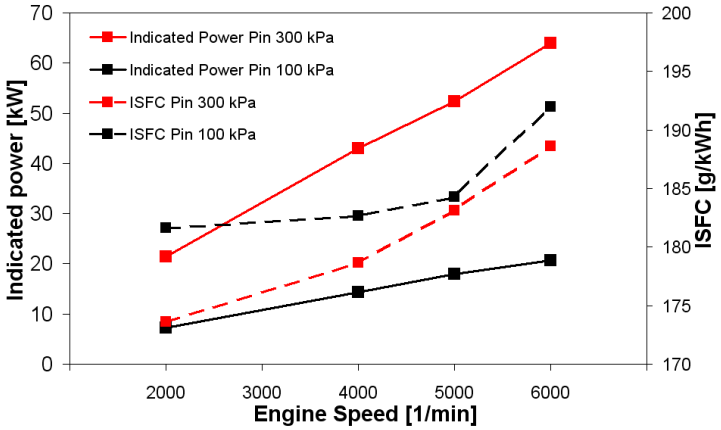

Fig. 3.48 Indicated power and ISFC (Φ=0.75, P_{in}: 100kPa, 300kPa, P_{ex} 100kPa, 270kPa respectively)

Fig. 3.48 shows engine performance versus engine speed for the naturally aspirated case and for an intake pressure of 300 kPa. A very high indicated specific power (64 kW) was obtained with 300 kPa intake pressure at 6000 rpm. The HCPC turbocharged engine is able to run properly in every operating condition considered, with more than 44% indicated thermal efficiency, demonstrating the robustness of the combustion concept. The engine indicated specific fuel consumption is always lower for the turbocharged case, than for the naturally aspirated one. In Figs. 3.49 and 3.50, pressure traces of compressor and combustor of the turbocharged and the naturally aspirated engine are respectively reported for different speeds. The pressure difference between compressor and combustor increase increasing engine speed due to higher pressure losses in the air transfer. Fig. 3.51 shows that the flow field is almost unchanged, but the velocity magnitude is over 500 m/s in the throat section of the transfer duct at 5000 and 6000 rpm. The average velocity in the throat section of the transfer duct does not change changing the turbocharging level, as Fig. 3.52 proves. Increasing engine speed from 2000 to 6000 rpm, indicated thermal efficiency decreases from 47% to 45% for the turbocharged case and from 46% to 44% for the naturally aspirated one due to higher pressure losses in the transfer phase. These results represent an important step forward in the HCPC engine development. As a matter of fact, the new HCPC engine with smaller compressor is able to run at the even better ISFC of Diesel engines at speeds that are typical of SI engines for passenger cars.

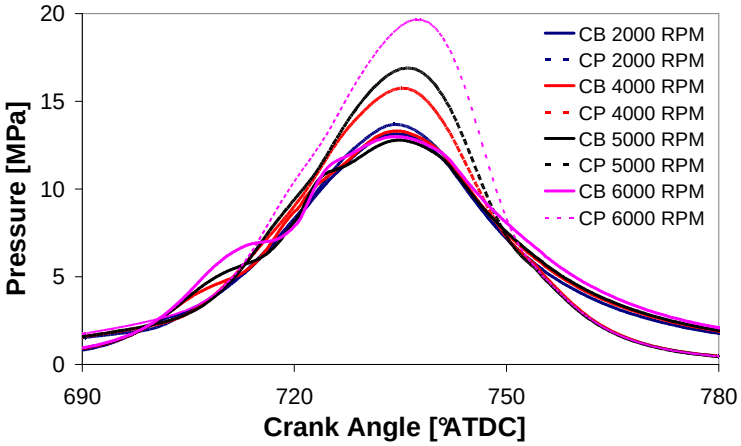

Fig. 3.49 CB and CP pressure traces at different engine speeds (P_{in}=300 kPa, P_{ex}=270 kPa).

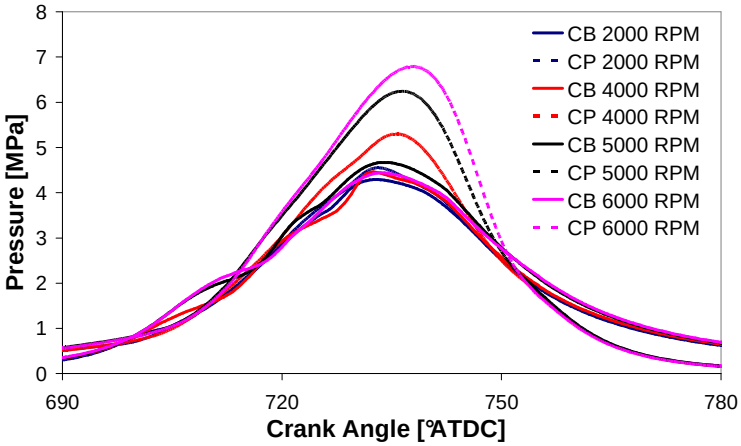

Fig. 3.50 CB and CP pressure traces at different engine speeds (P_{in}=100 kPa, P_{ex}=100 kPa).

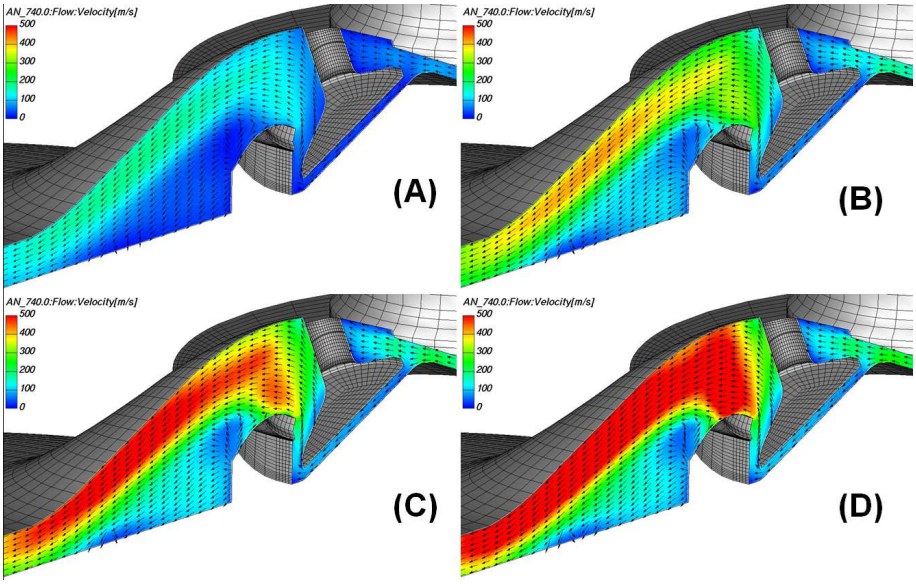

Fig. 3.51 Flow field in the symmetry plane 20°ATDC at 2000 RPM (A), 4000 RPM (B), 5000 RPM (C) and 6000 RPM (D) (P_{in}=300 kPa, P_{ex}=270 kPa).

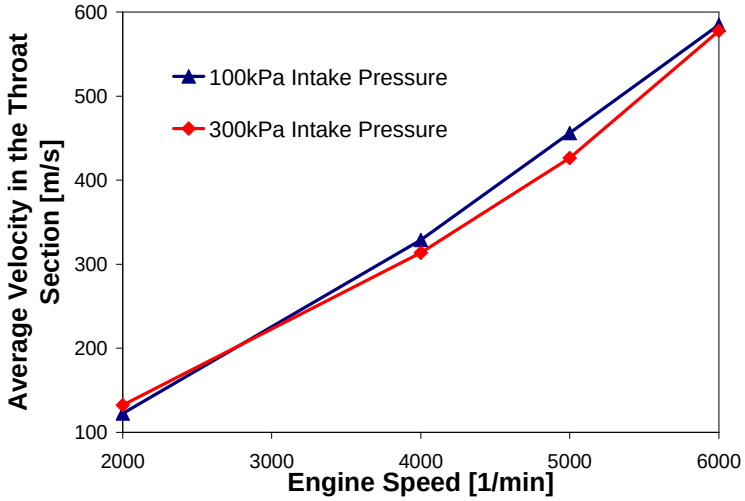

Fig. 3.52 Average velocity in the throat section (P_{in}: 100kPa, 300kPa, P_{ex} 100kPa, 270kPa respectively)

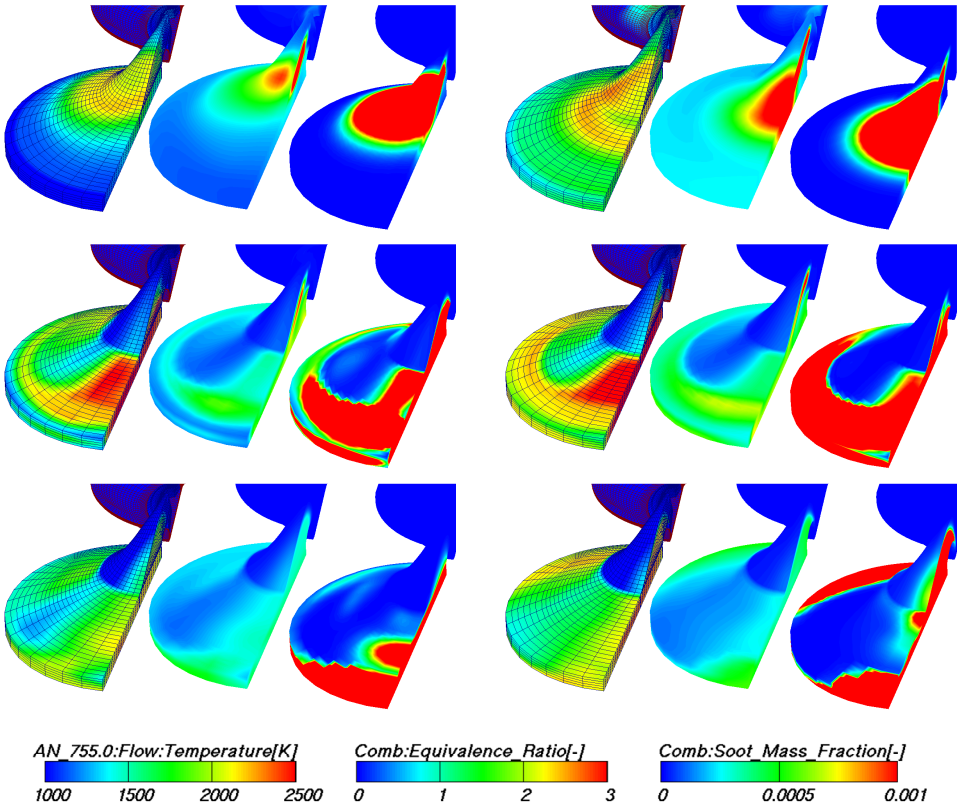

Fig. 3.53 From left to right: Temperature, Equivalence ratio and soot mass fraction mass maps during combustion at 5°, 20° and 35° ATDC at 2000 rpm (left) at 6000 (right) with P_{in}=300 kPa and P_{ex}=270 kPa

Figure 3.53 shows combustion behavior in terms of temperature, equivalence ratio and soot mass fraction at 2000 and 6000 rpm. Unlike in conventional Diesel engines, the speed of the combustion process increases along with the engine speed, keeping almost constant combustion quality and duration in terms of crank angle, like in SI engines. Pollutant emission behavior vs. engine speed, reported in Figure 3.54, confirms the validity of the HCPC combustion concept. Emissions are almost independent of the engine speed. soot and HC are orders of magnitude lower than the ones of a Diesel engine. The low CO emission trend confirms the high combustion efficiency even at high speeds. NO_X emissions are almost constant and similar to those of a conventional Diesel engine.

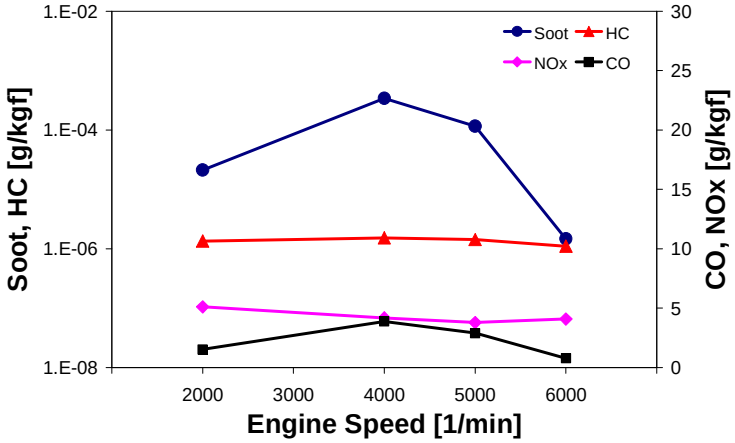

Fig. 3.54 Pollutant emissions vs. engine speed (Φ=0.75, P_{in}=300, P_{ex}=270 kPa).

3.5 HCPC vs CONVENTIONAL DIESEL COMBUSTION: CONCEPTUAL DIFFERENCES

Before proceeding to the description of the Heavy-Duty version of the HCPC, it is worth mentioning two fundamental conceptual differences between conventional Diesel combustion and HCPC.
The first difference regards the air-fuel mixture generation. In conventional Diesel combustion (Fig. 3.55), fuel injection happens when the piston is close to the combustion-TDC, therefore all the fuel is injected in all the trapped air. In the HCPC concept (Fig. 3.56) fuel is gradually injected in the pre-compressed air inside the transfer duct during the transfer phase. Therefore the combustion chamber is gradually fed with an almost homogeneous charge, which ideally burns completely while entering the combustor cylinder.
A second fundamental difference relies in the flow-field and in its influence on the mixing process.
In both engines mixing relies both on air and fuel momentum: injection is performed in both engines through a high pressure injection system, therefore spray momentum in the two cases is comparable.
The real difference relies in the air momentum: whereas in the conventional Diesel engine the air inside the cylinder is almost quiescent, apart from relatively low velocities induced by the swirl motion (Fig. 3.57), in the HCPC concept air momentum is much stronger leading to much higher velocity magnitude and a much better mixing (Fig. 3.58).

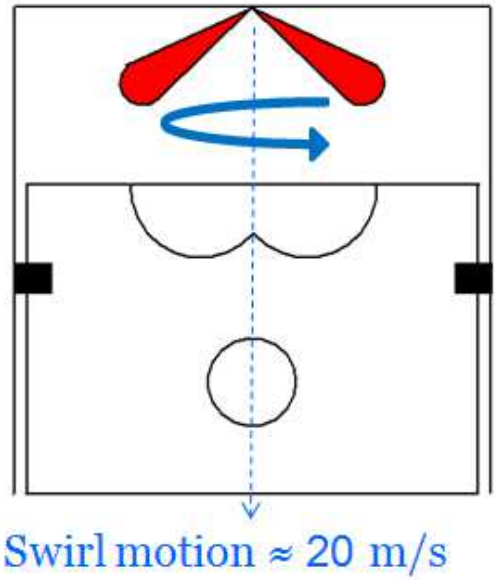

Fig. 3.55 Conventional Diesel mixture generation

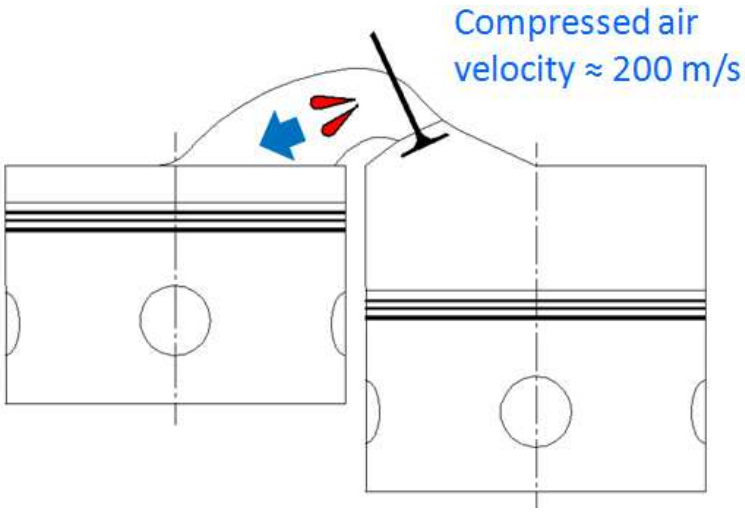

Fig. 3.56 HCPC mixture generation and air transfer

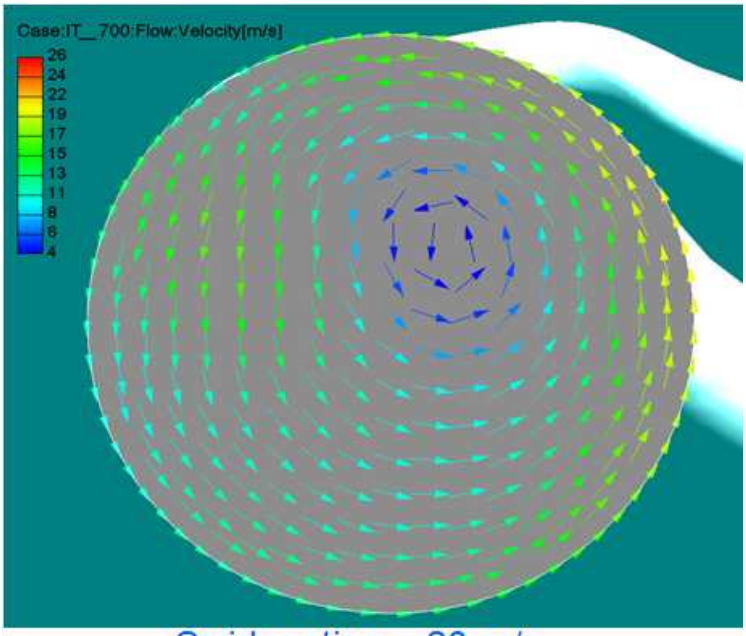

Fig. 3.57 Conventional Diesel in-cylinder flow field

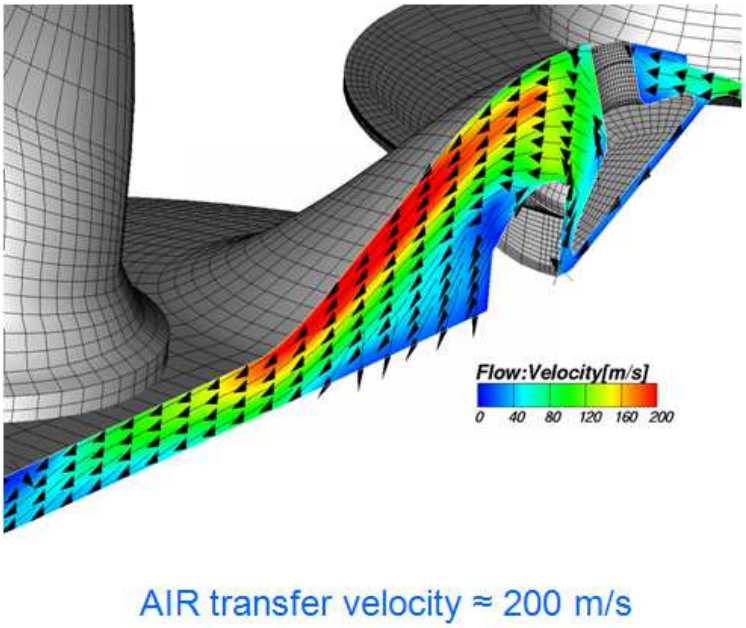

Fig. 3.58 HCPC transfer duct flow field

Chapter 4

HEAVY DUTY HCPC ENGINE

4.1 MOTIVATION

The latest part of the research on the HCPC engine, is focused on a Heavy-Duty application. The latest and the future pollutant emissions regulations, will require a stronger emissions reduction for Diesel engines than for Spark Ignited engines. These new regulations are likely to drive research and development in the Light-Duty applications towards different directions like downsized highly boosted gasoline engines, hybrid or electric vehicles, as well as CNG or LPG fuelled vehicles. The Diesel research will probably be more dedicated to Heavy-Duty applications, where electrification is not a real option, in particular for heavy trucks or extra-urban buses.
With this idea in mind, the study on the HCPC engine has been switched to a different application, and two different levels of displacement (9 and 13 liter engines) were studied. Prior to the CFD analysis of the new engine, an extensive code validation phase was performed.

4.2 13 LITER ENGINE

The results achieved with the Light-Duty engine motivated the research shown in this paper regarding the Heavy-Duty HCPC engine, especially because the low soot emissions that the HCPC engine produces at high loads have a stronger impact for a Heavy-Duty engine, which is more subject to these conditions than a Light-Duty one.
The Heavy-Duty HCPC engine configuration shown in this paper was obtained scaling the Light-Duty engine geometry studied before [36].
A previous extensive validation activity was performed in a standard Heavy-Duty Diesel engine. Special attention was paid to the calibration of the soot and NO_X models to obtain predictions as accurate as possible.

4.2.1 MODEL VALIDATION

Model validation was carried out, based on the experimental results obtained by Hardy et al. [37] on a single-cylinder Caterpillar SCOTE 3401E

Heavy-Duty Diesel engine at the Engine Research Center of the University of Wisconsin Madison. A diagram of the engine setup is shown in Fig. 4.1. The intake setup included a flexible intake boost pressure system that controls intake air pressure and a heater that controls intake air temperature. The engine specifications and operating conditions are given in Tab. 4.1 and 4.2.
The engine was operated with a double-injection strategy. The timing of the first injection was set at around -60° ATDC to achieve a partially-premixed combustion in the first part of the heat release rate. The second injection occurred near TDC, leading to a diffusive Diesel-like combustion. For other details of the experimental set-up refer to [37].

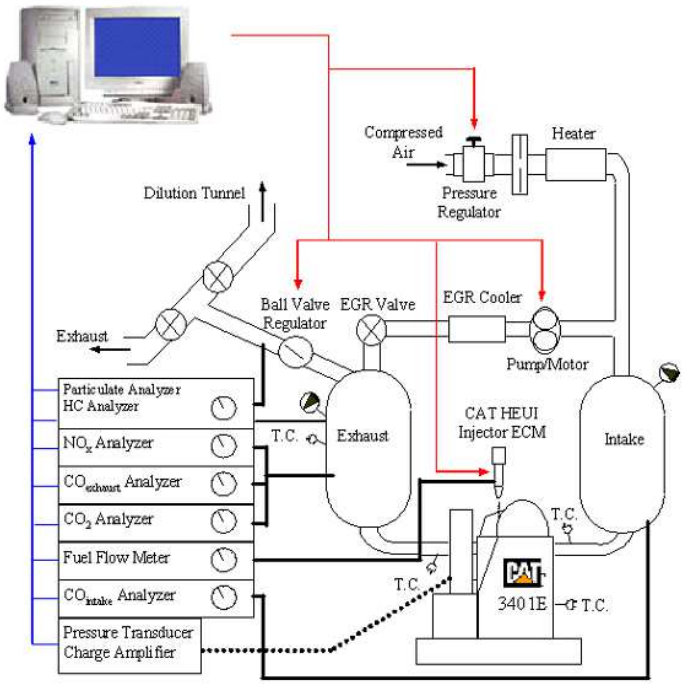

Fig. 4.1 Diagram of experimental engine setup for Caterpillar SCOTE 3401E

The simulation study was conducted using the AVL FIRE code with the models described in paragraph 3.2.2. As concerns the computational grid, a 60° sector mesh containing about 6700 cells at BDC was realized (Fig. 4.2). The mesh size was defined to obtain about the same cell size of the HCPC Heavy-Duty mesh.
Initial and boundary conditions for the calculation were obtained by the experimental measurements.

Bore	137.2 mm
Stroke	165.1 mm
Connecting Rod Length	261.6 mm
Squish Height	1.57 mm
Compression Ratio	16.1 : 1
Displacement	2.44 liters
Number of Valves	4
Number of Injector Nozzle Holes	6
Injector Nozzle Hole Diameter	0.158 mm
Injector Spray Angle (Included)	128°

Tab. 4.1 SCOTE 3401 E engine specifications

EVC	-355 deg ATDC
IVC	-143 deg ATDC
EVO	135 deg ATDC
IVO	335 deg ATDC
Engine Speed	1737 rpm
Engine Load	57%
Intake Temperature	32° C
Fuel rate	6.97 kg/hr
Fuel Injection Pressure	150 MPa
First Injection SOI	-65 to -50 deg ATDC
First Injection Duration	1000 to 1400 s
Main Injection SOI	-5 to +20 deg ATDC
Main Injection Duration	1650 to 1975 s
EGR %	0 to 30%
Boost Pressure	186.2 to 220.6 kPa

Tab. 4.2 Operating conditions

The simulation study was conducted using the AVL FIRE code with the models described in paragraph 3.2.2. As concerns the computational grid, a 60° sector mesh containing about 6700 cells at BDC was realized (Fig. 4.2). The mesh size was defined to obtain about the same cell size of the HCPC Heavy-Duty mesh.

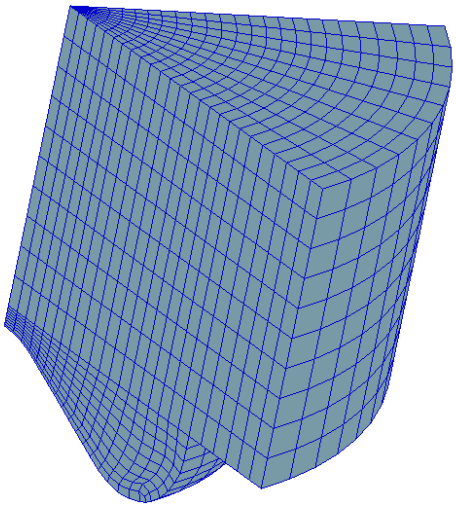

Fig. 4.2 Computational grid of Caterpillar SCOTE 3401E (6700 cells at BDC)

Initial and boundary conditions for the calculation were obtained by the experimental measurements.
During the validation activity, cylinder pressure and heat release rate curves, as well as emissions were compared varying three engine parameters: start timing of the main injection, boost pressure and EGR fraction. Conversely, start timing and duration of the pilot injection and the duration of the main injection were kept constant. Comparisons between experimental and numerical in-cylinder pressure and Heat Release Rate are shown in Figs. 4.3 to 4.8. Two cases for each parameter sweep are reported.

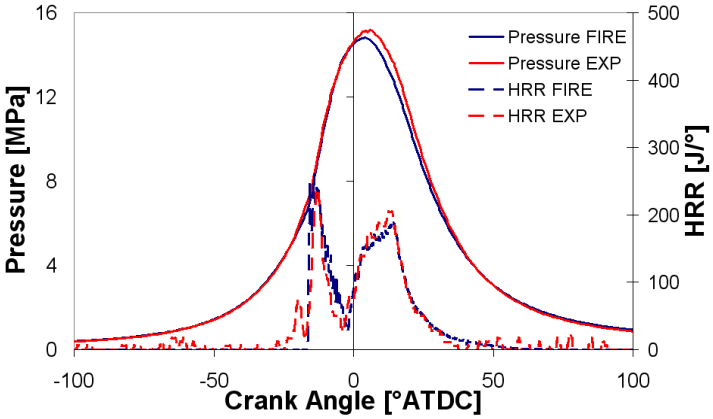

Fig. 4.3 Pressure and heat release rate main SOI -5°ATDC

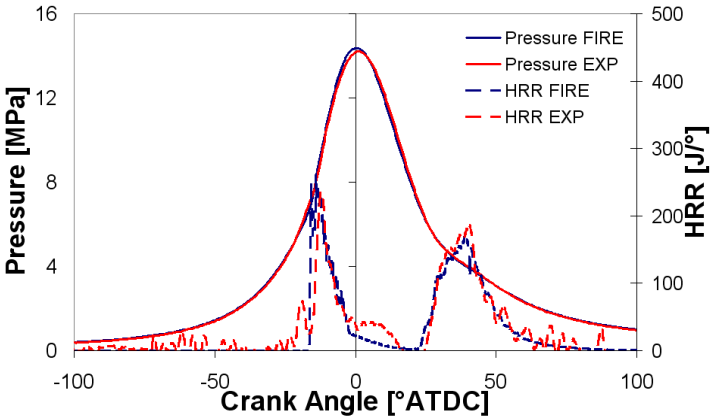

Fig. 4.4 Pressure and heat release rate main SOI 20°ATDC

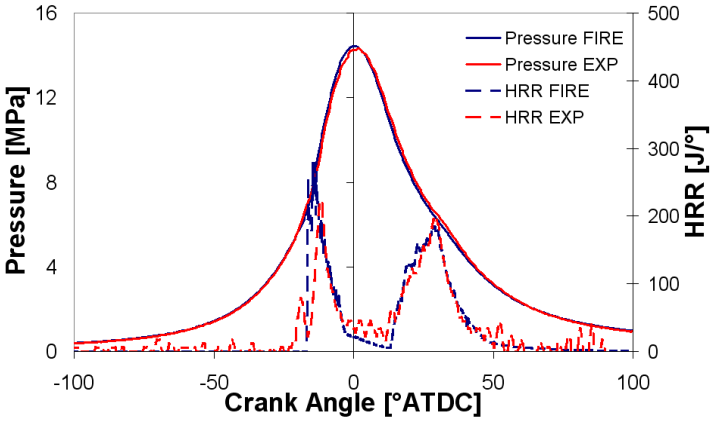

Fig. 4.5 Pressure and heat release rate EGR 0%

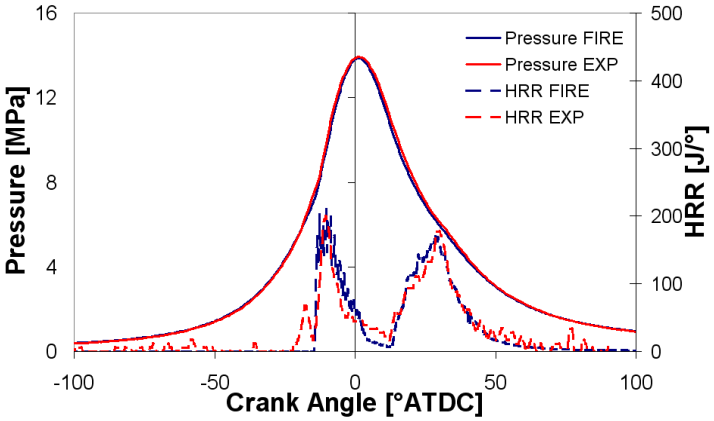

Fig. 4.6 Pressure and heat release rate EGR 30%

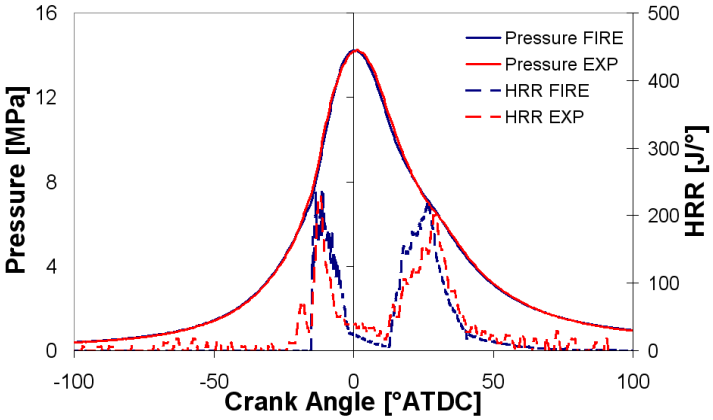

Fig. 4.7 Pressure and heat release rate intake pressure 0.26 MPa

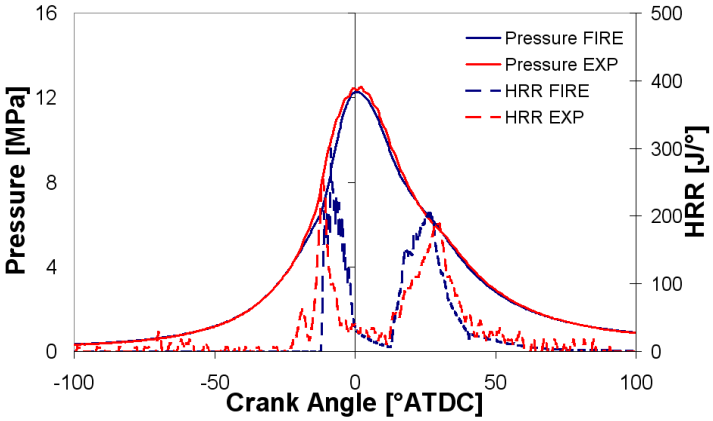

Fig. 4.8 Pressure and heat release rate intake pressure 0.21 MPa

In all the considered conditions the CFD model was able to reproduce pressure and heat release rate curves measured during the experiments almost perfectly. The only exception is the cold flame heat release rate, which could not be captured by the simplified ECFM-3Z combustion model that does not include detailed chemistry. Despite this limitation, the predicted emission behavior is in very good agreement with the experimental data. ECFM-3Z combustion model was chosen for its short calculation time. Only around 18 minutes were necessary, versus about 2 hours required by KIVA + CHEMKIN with the same grid size, to perform a sector-mesh calculation. This characteristic is very important in view of the time-consuming HCPC study, where multiple-cycle simulations are performed.

In Figs. 4.9 to 4.20, the emission results are reported. soot and NO_X results were also compared with those obtained by Cantrell et al. [38] using the KIVA-3V Release 2 code, coupled with the CHEMKIN detailed chemistry solver.

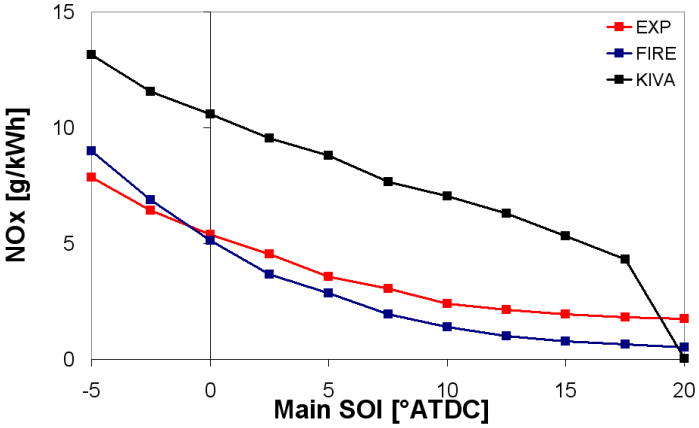

Fig. 4.9 NO_X emission comparison between CFD and experimental results with different main SOI

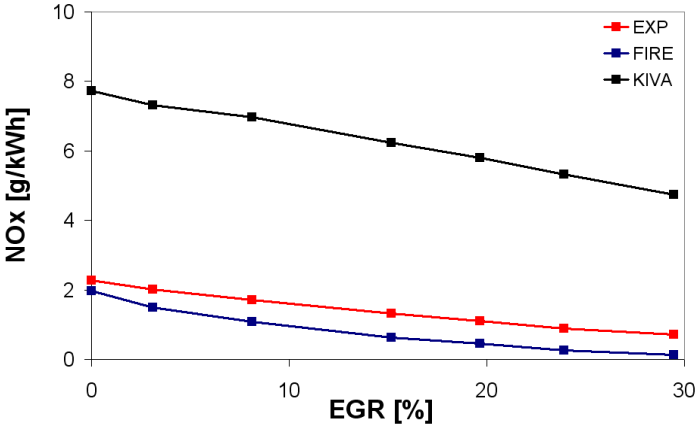

Fig. 4.10 NO_X emission comparison between CFD and experimental results with different EGR %

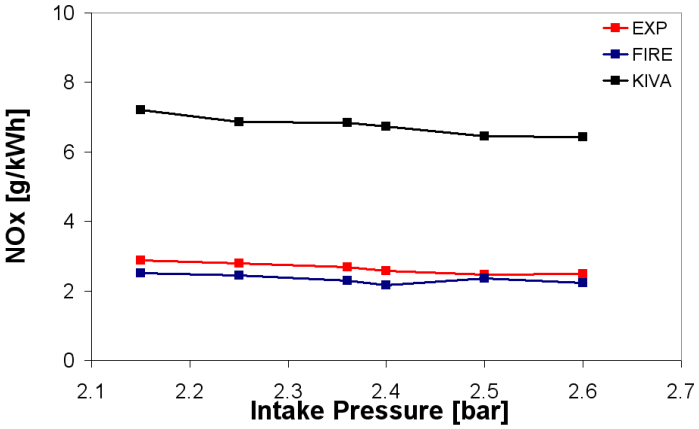

Fig. 4.11 NO_X emission comparison between CFD and experimental results with different intake pressures

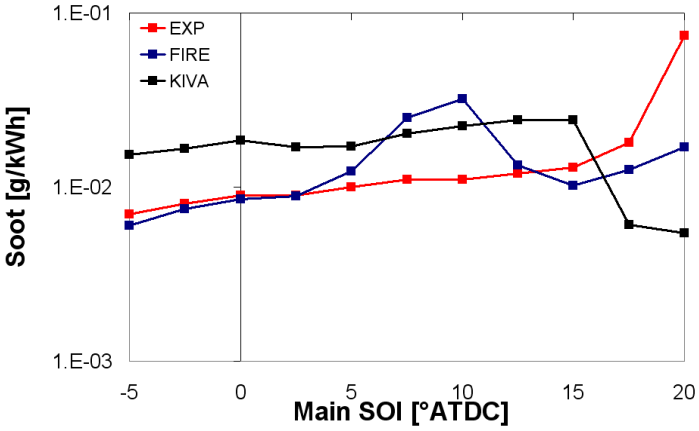

Fig. 4.12 soot emission comparison between CFD and experimental results with different main SOI

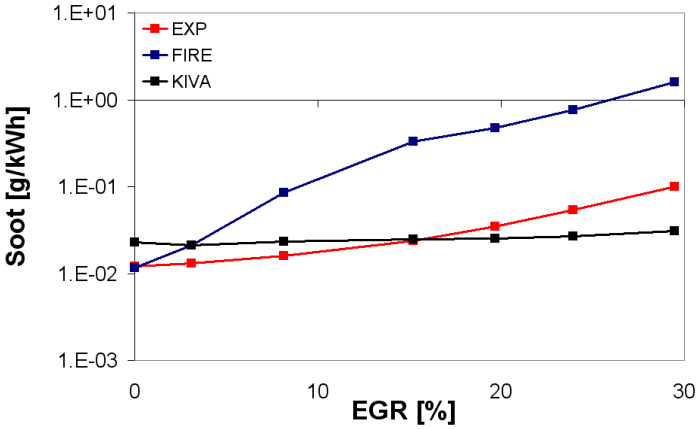

Fig. 4.13 soot emission comparison between CFD and experimental results with different EGR %

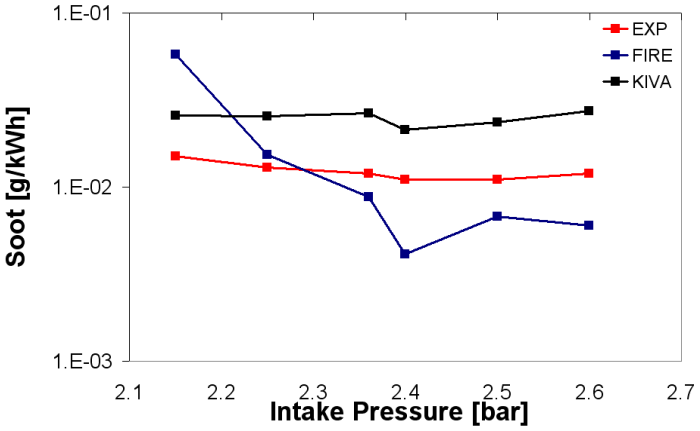

Fig. 4.14 soot emission comparison between CFD and experimental results with different intake pressures

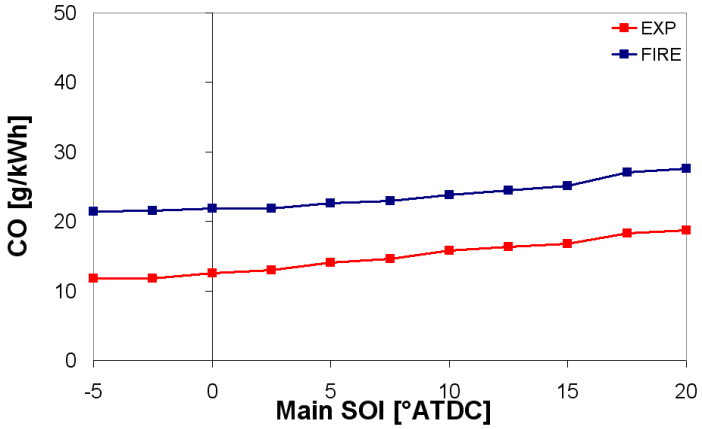

Fig. 4.15 CO emission comparison between CFD and experimental results with different main SOI

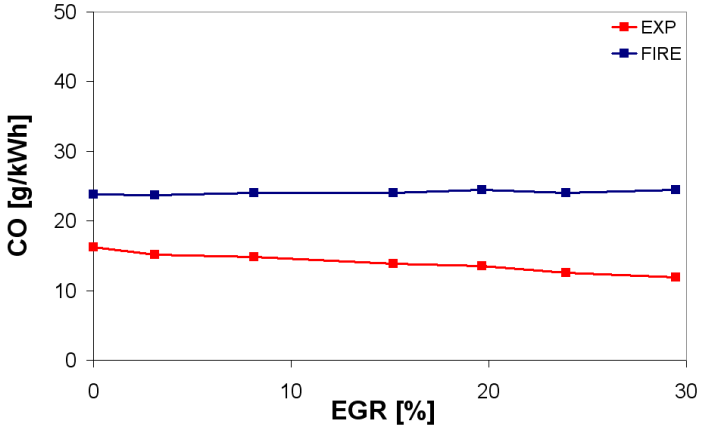

Fig. 4.16 CO emission comparison between CFD and experimental results with different EGR %

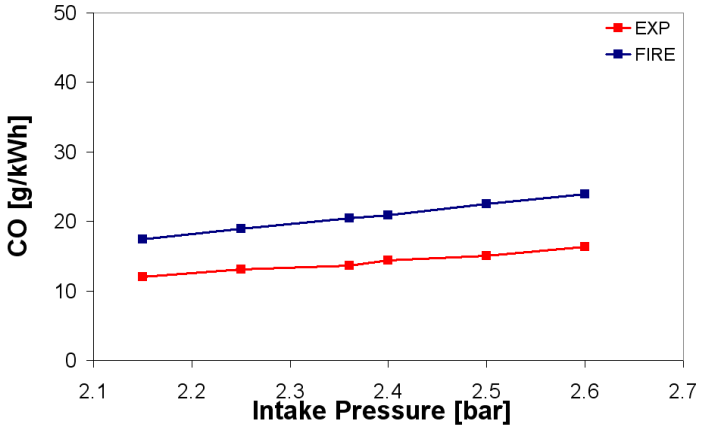

Fig. 4.17 CO emission comparison between CFD and experimental results with different intake pressures

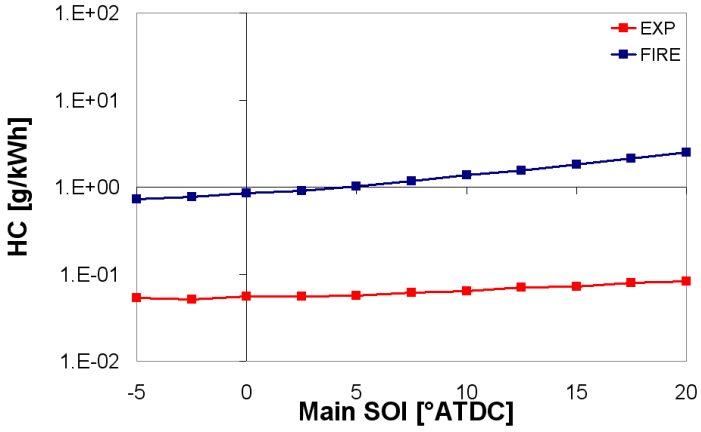

Fig. 4.18 HC emission comparison between CFD and experimental results with different main SOI sweep

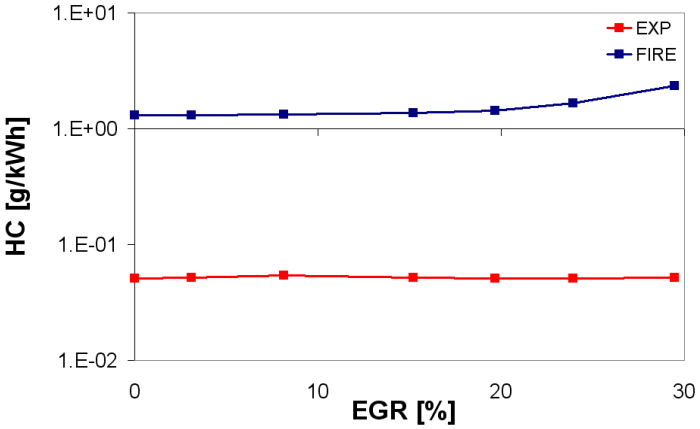

Fig. 4.19 HC emission comparison between CFD and experimental results with different EGR %

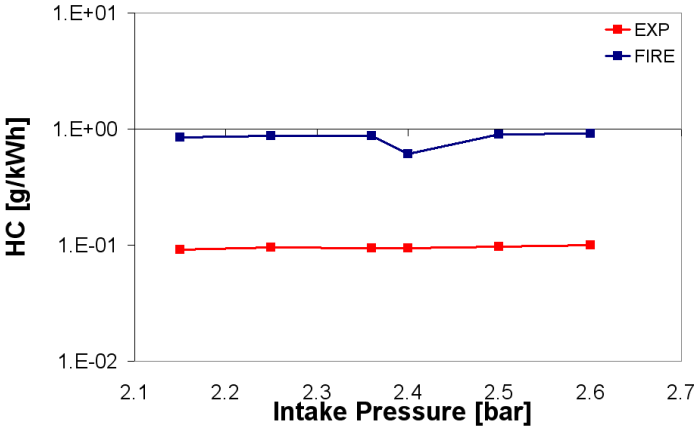

Fig. 4.20 HC emission comparison between CFD and experimental results with different intake pressures

In every condition with the AVL Fire code the NO_X emission trend and magnitude are very well captured.
soot trends are predicted reasonably well, although with larger error than NO_X. In the case of high levels of EGR, the model over-predicts the soot production. Nevertheless, in almost all cases the order of magnitude is in agreement with the experimental data. From the comparison with KIVA 3Vr2 results, it can be noticed how, despite FIRE was not coupled with a detailed chemistry solver, FIRE results can reproduce the emission trends with the same level of accuracy as KIVA, achieving even better results for NO_X emissions

CO and HC trends are closely reproduced by the FIRE model, even though the magnitudes are over-predicted in every case.
Taking the results of the validation study into account, the models were considered adequate to study the new HCPC engine concept.

4.2.2 HCPC HEAVY DUTY ENGINE

This paper shows the development of a new HCPC engine geometry, obtained scaling the light duty turbocharged-HCPC engine described I paragraph 3.4.A scaling factor of 1.69 was used, in order to obtain a total engine displacement of 13 liters with 3 HCPC units [39]. This displacement is widely employed in Diesel engines for Heavy-Duty road transportation; a conventional 6 cylinders heavy duty engine would correspond to 3 HCPC units (3 compressor and 3 combustor cylinders).

Engine sizing 1 (E-S 1)		
	Combustor	Compressor
Bore	145 mm	115 mm
Stroke	170 mm	170 mm
Geometric Compr. Ratio	161	171
Squish height	0.85 mm	0.85 mm
Total Displacement (3 HCPC units)	13118 cm^3	
Angle between cranks	30°	
IVO	35°ATDC	
IVO Effective	60°ATDC	
IVC	-101°ATDC	
IVC Effective	-126°ATDC	
TVO	-30°ATDC	
TVO Effective	-47°ATDC	
TVC	35 ATDC	
TVC Effective	52 ATDC	
EVO	138°ATDC	
EVO Effective	165°ATDC	
EVC	-36°ATDC	
EVC Effective	-9°ATDC	

Tab. 4.3 Engine sizing 1 specifications

Engine sizing 2 (E-S 2)		
	Combustor	Compressor
Bore	145 mm	115 mm
Stroke	175 mm	150 mm
Geometric Compr. Ratio	165	94
Squish height	0.85 mm	0.85 mm
Total Displacement (3 HCPC units)	12931 cm^3	
Angle between cranks	35°	
IVO	40° ATDC	
IVO Effective	65° ATDC	
IVC	-96° ATDC	
IVC Effective	-121° ATDC	
TVO	-30° ATDC	
TVO Effective	-47° ATDC	
TVC	40° ATDC	
TVC Effective	57° ATDC	
EVO	138° ATDC	
EVO Effective	165° ATDC	
EVC	-36° ATDC	
EVC Effective	-9° ATDC	

Tab. 4.4 Engine sizing 2 specifications

The new combustor and compressor bores were kept invariable, whereas two different strokes and two different angular phasing values between combustor and compressor were investigated. In Tab. 4.3 and 4.4 the two engine sizing specifications are given. They will be referred in the following as E-S 1 and E-S 2.

For E-S 2, the phasing between combustor and compressor was 35°, 5° more than in the previous Light-Duty turbocharged-HCPC engine. Therefore the effective closing timing of the transfer valve was set at 5° after the previous value, in order to maintain the same timing with respect to the compressor. The effective opening timing was kept at -30° ATDC, because it leads to lower pressure losses during the transfer phase. Likewise, the opening and closing timings of the intake valves were delayed by 5° in order to keep the same timings with respect to the compressor. For the E-S 1, the valve lift curves were maintained as in the previous turbocharged-HCPC engine. For both E-S 1 and E-S 2 valve lifts were scaled by the same factor used to scale the engine geometry.

Initial conditions for the simulation activity are given in Tab. 4.5. For the inlet and outlet pressure, a turbocharging system with 50% overall efficiency was assumed. Pilot injection was used to achieve stable ignition timing. A 7-hole injector located in the transfer duct was employed, in the same position as in the previous part of the research activity (Fig. 3.29). Spray boundary conditions used in the simulations are summarized in Tab. 4.6. Computational grids containing about 85000 cells at TDC (half model) were generated by means of the ANSYS ICEM-CFD software.

Engine speed	600 - 2200 rpm
Inlet T, P	363 K, 400 kPa
Outlet P	363 kPa
Combustor Initial T, P	1124 K, 10.5 bar
Compressor Initial T, P	564 K, 19.5 bar
Simulation Start	330°ATDC
Equivalence Ratio	0.8
Simulation End	1050° ATDC (2°cycle)

Tab. 4.5 Initial and boundary condition

Injection Type	Transfer Duct Injection
Fuel	N-Tetradecane
Fuel Temperature	363 K
SOI (Pilot injection)	-8° ATDC
EOI (Pilot injection)	-6° ATDC
SOI (Main injection)	0° ATDC
EOI (Main injection)	E-S 1: 25° ATDC E-S 2: 20° ATDC
Injector	7 - Hole
Fuel Injected	ES1: 330 mg ES2: 260 mg
Nozzle Diameter	300 μm
Cone Angle	12°
Injection rate	Square profile

Tab. 4.6 Injection boundary condition

Compressor piston	503 K
Compressor head	503 K
Compressor liner	373 K
Combustor piston	553 K
Combustor head	553 K
Combustor liner	433 K
Transfer duct	503 K
Intake duct	353 K
Exhaust duct	503 K
Transfer valve	553 K
Intake valve	373 K
Exhaust valve	503 K

Tab.4.7 Boundary condition: wall temperatures

4.2.3 RESULTS AND DISCUSSION

In Fig. 4.21 indicated power and torque for the two engine sizings are given. Both engines deliver very high torque values (over 3000 Nm for E-S 1), which are almost constant over all the engine speed range. Indicated power reaches 690 kW for E-S 1 and 600 kW for E-S 2, at 2200 RPM. This is due to the smaller compressor displacement of E-S 2, which leads to lower trapped mass in the compressor and in the combustor (Fig. 4.22).
On the other hand, E-S 2 allows higher efficiency (Fig. 4.23), almost 50% for all engine speeds. This depends on the lower compression ratio and larger expansion ratio as well as on the lower pressure losses during the air transfer phase, as shown by Fig. 4.24.

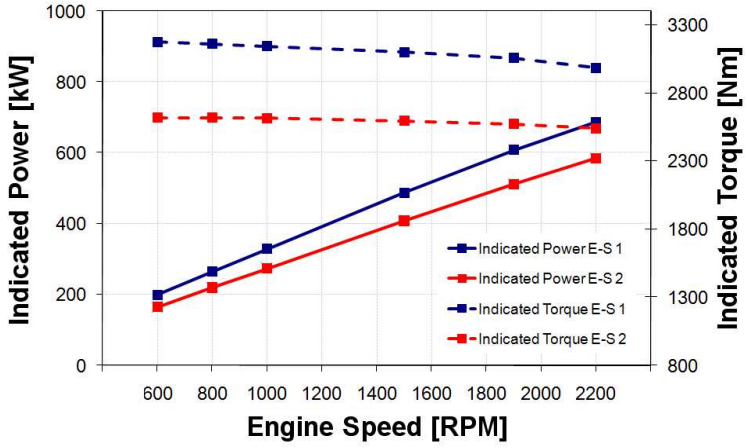

Fig. 4.21 Indicated power and torque vs. engine speed

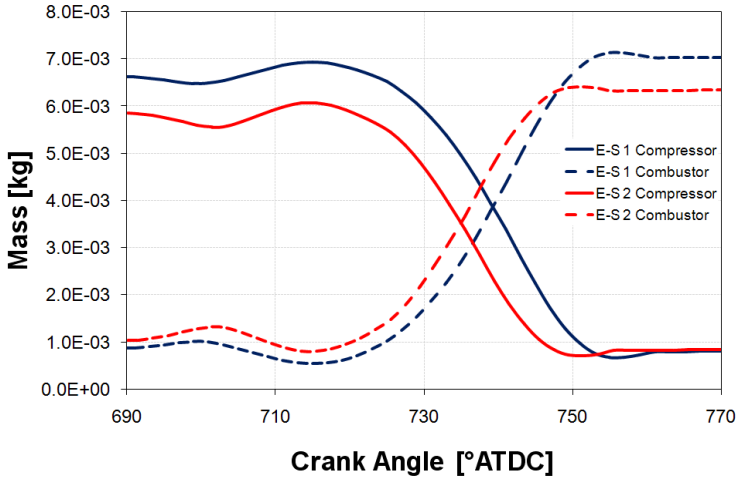

Fig. 4.22 Combustor and compressor mass vs. crank angle for E-S 1 and E-S 2 during the transfer process between the two cylinders.

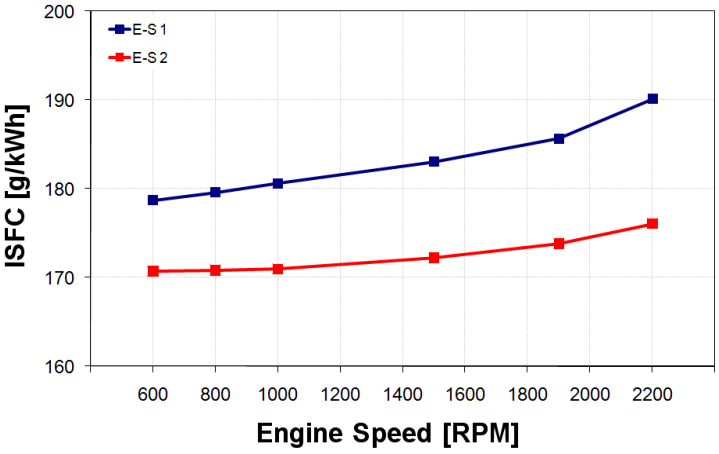

Fig. 4.23 Indicated Specific Fuel Consumption vs. engine speed

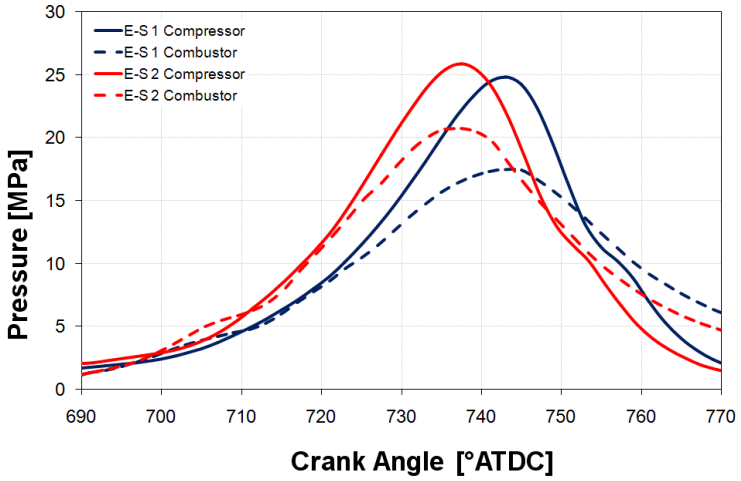

Fig. 4.24 Pressure traces vs. crank angle at 2200 RPM

Fig. 4.24 also confirms the results achieved during the previous parts of the research, showing a very smooth and almost linear in-cylinder pressure rise, which is very different from what occurs in conventional Diesel engines. This result can be better seen in Fig. 4.25, where peak pressure rise rate in the combustor cylinder shows very low maximum values (smaller than 1 MPa) for this kind of application. Engine sizing 1 allows lower PPRR values thanks to the wider phasing between combustor and compressor.

Pollutant emission behavior vs. engine speed, reported in Figs. 4.26-27, confirms the results of the previous turbocharged-HCPC engine. Emissions are almost independent of engine speed and no noticeable difference occurs between the t wo engine sizings. soot and HC are orders of

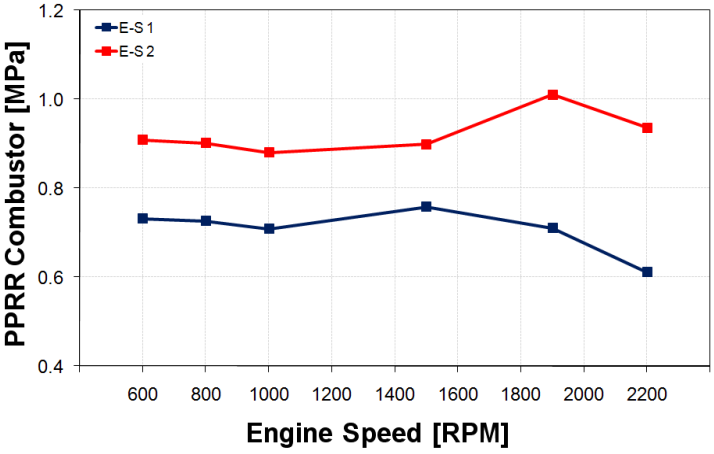

Fig. 4.25 Peak Pressure Rise Rate

magnitude lower than the ones of a conventional Diesel engine. CO emissions are much lower than those seen in the smaller turbocharged-HCPC engine. This result confirms the high efficiency of the combustion process. NO_X emissions are almost constant and similar to those of a conventional Diesel engine.

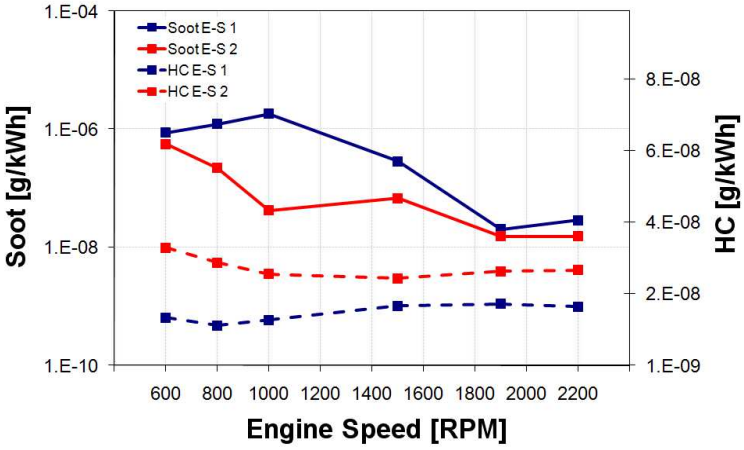

Fig. 4.26 soot and HC emissions vs. engine speed

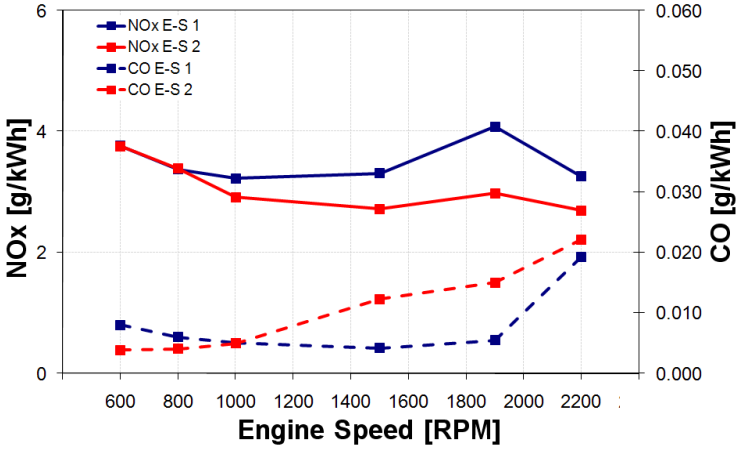

Fig. 4.27 NO_X and CO emissions

4.2.4 ADIABATIC CASE RESULTS

The high velocity of the air transfer from the compressor to the combustor during combustion produces higher heat losses than in a conventional Diesel engine, as shown in paragraph 3.3.4. In order to quantify these losses, an adiabatic simulation was conducted on E-S 2. Cylinder heads,

pistons and transfer duct surface where considered adiabatic in the calculation.
The results of this analysis are shown in Tab. 4.8. The adiabatic case shows a big jump in the indicated efficiency, from 48% to 58%, confirming the results achieved with the same kind of analysis on the Light-Duty HCPC engine.

	NON ADIABATIC	ADIABATIC
Indicated Power [kW]	512	608
Indicated Torque [Nm]	2570	3055
ISFC [g/kWh]	174	146
PPRR [MPa/°]	1.01	1.01
soot [g/kWh]	1.5 E-08	1.0 E-08
NO_X [g/kWh]	3.0	6.6
CO [g/kWh]	0.015	0.007
HC [g/kWh]	2.7 E-08	1.7 E-08

Tab. 4.8 Wall insulation effect (1900 RPM, Phi 0.8)

4.3 9 LITER ENGINE

The results shown so far prove the validity of the HCPC engine for light and Heavy Duty applications, in particular regarding soot emissions, maintaining an indicated efficiency comparable, or even better, with a conventional Diesel engine. NO_X emissions on the other hand, were shown to be on the same level of those produced by a conventional Diesel engine, if no EGR was used. In the latest part of the research a different approach was tested, with the aim of realizing an HCPC engine which could comply with EURO 6 / EPA 2010 regulations, without coupling the engine with complicated, and expensive, aftertreatment systems, such as SCR, LNT or DPF, using only a conventional oxidizing catalyst to reduce HC and CO emissions level. In order to achieve ultra-low in-cylinder NO_X and soot emissions a Low-Temperature HCPC strategy was tested. To achieve such low combustion temperatures, the external turbocharging system was modified, consisting in a dual-stage turbocharger, with intermediate intercooling. In this way the HCPC compressor receives intake air at higher pressure and lower temperature with respect to previous applications, leading to lower end-of-compression temperatures and therefore lower peak temperatures during combustion. In order to achieve this results, also

the injection rate was improved, to obtain a more homogeneous charge, which helps lowering peak combustion temperatures as well.
EGR is also used to lower combustion temperatures and oxygen content, with benefits for NO_X emissions. In the HCPC engine, using EGR does not increase soot emissions to excessive levels, given the ultra-low soot intrinsic production.
The ratio between combustor and compressor cylinders displacement was also increased, being the turbocharging system compression ratio higher than for those used in previous stages of the research, as will be shown in the next paragraph.
The new approach was tested on the new HCPC engine sizing, so it could be compared with available benchmark results from a latest generation, EURO 6 compliant, conventional Diesel engine, as shown in the next paragraph. It is worth mentioning that the benchmark engine runs on a no EGR strategy, and it is coupled with a latest-generation DPF + SCR aftertreatment system. Using an SCR system allows moving the NO_X – indicated efficiency trade-off towards the latter, but requires an additional tank and injection system for ammonia in the exhaust line to operate the catalytic converter.

4.3.1 MODEL VALIDATION

Experimental results for the new model validation activity were obtained directly from the benchmark engine OEM, for two different load conditions, full (1700 rpm, 23 bar IMEP) and partial load (1400 rpm, 12 bar IMEP).
The benchmark engine is a 6 cylinder 9 liter Heavy-Duty Diesel engine, which correspond to a 3 HCPC unit 9 liter engine.
Geometric specification for the new HCPC engine sizing are given in Tab. 4.9.

CB bore x stroke [mm]	135x160
CP bore x stroke [mm]	107x90
Angular Phasing	30°
Displacement 3 Units [cc]	9054

Tab. 4.9 9l HCPC engine specifications

In Fig. 4.28 the computational grid used for the validation activity is shown: full cycle simulations of the two load conditions previously described were tested.
Differently from the previous validations, a kinetic soot emission model was used, which is available in the 2011 version of AVL FIRE code.

The basis of this model is a detailed chemical reaction scheme for the calculation of soot formation and oxidation. The complete detailed kinetic scheme of the soot formation process incorporates 1850 gas-phase reactions 186 species and 100 heterogeneous reactions.
The current model contains a reduced number of species and reactions and has been developed in order to provide a computationally efficient kinetic overall soot model. The model can describe the behavior of soot formation and oxidation for different fuel classes [40].
The fuel used in the calculation is tetradecane, whose reduced reaction mechanism is shown in Tab. 4.10.

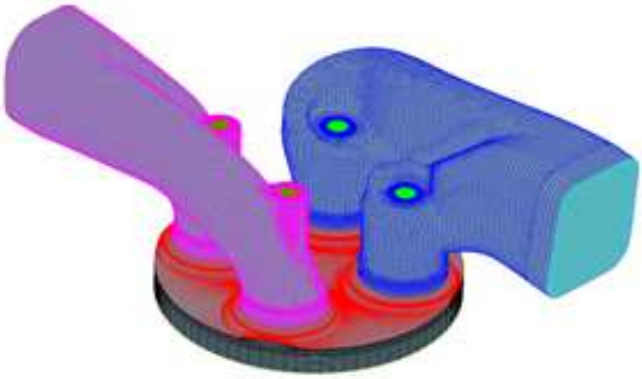

Fig. 4.28 Computational grid of the Benchmark-EURO 6 engine. Bore x Stroke: 117x135 mm, Displacement (6 cylinders): 8710 cm3

1	$C_{14}H_{30} + 7O_2 = 14CO + 15H_2$
2	$H_2 + H_2 + O_2 = H_2O + H_2O$
3	$CO + CO + O_2 = CO_2 + CO_2$
4,5	$CO + H_2O = CO_2 + H_2$
6	$C_{14}H_{30} + C_{14}H_{30} = 28C + 30H_2$
7	$C + C + O_2 = CO + CO$
8	$C + H_2O = CO + H_2$

Tab. 4.10 soot emissions kinetic model for tetradecane

The Kennedy-Hiroyasu-Magnussen model which was used in the previous part of the research activity, is not a fully predictive model, therefore a parameter needed to be tuned in order to adjust the model behavior. In the kinetic model, instead, no parameter has to be tuned, making the results more reliable.

In Figs. 4.29 and 4.30, experimental vs CFD in-cylinder pressure and heat release rate traces are shown, both for the full and partial load conditions. The results are satisfactory in both load condition, with better agreement between experimental and CFD traces for the full load condition.

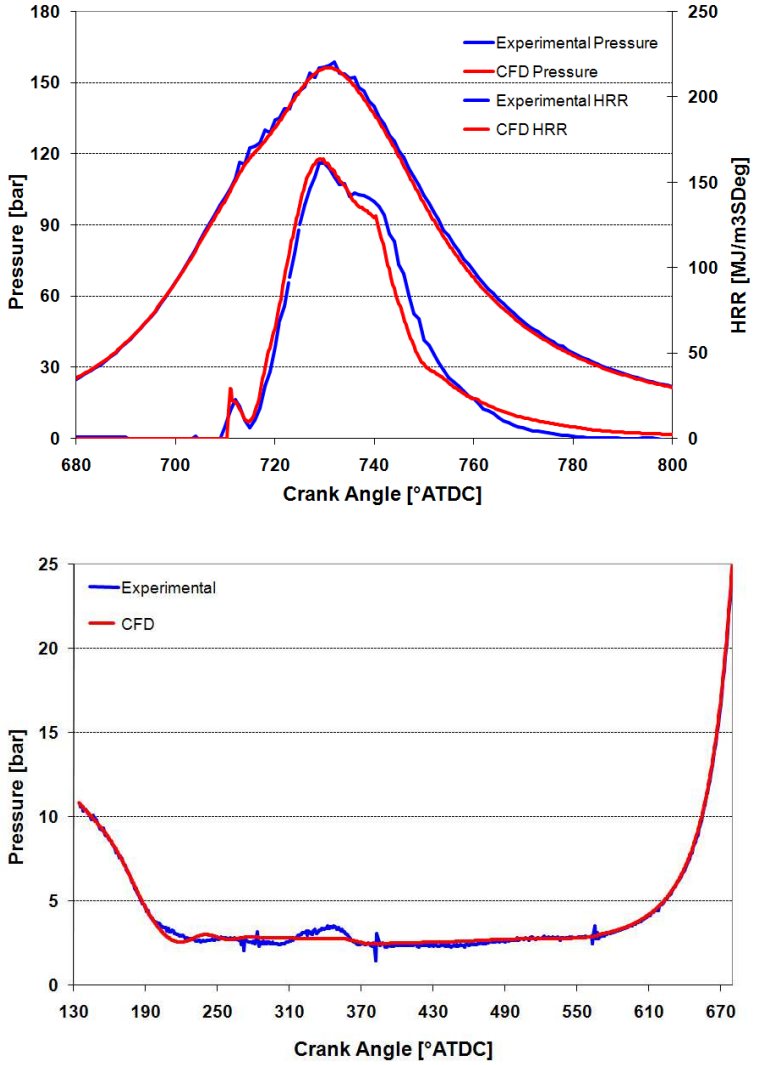

Fig. 4.29: Pressure and HRR traces for the full load condition

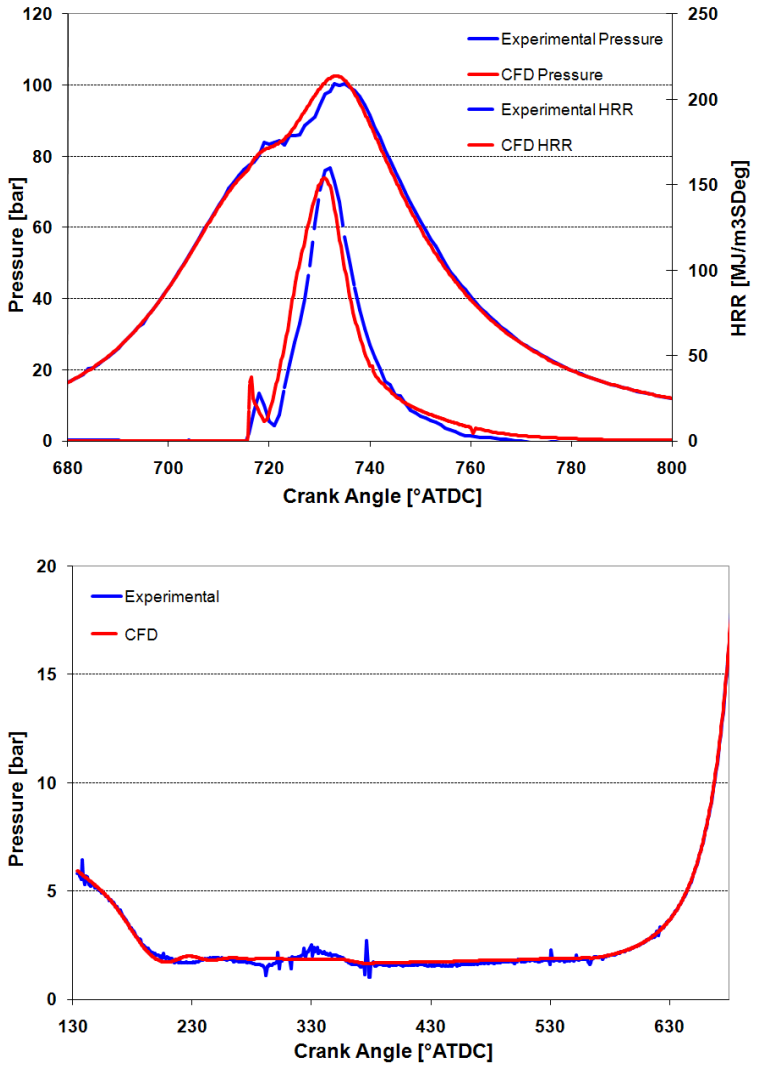

Fig. 4.30: Pressure and HRR traces for the full partial condition

4.3.2: 9 LITER ENGINE RESULTS

Tabs. 4.11 and 4.12 show the boundary condition used for the CFD calculations for HCPC and conventional Diesel engines, for both load conditions. The two engines were compared keeping the same injector, injection characteristics, amount of fuel injected and engine load in both analyzed conditions.

	Full Load (1700 rpm, 23 bar IMEP)		
	Intake pressure [bar]	Eq. Ratio [-]	EGR %
HCPC	5.1	0.8	20%
Benchmark EURO 6	2.7	0.6	0%

Tab 4.11 Full load condition boundary condition

	Partial Load (1400 rpm, 12 bar IMEP)		
	Intake pressure [bar]	Eq. Ratio [-]	EGR %
HCPC	2.7	0.8	20%
Benchmark EURO 6	1.8	0.4	0%

Tab 4.12 Partial load condition boundary condition

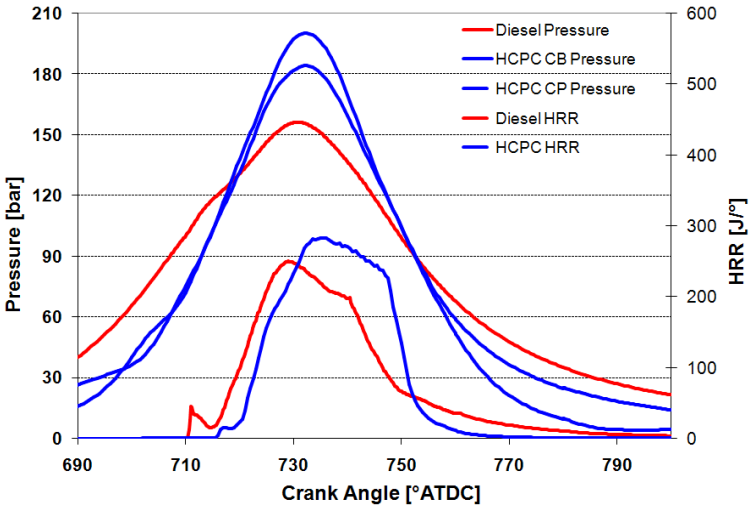

Fig. 4.31: Pressure and HRR traces in HCPC and conventional Diesel engine, for the full load condition

It can be noticed how the HCPC engine operates with much higher turbocharging pressure, than the conventional Diesel ones. Such pressures can be reached with the HCPC concept thanks to the much higher exhaust temperature, which lead to higher enthalpy in the exhaust gas. Higher exhaust temperature can be achieved thanks to the fact that the HCPC engine operates at higher equivalence ratio (around 0.8 in both load conditions), with respect to the conventional Diesel one.

In Figs. 4.31 and 4.32 results in term of in-cylinder pressure and HRR traces for the HCPC and the conventional Diesel engine are shown, for both load conditions.
In the full load condition HCPC pressure maximum values are slightly higher than in the conventional Diesel, but still under acceptable values. Moreover the highest maximum pressure value is seen in the compressor cylinder, which can tolerate higher pressure values, due to its relatively small bore (Tab. 4.9), leading to acceptable forces acting on the piston.

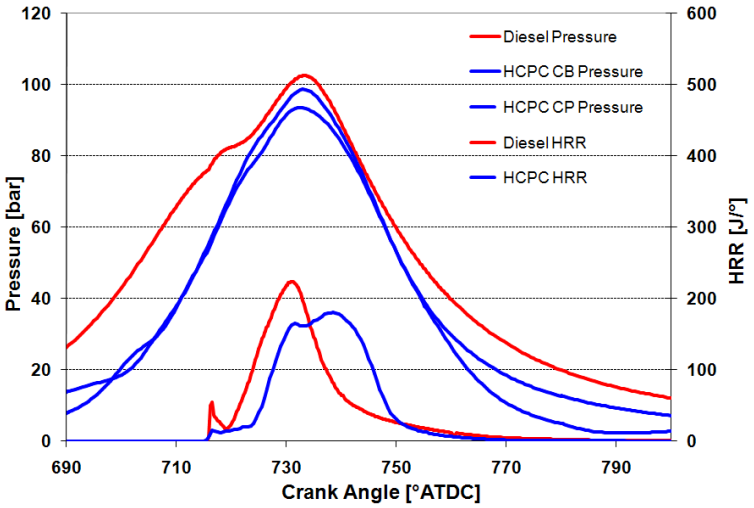

Fig. 4.32: Pressure and HRR traces in HCPC and conventional Diesel engine, for the partial load condition

In Tabs. 4.13 and 4.14 pollutant emissions results as well as indicated thermal efficiency are reported. As regards efficiency HCPC is in advantage for the full load condition, whereas Diesel delivers slightly better results for the partial load condition. As regards emissions instead, HCPC is always in advantage, with impressive results especially for NO_X emissions. As a matter of fact these results will allow the Low Temperature HCPC engine to operate in both load conditions with NO_X and soot emission levels lower than those set by the EURO 6 regulations, without coupling the engine with sophisticated aftertreatment systems.

Full Load		
	HCPC	Benchmark EURO 6
Thermal Ind. Efficiency	47.0 %	45.9%
HC [g/kWh]	0.06	0.4
CO [g/kWh]	2.0	6.5
soot [g/kWh]	0.007	0.034
NO_X [g/kWh]	0.13	9.6

Tab 4.13 Efficiency and emissions results for the full load condition

Partial Load		
	HCPC	Benchmark EURO 6
Thermal Ind. Efficiency	46.4%	47.9%
HC [g/kWh]	0.06	0.4
CO [g/kWh]	3.2	7.8
soot [g/kWh]	0.008	0.011
NO_X [g/kWh]	0.11	3.6

Tab 4.14 Efficiency and emissions results for the partial load condition

4.3.3 Φ-T ANALYSIS

In order to give more insight into the results presented in the last paragraph, an equivalence ratio – temperature map based analysis was carried out, plotting results from both CFD models for HCPC and EURO 6 conventional Diesel engine.
As expected, Fig 4.33 shows a classic behavior for the conventional Diesel engine, whit many points in the map touching both soot and NO_X generation areas, for most of the combustion duration.

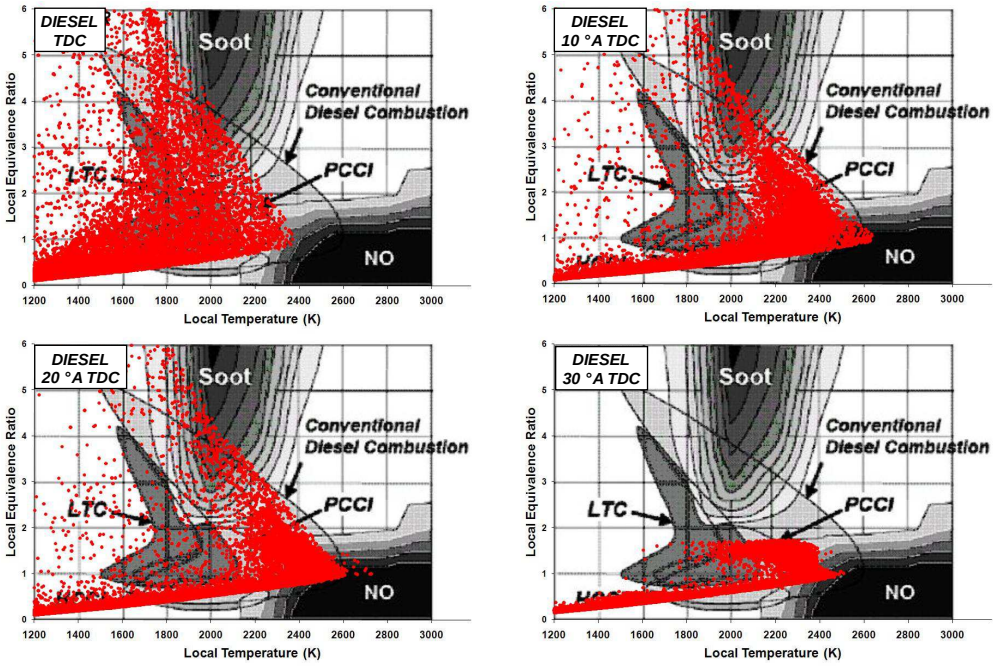

Fig 4.33 Φ-temperature maps for EURO 6 conventional Diesel engine

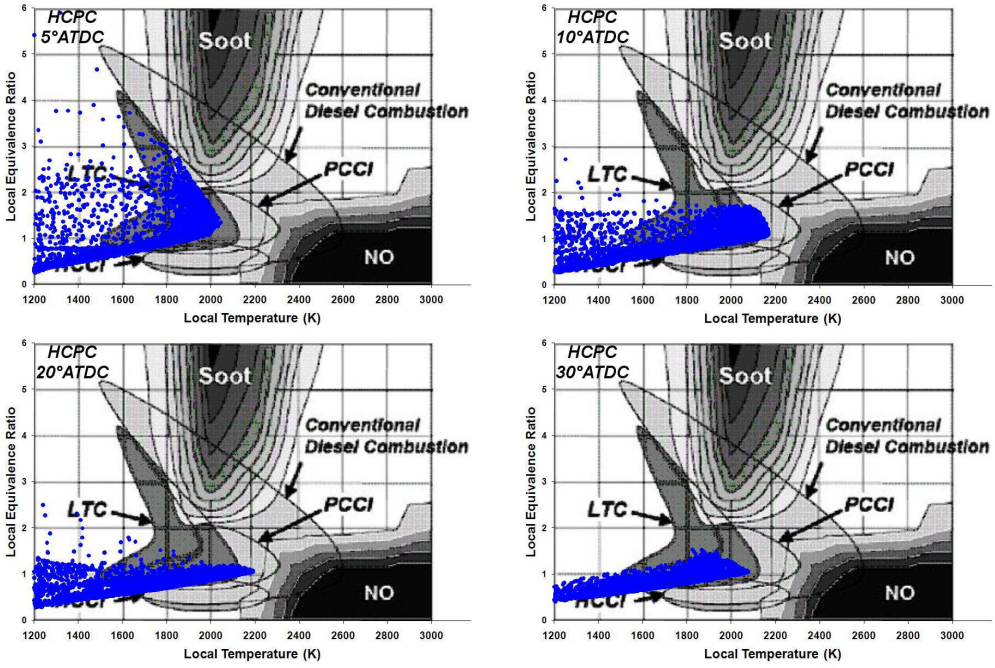

Fig 4.34 Φ-temperature maps for Low-Temperature HCPC engine

Fig. 4.34 shows the Φ-temperature maps for Low-Temperature HCPC concept. Local temperature is now much lower than in previous stages of the research activity (i.e. Fig. 2.40), leading to much lower NO_X emissions. It can be noticed how HCPC results are mostly covering the LTC gray area, with the advantage of not needing high EGR rates or diluted charge to moderate combustion reactions, thus achieving very high BMEPs, and covering all engine operating range.
Therefore the HCPC engine operating in Low-Temperature combustion can comply with the EURO 6 / EPA 2010 regulations just using an EGR system and a conventional Diesel Oxidizing Catalyst (DOC), without needing a latest-generation aftertreatment system (SCR or LNT + DPF).
HCPC engine will probably be also ready for future regulations (i.e. EURO 7), coupling the engine with SCR + DPF, whereas conventional Diesel engine will require further research and investments to achieve the same targets.
As regards indicated efficiency, which is at the current stage of the research on the same level of that of a conventional Diesel engine, major improvements can come from insulating engine walls as shown in paragraph 3.3.4. Indicated efficiency higher than 55% can be reached in this scenario, even though the increase in combustion temperature will increase NO_X emissions as well. An SCR/LNT system will then be required to comply with emission regulations.

Chapter 5

CONCLUSIONS

The research activity presented in this thesis suggests that Homogeneous Charge Progressive Combustion (HCPC) can represent a next-generation combustion mode for internal combustion engines that can simultaneously reduce exhaust emissions and substantially improve thermal efficiency.
The presented research activity was focused on the design and development of an innovative combustion system for Diesel engines. A new approach for a low emission – high efficiency Diesel combustion was conceived: the basic idea is to control the heat release rate by a gradual supply of an almost homogeneous charge in the combustion chamber, without relying on exhaust gas recirculation or extremely diluted mixtures to moderate the combustion reactions. In this way the typical limitations of limitations of HCCI/LTC Diesel combustion can be overcome.
The concept feasibility was proven in the early stages of the research, and a possible solution to realize HCPC combustion was chosen, based on the split-cycle concept. A novel split-cycle concept (patent pending [31]) was developed, where the thermodynamic cycle is accomplished in 2 volumes (compressor cylinder and transfer duct + combustor cylinder), differently from the other split cycle concept described in the scientific and technical literature. An high efficiency Miller cycle can therefore be realized with the HCPC engine.
Light-Duty and Heavy-Duty versions of the engine were studied, by means of CFD analysis. The results of the simulation activities are summarized in the following paragraphs.

5.1 LIGHT-DUTY HCPC ENGINE

An intensive simulation activity was carried on the Light-Duty version of the HCPC engine. Starting from a baseline geometry, studies were conducted to improve the transfer duct and engine head geometry, to a final configuration that delivers promising results. High efficiency (46%) and power density can be obtained with a naturally aspired engine. NO_X emissions are of the same order of magnitude as those of a Diesel engine, but it is possible to reach global equivalence ratios up to 0.85 with almost zero soot emissions. Moreover HCPC combustion quality is not worsened by increased engine speed, as it happens in conventional Diesel engines.

Clean Diesel combustion can be achieved using a moderate level of external cooled EGR that allows reducing NO_x emissions to levels typical of low-temperature combustion. Finally, insulating the engine walls it is possible to increase the indicated thermal efficiency to ideally 56 % (ISFC 151 g/kWh) when all the combustor and compressor walls (except the cylinder liners) are assumed to be adiabatic.

In a next stage of the research activity a new version of the engine with a smaller compressor and coupled with an external turbocharging system was studied, with benefits in terms of specific power and efficiency. Indeed turbocharging allows using a compressor of only 250 cm^3, half of the displacement of the compressor adopted for the naturally aspirated engine. Different intake pressures were considered from 100 to 300kPa adjusting the fuel injected accordingly to maintain the global equivalence ratio at 0.75. Higher fuel efficiency was attained compared to the 500 cm^3 compressor configuration, keeping the same pollutant emission behavior. Moreover, the new engine configuration allows reaching 6000 RPM keeping high indicated efficiency (45%), besides clean combustion. In conclusion the turbocharged Light-Duty HCPC engine can run at even better ISFC of Diesel engines at speeds that are typical of SI engines for passenger cars.

5.2 HEAVY-DUTY HCPC ENGINE

The last part of the research activity has been focused on an Heavy-Duty application of the HCPC engine. Two different engine were tested, respectively with a displacement of 13 l and 9 l. Prior to the study, a validation activity was performed for both engines, on two comparable Heavy-Duty conventional Diesel engines.
As regards the 13 l version, the geometry was obtained by scaling the small turbocharged Light-Duty HCPC engine. Two different engine sizings were studied, both with about 13 liters total displacement (3 HCPC units), but with different combustor and compressor strokes, and different angular phasing values between combustor and compressor. The results show that the two sizings respectively correspond to high-power and to high-efficiency configurations. Maximum indicated power (690 kW) was achieved with engine sizing 1, whereas maximum indicated efficiency (49%) was obtained with engine sizing 2. Both engine sizings confirm the results attained with the turbocharged Light-Duty HCPC engine in terms of pollutant emissions, showing ultra-low soot and HC emissions, and NO_X emissions in the same order of magnitude of the ones of conventional Diesel engines. An improvement in CO emissions was achieved with respect to the turbocharged Light-Duty HCPC engine. Finally, an adiabatic calculation was performed on engine sizing 2, confirming the importance of the heat

transfer losses during the air transfer phase, due to the high velocity of the air transfer from the compressor to the combustor cylinder.

As regards the 9 l version of the HCPC engine, a Low-Temperature HCPC concept was tested, with the aim of realizing an engine capable of complying with latest emission regulations (i.e. EURO 6), without needing latest-generation aftertreatment systems, like SCR/LNT or DPF.
The HCPC engine was compared with a latest-generation EURO 6 conventional Diesel engine, in two load conditions (full and partial). HCPC delivers slightly better thermal indicated efficiency for the full load condition (47% vs 45.9%), whereas conventional Diesel engine is in advantage for the partial load condition (46.5% vs 47.9%). As regards pollutant emissions, instead, HCPC engine is in strong advantage with respect to the conventional Diesel engine, in particular as far as NO_X emissions are concerned, which are one order of magnitude lower in the HCPC engine. HCPC is actually below the EURO 6 Heavy-Duty Diesel engine emission limits for both NO_X and soot, without needing SCR/LNT or DPF catalytic systems.
This result is encouraging also for emissions regulations to come (i.e. EURO 7), for which HCPC engine will probably be ready, if coupled with SCR/LNT systems, with minor adjustments. The conventional Diesel engine, instead, will struggle to meet this future regulations, and much research and investments will be required to achieve this result.

BIBLIOGRAPHY

1. http://www.Dieselnet.com/standards/.
2. Dec, J. E., "A Conceptual Model of D.I. Diesel Combustion Based on Laser-Sheet Imaging," SAE Paper 970873, 1997.
3. J.E. Dec, “Advanced compression-ignition engines, understanding the in-cylinder processes”, Proceedings of the Combustion Institute 32 (2009) 2727–2742
4. J.E. Dec, R.E. Canaan,” PLIF Imaging of NO Formation in a DI Diesel Engine”, SAE Trans.paper 980147 107 (3) (1998) 176–204.
5. F. Zhao, F., T.W. Asmus, D.N. Assanis, J.E. Dec., J.A. Eng, P.M. Najt, “Homogeneous Charge Compression Ignition (HCCI) Engines: Key Research and Development Issues”, Society of Automotive Engineers, Warrendale, PA, 2003.
6. X. Lu et al., “Fuel design and management for the control of advanced compression-ignition combustion modes”, Progress in Energy and Combustion Science 37 (2011) 741e783
7. S. Kokjohn, R. Hanson, D. Splitter, J. Kaddatz and R. D. Reitz, “Fuel Reactivity Controlled Compression Ignition (RCCI) Combustion in Light- and Heavy-Duty Engines”
8. D. Tamagna, “Innovative combustion strategies for land vehicles engines”, Doctoral thesis, University of Pisa.
9. AVL FIRE^{TM} User’s guide version 8.5, AVL LIST GmbH, 2006
10. AVL FIRE^{TM} Combustion manual version 8.5, AVL LIST GmbH, 2006
11. Dukowicz, J.K.: Particle-Fluid Numerical Model for Liquid Spray of Computational Physics 35,229-253(1980).
12. Dukovitcz, J.K.: Quasi-Steady Droplet Change in the Presence of Convection, Los Alamos Scientific Laboratory, LA7997-MS.
13. AVL BOOST^{TM} User’s guide version 5.0, AVL LIST GmbH, 2006.
14. Musu, E., Gentili, R.,Reitz, R., “Homogeneous Charge Progressive Combustion (HCPC): CFD Study of an Innovative Diesel HCCI Concept”, Technical Paper 2009-01-1344 2009
15. Beale, J.C., and Reitz, R.D., “Modeling Spray Atomization with the Kelvin-Helmholtz/Rayleigh- Taylor Hybrid Model,” Atomization and Sprays, Vol. 9, pp.623-650, (1999).
16. AVL FIRE^{TM} Combustion manual version 8.52, AVL LIST GmbH, (2007).

17. A. Patel, S.C. Kong, and R.D. Reitz, “Development and Validation of a Reduced Reaction Mechanism for HCCI Engine Simulations,” SAE 2004-01-0558 (2004).

18. Richard Opat, Youngchul Ra, Manuel A. Gonzalez D., Roger Krieger, Rolf D. Reitz, David E. Foster, Russell P. Durrett and Robert M. Siewert, “Investigation of Mixing and Temperature Effects on HC/CO Emissions for Highly Dilute Low Temperature Combustion in a Light Duty Diesel Engine” SAE Technical Paper No. 2007-01-0193, (2007).

19. Tamagna, D., Ra, Y., Reitz, R. D., “Multidimensional Simulation of PCCI Combustion Using Gasoline and Dual-Fuel Direct Injection with Detailed Chemical Kinetics”, SAE Technical Paper No. 2007-01-0190, (2007).

20. Babajimopoulos A., Assanis D. N., Flowers D. L., Aceves S. M., Hessel R. P.: “A fully coupled computational fluid dynamics and multi-zone model with detailed chemical kinetics for the simulation of premixed charge compression ignition engines”, International Journal of Engine Research, Volume 6, Number 5 / 2005, pages 497-512 (2005).

21. Yutaka Murata, Jin Kusaka, Yasuhiro Daisho, Daisuke Kawano, Hisakazu Suzuki, Haijime Ishii, Yuichi Goto, “Miller-PCCI Combustion in an HSDI Diesel Engine with VVT”, SAE Technical Paper No. 2008-01-0644 (2008).

22. Musu E., Rossi R., Gentili R., “Improvements in efficiency and mixture formation for an innovative Diesel HCCI concept”, ASME ICEF 2009, paper n°2009-14046.

23. Musu E., Rossi R., Gentili R., “HCPC: A New combustion system to lower Diesel engine emission”, F2010B103, Budapest, FISITA 2010

24. Backus Water Motor Co., Newark, N.J., “The Backus gas engine”, American Machinist Magazine -- January 15, 1891

25. J. Koenig, “Internal Combustion Engine”, U.S. Patent 1111841, Sept 29th 1914

26. Jukka T. Tianen, Ari Sarineen, Tore Grönlund, Martti J. Larmi, “Novel Two-Stroke Engine Concept, Feasibility Study” SAE Technical Paper No. 2003-01-3211, (2003).

27. Tore Grönlund, Martti J. Larmi, “Valve Train Design for a New Gas Exchange Process” SAE Technical Paper No. 2004-01-0607, (2004).

28. http://www.tourengine.com/

29. http://www.scuderiengine.com/

30. Coney W. M., Linnemann C., Morgan E.R., "A Novel Internal Combustion Engine With Simultaneous Injection of Fuel and Pre-Compressed Pre-Heated Air" ASME Paper No. ICEF2002-485 (2002).

31. Gentili R., Musu E., Rossi R., “Split-Cycle Engine”, WO2011045642, International Patent Application

32. Musu E., Rossi R., Gentili R., Reitz Rolf D., “Clean Diesel Combustion by means of the HCPC Concept”, SAE Int. J. Engines 3(1):964-981, 2010

33. Kokjohn, S.L. and Reitz, R.D., “A Computational Investigation of Two-Stage Combustion in a Light-Duty Engine,” SAE Int. J. Engines 1(1):1083-1104, 2008. 40.

34. Kokjohn, S.L., Swor, T.A., Andrie, M.J., and Reitz R.D., “Experiments and Modeling of Adaptive Injection Strategies (AIS) in Low Emission Diesel Engines,” SAE Int. J. Engines 2(1):16-32, 2009

35. Malgrem, A., Sidders, J., Stephenson, P., and Coney, M., “Experiments and Simulations of Quasi-Isothermal Compressor for a Novel High Efficiency Engine,” IMechE Conference Transaction, International Conference on Compressors and Their System, pages 461-472, 2003.

36. Musu E., Rossi R., Gentili R., Reitz Rolf D., “Heavy Duty HCPC”, SAE 2010 Powertrains, Fuels and Lubricants Meeting, Kyoto, 30/08/2011-02/09/2011, JSAE 20119324/SAE 2011-01-1824

37. Hardy, W.L., “An Experimental Investigation of Advanced Diesel Combustion Strategies for Emissions Reductions in a Heavy-Duty Diesel Engine at High Speed and Medium Load,” Master’s Thesis, University of Wisconsin-Madison, 2005.

38. Cantrell B. A., Ge H., Reitz R. D., Rutland C. J., “Validation of advanced combustion models applied to Two-Stage combustion in Heavy Duty engine”, SAE Technical Paper No. 2009-01-0714 (2009).

39. Lee C., Reitz R. D. and Kurtz, Eric “A Numerical Study on Diesel Engine Size-Scaling in Low Temperature Combustion Operation”, Numerical Heat Transfer, Part A: Applications, 58: 9, 681 — 701 (2010)

40. AVL FIRE, “CFD-Solver v2011 01 Combustion-Emission Manual”, AVL LIST GmbH, 2011

41. Tamagna Daniele, Musu Ettore, Gentili Roberto,A Preliminary Study Towards an Innovative Diesel HCCI Combustion, 2007 Fall Technical Conference of the ASME Internal Combustion Engine Division, pp 1-14, Charleston (SC),vol. CD & ASME Paper ICEF2007-1743

42. Arnold S., “Turbocharging technologies to meet critical performance demands of ultra-low emissions Diesel engines”, 19th Cliff Garret Turbomachinery award lecture, SAE 2004-01-1359

43. Winkler, N. and Ångström, H., "Simulations and Measurements of a Two-Stage Turbocharged Heavy-Duty Diesel Engine Including EGR in Transient Operation," SAE Technical Paper 2008-01-0539, 2008, doi:10.4271/2008-01-0539.

44. Arnold, S., "Turbocharging Technologies to Meet Critical Performance Demands of Ultra-Low Emissions Diesel Engines," SAE Technical Paper 2004-01-1359, 2004, doi:10.4271/2004-01-1359.

45. Kobayashi, M., Aoyagi, Y., Adachi, T., Murayama, T. et al., "Effective BSFC and NOx Reduction on Super Clean Diesel of Heavy Duty Diesel Engine by High Boosting and High EGR Rate," SAE Technical Paper 2011-01-0369, 2011, doi:10.4271/2011-01-0369.

46. Martinez-Frias, J., Aceves, S., Flowers, D., Smith, J. et al., "HCCI Engine Control by Thermal Management," SAE Technical Paper 2000-01-2869, 2000, doi:10.4271/2000-01-2869.

47. Yang, J., Culp, T., and Kenney, T., "Development of a Gasoline Engine System Using HCCI Technology - The Concept and the Test Results," SAE Technical Paper 2002-01-2832, 2002, doi:10.4271/2002-01-2832

48. Marriott, C. and Reitz, R., "Experimental Investigation of Direct Injection-Gasoline for Premixed Compression Ignited Combustion Phasing Control," SAE Technical Paper 2002-01-0418, 2002, doi:10.4271/2002-01-0418.

49. Odaka, M., Suzuki, H., Koike, N., and Ishii, H., "Search for Optimizing Control Method of Homogeneous Charge Diesel Combustion," SAE Technical Paper 1999-01-0184, 1999, doi:10.4271/1999-01-0184.

50. Hiraya, K., Hasegawa, K., Urushihara, T., Iiyama, A. et al., "A Study on Gasoline Fueled Compression Ignition Engine ~ A Trial of Operation Region Expansion ~," SAE Technical Paper 2002-01-0416, 2002, doi:10.4271/2002-01-0416.

51. Christensen M. et al., “Demonstrating the multi fuel capability of a homogeneous charge compression ignition engine with variable compression ratio”, SAE Technical Paper No. 1999-01-3679, (1999).

52. Haraldsson G. et al., “HCCI combustion phasing in a multi cylinder engine using variable compression ratio”, SAE Technical Paper No. 2002-01-2858, (2002).

53. Zhao H. et al.., “Understanding the effects of recycled burnt gases on the controlled autoignition (CAI) combustion in four-stroke gasoline engines”, SAE Technical Paper No. 2001-01-3607, (2001).

54. Nishijima, Y., Asaumi, Y., Aoyagi, Y., “Inpingement spray system with direct water injection for premixed lean diesel combustion control”, SAE Technical Paper No. 2002-01-0109 (2002).

55. Kaneko N., Ando, H., Ogawa, H., and Miyamoto, N., “Expansion of the operating range with in-cylinder water injection in a premixed charge compression ignition engine”, SAE Technical Paper No. 2002-01-1743, (2002).

56. Ricklin P. U. et al., “The effects of NO_X addition on the auto-ignition behavior of natural gas under HCCI conditions“, SAE Technical Paper No. , (2002).

57. Furutani M. et al., “An ultra-lean premixed compression-ignition engine concept and its characteristics”, Proceedings of COMODIA ’98, pp. 173-177 (1998).

58. Reitz R.D., Hanson R., Splitter D.,Kokjohn S.L., "Improving Fuel Efficiency with Fuel-Reactivity-Controlled Combustion" ERC Symposium 2009", www.erc.wisc.edu/documents/symp09-Reitz.pdf

59. Okude K., Mori K., Shiino S., Moriya T., “Premixed Compression Ingnition (PCI) Combustion for Simultaneous Reduction of NOx and Soot in Diesel Engine”, SAE Technical Paper No. 2004-01-1907, (2004).

60. Bessonette P. W., Schleyer C. H., Duffy K. P., Hardy W. L., Liechty M. P., “Effects of Fuel Property Changes on Heavy-Duty HCCI Combustion”, SAE Technical Paper No. 2007-01-0191.

61. Olsson J. O., Tunestal P., Johansson B., “Boosting for High Load HCCI”, SAE Technical Paper No. 2004-01-0940, (2004).

62. Yao M., Liu H., Zhang B., Zheng Z., “The influence of Boost Pressure and Fuel Chemistry on Combustion and Performance of a HCCI Engine”, SAE Technical Paper No. 2008-01-0051, (2008).

63. Ryan III, T. W. and Callahan, T. J., “Homogeneous Charge Compression Ignition of Diesel Fuel”, SAE Technical Paper No. 961160, (1996).

64. Gray A. and Ryan III, T. W., “Homogeneous charge compression ignition (HCCI) of diesel fuel”, SAE Technical Paper No. 971676, (1997).

65. Takeda, Y., Nakagome, K., and Niimura, K., “Emission Characteristics of Premixed Lean Diesel Combustion with Extremely Early Staged Fuel Injection”, SAE Technical Paper No. 961163, (1996).

66. Kimura, S., Aoki, O., Ogawa, H., Muranaka, S., and Enomoto, Y.,”New Combustion Concept for Ultra-Clean and High-Efficiency Small DI Diesel Engines”, SAE Technical Paper No. 1999-01-3681, (1999).

67. Mase, Y., Kawashina, J.-I., Sato, T., and Euguchi, M., “Nissan’s new multivalve DI diesel engine series”, SAE Technical Paper No. 981039, (1998).

68. Musu E., Rossi R., Gentili R., "Improvements in Efficiency and Mixture Formation for an Innovative Diesel HCCI Concept" ASME Paper No. ICEF2009-14046 (2009).

69. Kokjohn S. L., Reitz R. D., "A computational Investigation of Two-Stage Combustion in a Light-Duty Engine" , SAE Technical Paper No. 2008-01-2412, (2008).

70. Kokjohn S. L., Thaddeus A. S., Andrie M. J., Reitz R. D., "Experiments and Modeling of Adaptive Injection Strategies (AIS) in low Emission Diesel Engines" SAE Technical Paper No. 2009-01-0127, (2009).

71. Malgrem A., Sidders J., Stephenson P., Coney M., "Experiments and Simulations of a Quasi-Isothermal Compressor for a Novel High Efficiency Engine" SAE Technical Paper No. 2003-04-0137, (2003).